Identification of Factors Regulating Cytoplasmic and Nuclear Lipid Droplets

by

Jonghwa Lee

Submitted in partial fulfilment of the requirements
for the degree of Doctor of Philosophy

at

Dalhousie University
Halifax, Nova Scotia
November 2019

TABLE OF CONTENTS

LIST OF TABLES

LIST OF FIGURES

ABSTRACT

Lipid droplets (LDs) are cellular metabolic energy reservoirs composed of a neutral lipid core of triglycerides (TG) and cholesterol esters (CE) that is surrounded by a surface monolayer of phospholipids and embedded proteins. The most quantitatively significant phospholipid in eukaryotic cellular membranes is phosphatidylcholine (PC), which is *de novo* synthesized by the CDP-choline pathway under the control of the rate-limiting enzyme CTP:phosphocholine cytidylyltransferase (CCT) α. In the liver and intestine, the neutral lipids in LDs are hydrolyzed, re-esterified and assembled into lipoproteins for secretion. Increased PC synthesis is required for LD biogenesis and hepatic lipoprotein secretion. The aim of this project was to investigate mechanisms involved in regulating TG and PC biosynthesis during LD biogenesis and cellular lipid metabolism. Knockout of CCTα in intestinal-derived Caco2 cells (CCTα-KO cells) was used to determine how PC metabolism controls TG storage in LDs and secretion in chylomicrons. CCTα-KO cells had significantly decreased *de novo* PC synthesis and number of cytosolic LDs (cLDs), but increased droplet size and TG mass. Secretion of chylomicrons was reduced in differentiated CCTα-KO cells, indicating a specific requirement for the CDP-choline pathway in intestinal cell TG storage and secretion in lipoproteins. CCTα-KO cells also had a significant reduction in nuclear LDs (nLDs), which have CCTα and promyelocytic leukemia nuclear bodies (PML-NBs) coating the surface. Using PML knockout U2OS cells, we show that PML-NBs are critical for regulating the size and number of cLDs and nLDs in response to exogenous fatty acids. PML deficiency diminished both cLDs and nLDs, prevented recruitment of CCTα and LIPIN-1 to nLDs, and reduced PC and TG synthesis. Our research highlights the importance of coordinated regulation of PC and TG metabolism for the formation and function of LDs in the cytoplasm and nucleus.

LIST OF ABBREVIATIONS USED

ACAT	Acyl-CoA acyltransferase
ACSL	Acyl-CoA synthetase
AGPAT	1-acyl-*sn*-G3P acyltransferase
Apo	Apolipoprotein
ATGL	Adipose triglyceride lipase
ATP	Adenosine triphosphate
BAT	Brown adipose tissue
BSA	Bovine serum albumin
cAMP	Cyclic adenosine monophosphate
CCT	CTP:phosphocholine cytidylyltransferase
CDP	Cytidine 5'-diphosphate
CDS	Chanarin-Dorfman Syndrome
CE	Cholesterol ester
C/EBP	CAAT/enhancer-binding protein
CEPT	Choline/ethanolamine phosphotransferase
CGI-58	Comparative gene identification-58
CGL	Congenital generalised lipodystrophy
CHT	High-affinity choline transporter
CIDE	Cell death-inducing DEFA-like effector
CK	Choline kinase
cLD	Cytoplasmic LD
CMP	Cytidine 5'-monophosphate
CPT	Choline phosphotransferase
CRISPR	Clustered regularly interspaced short palindromic repeats
CTP	Cytidine 5'-triphosphate
CL	Cardiolipin
CLT	Choline transporter-like proteins
CoA	Coenzyme A
DG	Diacylglycerol
DGAT	Diacylglycerol acyltransferase
DMEM	Dulbecco's Modified Eagle Serum
ER	Endoplasmic reticulum
FASN	Fatty acid synthase
FAT	Fatty acid translocase
FATP	Fatty acid transport protein
FBS	Fetal bovine serum
G3P	Glycerol-3-phosphate
GFP	Green fluorescent protein
GPAT	G3P acyltransferase
GPC	Glycerophosphocholine
HDL	High-density lipoprotein
HMG-CoA	3-hydroxy-3-methyl-glutaryl-coenzyme A
HNF	Hepatocyte nuclear factor
HSL	Hormone-sensitive lipase

IDL	Intermediate-density lipoprotein
IMM	Inner mitochondrial membrane
INM	Inner nuclear membrane
IP_3	Inositol 1,4,5-triphosphate
KO	Knockout
LAL	Lysosomal acid lipase
LC3	Microtubule-associated protein light chain 3
LD	Lipid droplet
LDL	Low-density lipoprotein
LMA/C	Lamin A/C
LPAAT	Lysophosphatidic acid acyltransferase
LPCAT	Lyso-PC acyltransferase
LPDS	Lipoprotein-deficient serum
LPLAT	Lysophospholipid acyltransferase
LSC	Liquid scintillation counter
MAM	Mitochondrial-associated membranes
MAPK	Mitogen activated protein kinase
MBOAT	Membrane bound *O*-acyltransferase
MG	Monoacylglycerol
MGAT	Monoacylglycerol acyltransferase
MGL	Monoacylglycerol lipase
MTP	Microsomal triglyceride transfer protein
mRNA	Messenger RNA
NAFLD	Non-alcoholic fatty liver disease
NE	Nuclear envelope
NEM	*N*-ethylmaleimide
nLD	Nuclear LD
NLS	Nuclear localization signal
NR	Nuclear reticulum
OCT	Organic cation transporter
OMM	Outer mitochondrial membrane
ONM	Outer nuclear membrane
PA	Phosphatidic acid
PABP	PA binding protein
PAP	PA phosphatase
PC	Phosphatidylcholine
pChol	Phoshocholine
PCTV	Prechylomicron transport vesicle
PE	Phosphatidylethanolamine
PEMT	PE *N*-methyltransferase
PGC-1α	PPARγ coactivator-1α
PH	Pleckstrin homology
PI	Phosphatidylinositol
PIP_2	PI 4,5-biophosphate
PKA	Protein kinase A
PKC	Protein kinase C

PLA_2	Phospholipase A_2
PLC	Phospholipase C
PLD	Phospholipase D
Plin	Perilipin
PML	promyelocytic leukemia protein
PML-NBs	PML nuclear bodies
PNPLA3	Patatin-like phospholipase domain-containing protein 3
PPAR	Peroxisome proliferator-activated receptor
PS	Phosphatidylserine
SCD-1	Stearoyl-CoA desaturase-1
SDS	Sodium dodecyl sulphate
SDS-PAGE	SDS-polyacrylamide gel electrophoresis
siRNA	Small interfering RNA
SNARE	Soluble NSF attachment protein receptor
SREBP	Sterol regulatory element-binding protein
TER	Transepithelial resistance
TG	Triglycerides
TLC	Thin layer chromatography
TPD	Transepithelial potential difference
VLDL	Very-low density lipoprotein
WAT	White adipose tissue
XBP1	X-box binding protein

ACKNOWLEDGMENTS

I would like to gratefully thank my supervisor, Dr. Neale Ridgway, for his guidance and the opportunity to work in his lab. Dr. Ridgway has been an excellent supervisor. I am grateful for his patience, kindness and encouragement throughout my degree. I sincerely thank him for the time he has devoted to me and everything that I have learned from his laboratory.

To all the members of the Ridgway lab, thank you for being there for me. I truly appreciate your time for helping me both technically and emotionally, and most importantly, for being great friends. Additionally, I would like to acknowledge the members of the ARC for sharing their knowledge and lab techniques. Special thanks to Rob Douglas for maintaining cell cultures as well as technical supports.

This work was funded by an operating grant from the Canadian Institute for Health Research (CIHR).

Finally, to my family and friends, thank you so much for your support, encouragement and understanding throughout my life. Without them, I could never succeed in my degree.

CHAPTER 1: Introduction

1.1 Overview

Triglycerides (TG) and phospholipids are the major glycerolipid classes with key physiological roles in energy homeostasis, membrane biogenesis and cell proliferation (1). In mammals, excess fatty acids are esterified to form TG and cholesterol esters (CE), which are stored in a highly-condensed state in the core of lipid droplets (LDs) (2,3). TG stored in the large unilocular LDs within adipocytes serve as the main storage depots for fatty acids, but hepatocytes and enterocytes also have the capacity to store TG in LDs as well as assemble and secrete in lipoproteins for delivery to peripheral tissues. The neutral lipid core of LDs is surrounded by a monolayer of phospholipids, primarily phosphatidylcholine (PC), that stabilizes and controls the storage and mobilization of lipids (2,4). Thus, coordinated biosynthesis of TG and PC is required for LD biogenesis, and disruption in the balance between lipid storage and surface monolayer can lead to pathological conditions such as diabetes, obesity (5) non-alcoholic fatty liver disease (NAFLD) (6) or lipodystrophy (7).

The CDP-choline pathway or Kennedy pathway synthesizes the majority of PC for cellular membranes in mammalian cells (2,8). The rate-limiting step in this pathway is catalyzed by CTP:phosphocholine cytidylyltransferase (CCT) α and β isoforms, which are soluble enzymes that undergo activation upon translocation to membranes in response to lipid activators such as fatty acids (9,10). The more abundant and ubiquitously expressed isoform CCTα has been shown to increase PC synthesis for LD biogenesis and hepatic lipoprotein secretion in various cellular and animal models (2,11,12). LDs are

proposed to form in the endoplasmic reticulum (ER) and bud into the cytoplasm. However, recent studies demonstrate that LDs are not only present in the cytoplasm (cytoplasmic LDs; cLDs) but also in the nucleus (nuclear LDs; nLDs) of certain cell types (13,14). Similar to cLDs, the frequency and size of nLDs increase or decrease following fatty acid treatment or removal, respectively (13). Interestingly, nLDs associate with CCTα and promyelocytic leukemia nuclear bodies (PML-NBs), dynamic sub-nuclear structures that regulate gene expression and stress response (14). These findings suggest that nLDs could be active sites for PC synthesis and provide a platform for the assembly of enzymes and/or transcription factors involved in fatty acid homeostasis.

The main purpose of this thesis research is to understand how PC and TG metabolism are regulated and control LD biogenesis and lipoprotein secretion. Using intestinal-derived Caco2 cells with knockout of CCTα, we examined the contribution of CCTα and PC synthesis to the formation of cLDs and nLDs, as well as the partitioning of TG into storage and secretory pathways. The biological significance of PML-NBs and nLDs in regulating TG and PC homeostasis was also investigated using human osteosarcoma U2OS cells with knockout of PML. This introductory chapter summarizes current understanding of TG and PC biosynthetic pathways and their role in regulating LD biogenesis and lipid metabolism and will introduce novel concepts in nuclear lipid regulation and biology of nLDs.

1.2 Glycerolipids and Lipid Droplet

1.2.1 Triglyceride Properties and Function

TG is composed of a glycerol backbone esterified to three fatty acids (**Fig. 1.1A**), whose length and degree of saturation determine the physical and chemical properties of TG such as melting point (15). The highly reduced and anhydrous hydrocarbon tail of the acyl chains makes TG an efficient form of cellular energy storage (15). In mammals, TG stored in adipose tissue serves as the main energy source through lipolysis, the process by which free fatty acids are released from TG (2). Hepatocytes and enterocytes also contain prominent amounts of TG stored in LDs that are hydrolyzed, re-esterified and assembled to form lipoproteins that transport fatty acids to other tissues (4). TG hydrolysis also provides diacylglycerol (DG), a precursor of the major phospholipids and membrane biogenesis (16). In addition to energy storage and membrane biogenesis, TG synthesis protects cells against fatty acid-induced toxicity (17).

1.2.2 Phospholipid Properties and Function

Phospholipids are composed of two fatty acyl chains esterified at the *sn*-1 and *sn*-2 positions and a polar head group with a phosphodiester bond at the *sn*-3 position of glycerol (18). Because of their amphiphilic properties, phospholipids can form lipid monolayers and bilayers, and are the major components of biological membranes that comprise a semi-permeable barrier to the external environment (1). In addition to structural roles, phospholipids can also associate with and regulate the function of membrane proteins, and are precursors for signaling molecules.

The major phospholipids are phosphatidylcholine (PC), phosphatidylethanolamine (PE), phosphatidylinositol (PI), and phosphatidylserine (PS) (18) (**Fig. 1.1B)**. PE, which makes up 20-30% of total membrane content, induces negative curvature into lipid bilayers due to its conical shape arising from the small polar head group (19). PI, which composes 5-15% of total membrane content, can be phosphorylated at the 3', 4' or 5' positions of the inositol ring, resulting in positional isomers with specialized functions (20). PS constitutes up to 10% of membrane phospholipid and is asymmetrically distributed between the bilayer leaflets (21). This asymmetry is determined by the balance between the flippase and scramblase activities, and plays an important role in apoptosis (22).

PC is the most abundant phospholipid in eukaryotic membrane bilayers, comprising 40-60% of total membrane lipids (23). PC has a large phosphocholine head group, making it cylindrical in shape and ideal for forming planar membranes with increased stability and rigidity (9). PC is also a major component of the surface monolayers of serum lipoproteins, lung surfactant and LDs. PC is not only involved in membrane structure, but also serves as a source for signaling molecules released through hydrolysis by different phospholipases (8). For example, PC hydrolysis by phospholipase A_2 (PLA_2) results in the formation of arachidonic acid, which is metabolized to leukotrienes and prostaglandins (24). Phospholipase D (PLD)-mediated hydrolysis of PC releases phosphatidic acid (PA), a precursor for other bioactive lipids (25) and an inducer of inflammation (26). Cleavage of the phosphocholine head group by phospholipase C (PLC) releases DG, a potent activator of protein kinase C (PKC) (27).

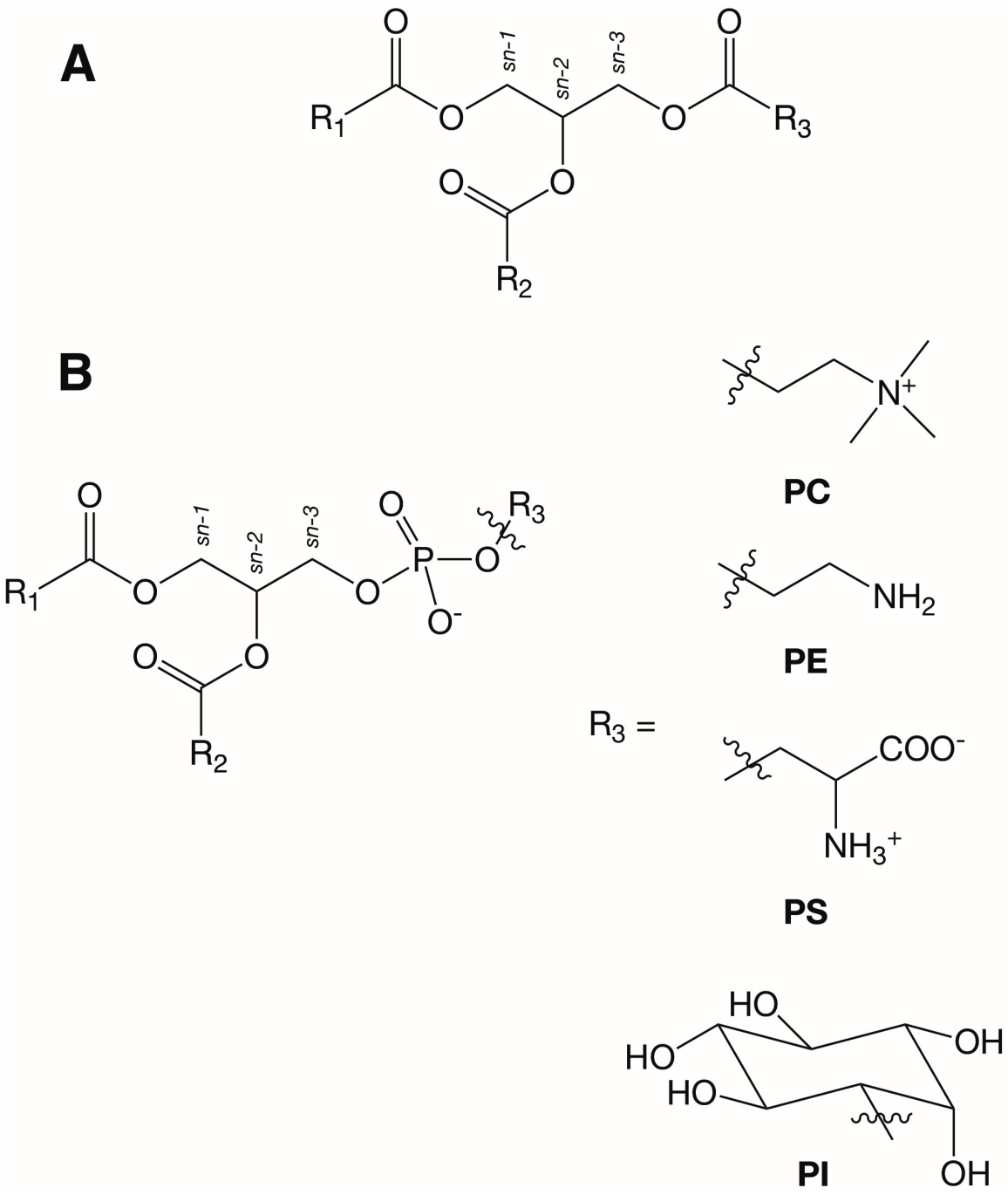

Figure 1.1. Structure of glycerolipids. Structure of TG composed of a glycerol backbone esterified with three fatty acyl chains. Fatty acyl chains are indicated by R_1, R_2 and R_3 **(A)**. Structure of major phospholipids composed of a glycerol backboned esterified with two fatty acyl chains and a hydrophilic head consisting of a phosphate group. Fatty acyl chains are indicated by R_1 and R_2. Polar head groups are indicated by R_3 **(B)**.

1.2.3 Lipid Droplet Function and Composition

Excess fatty acids are esterified to form TG and CE that are packaged into LD for storage and lipolysis (28). In white adipocytes, the neutral lipid core is primarily composed of TG, but in most cell types, TG and CE coexist in various ratios. When fatty acids are needed for energy generation, membrane biogenesis or hormone synthesis, LD-associated lipases release neutral lipids as free fatty acids. Thus, LDs constantly form, grow and shrink, with diameters ranging from 0.1-5 μm in nonadipocytes to ~100 μm in white adipocytes, depending on the metabolic state of the cell (29).

During LD formation and expansion, surface phospholipid addition must be coordinated with increased neutral lipid core volume to maintain optimal surface to volume ratio (30). The most quantitatively significant phospholipid in mammalian LDs is PC, and conditions that result in PC deficiency lead to abnormal LD morphology. Inhibition of PC synthesis by silencing CCTα in oleate-treated rat intestinal epithelial (IEC-18) cells resulted in the formation of enlarged LDs with reduced TG mass (2) due to increased surface tension that leads to LD fusion (31) (discussed in Section *1.5.2*), indicating that the CDP-choline pathway is an important contributor to LD biogenesis and stability.

Exceeding or saturating the neutral lipid storage capacity of LDs is associated with several human diseases (28,32). For example, TG deposition in adipocytes is increased in hyperphagia-induced obesity (32). Increased adipose TG storage also results in elevated levels of circulating fatty acids that may accumulate in skeletal muscle or liver, leading to the development of insulin resistance and hepatic steatosis (28,32). With

increasing worldwide prevalence of these diseases (33,34), a better understanding of glycerolipid metabolism and LD biogenesis is of considerable importance.

In eukaryotic cells, TG is synthesized by the successive fatty acylation of glycerol-3-phosphate (G3P) in the endoplasmic reticulum (ER). In the G3P pathway, phosphatidic acid (PA) and diacylglycerol (DG) are central intermediates for TG synthesis, but also serve as precursors for phospholipid synthesis (**Fig. 1.2**). PA, produced by sequential acylation of G3P by glycerol-3-phosphate acyltransferases (GPATs) and 1-acyl-*sn*-glycerol-3-phosphate acyltransferases (AGPATs), is the substrate for CDP-DG, a precursor for PI, phosphatidylglycerol (PG) and cardiolipin (CL). DG produced by dephosphorylation of PA by PA phosphatases (LIPINs) is the substrate for TG synthesis by diacylglycerol acyltransferases (DGATs) or PC and PE synthesis by the CDP-choline/ethanolamine pathway. The enzymology and regulation of the G3P and CDP-choline pathways are discussed further in **Section 1.3** and **1.4**, respectively.

1.3 Enzymes of the Glycerol-3-Phosphate Pathway

1.3.1 Triglyceride Synthesis

In mammals, two TG biosynthetic pathways have been identified: the G3P and monoacylglycerol (MG) pathways (15). In both pathways, CoA-activated fatty acids are utilized as acyl donors (35), and DG is acylated by DGATs to form TG. The MG pathway is important in the small intestine to synthesize TG by re-esterification of MG derived from the diet (36). As a result, intestine-specific deletion of MGAT in mice delayed fat absorption and decreased food intake (37). In contrast, the G3P pathway is present in most cells, including enterocytes (3,15). Although considerable knowledge has

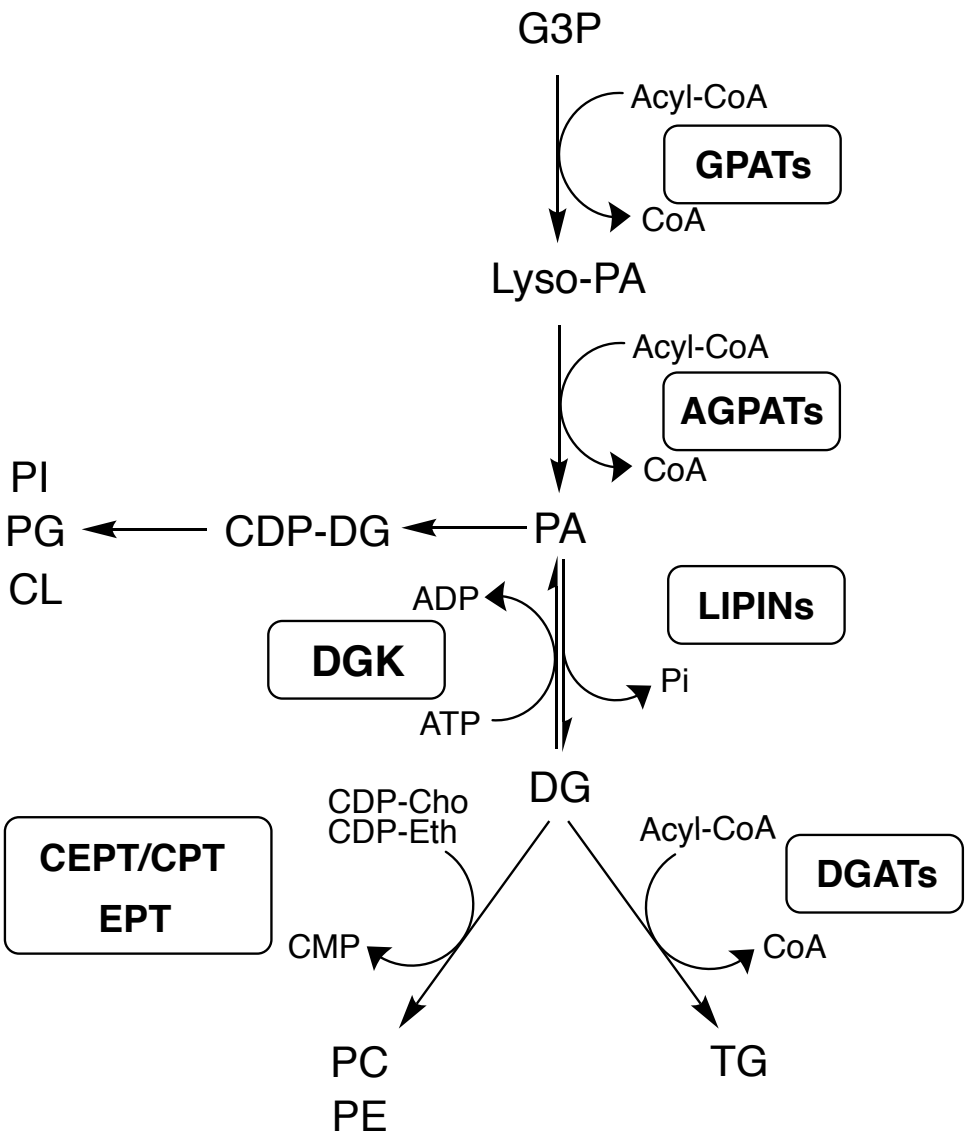

Figure 1.2. The G3P pathway. The biosynthesis of TG and phospholipids occurs through the G3P pathway involving sequential acylation and dephosphorylation reactions catalyzed by GPATs, AGPATs, LIPINs, and DGATs. PA and DG are central intermediates that are also substrates for the CDP-DG and CDP-choline/ethanolamine pathways for phospholipid synthesis, respectively. Enzymes are indicated in boxes.

been gained about G3P pathway, recent molecular, genetic and physiological studies have demonstrated new insights into its complexity (38). TG biosynthetic enzymes often exist as isoforms that are encoded by the separate genes or alternative splicing, and further modified by post-translational modifications (39). While these isoenzymes catalyze the same reactions, they have distinct functional roles in the G3P pathway. For example, DGAT2, but not DGAT1, relocates from the ER to the surface of expanding LDs during fatty acid-induced LD biogenesis (40,41). This section highlights the role of G3P pathway enzymes during TG metabolism and LD biogenesis. The substrate specificity and tissue and subcellular distributions of these enzymes are summarized in **Table 1.1**.

1.3.2 Glycerol-3-Phosphate Acyltransferases

The first committed step of the G3P pathway is the acylation of G3P to form 1-acyl-*sn*-glycerol-3-phosphate (lysophosphatidic acid, lyso-PA) by the GPAT family of enzymes (42-44). This step is considered to be the rate-limiting because GPATs exhibit the lowest specific activity of all enzymes in the pathway (42). GPATs are found in most tissues including adipose, liver, lung, kidney, muscle, intestinal mucosa, and brain (43). Four mammalian GPAT members have been identified that have distinct subcellular localization and biochemical properties; *N*-ethylmaleimide (NEM)-resistant GPAT1 and NEM-sensitive GPAT2 are on the outer mitochondrial membrane (OMM), and NEM-sensitive GPAT3 and GPAT4 are localized to the ER (42,43,45,46). Amino acid sequence alignment reveals that GPAT isoforms are members of the pfam01553 family with four motifs that are highly conserved among glycerolipid acyltransferases, suggesting that these motifs are a catalytically important region (43,45-47).

Table 1.1. Substrate preference and subcellular/tissue distribution of G3P enzymes.

	Acyl-CoA preference	Subcellular distribution	Tissue distribution
GPAT1	16:0 > 18:0 > 18:1 (48)	Mitochondria (48)	[m]WAT > liver > muscle > brain > kidney > lung (49)
GPAT2	No preference (50)	Mitochondria (50)	[m]Testis > liver > BAT > brain > lung > heart (49)
GPAT3	16:0, 18:1, 18:2 (51)	ER (51)	[m]WAT > small intestine > BAT > kidney > heart > colon (51)
GPAT4	No preference (52)	ER (52) and LD (40)	[m]BAT > testis > liver > kidney > brain > intestine > WAT > heart > skeletal muscle (53)
AGPAT1	14:0, 16:0, 16:1, 18:2, 18:3, 18:0, 18:1 (54,55)	ER (56)	[h]Liver > pancreas > lung > heart > small intestine > skeletal muscle (57,58)
AGPAT2	14:0, 16:0, 18:1, 18:2, 18:0, 20:4 (55)	ER (59)	[h]Heart > liver > WAT (58,60)
AGPAT3	18:1, 18:2, 20:4 (61)	ER, NE (61) and LD (40)	[h]Testis > WAT > liver > kidney > heart, brain > lung (62)
AGPAT4	18:1, 18:2, 20:4, 22:6 (63)	ER (63)	[h]Brain > skeletal muscle > spleen (63)
AGPAT5	16:0, 18:0, 18:1, 20:4 (61)	ER, NE, and mitochondria (61)	[h]Brain > WAT > heart > kidney > liver > lung (64)
LIPIN-1	-	Nucleus, ER (65) and LD (66,67)	[h]WAT > skeletal muscle > small intestine (68)

LIPIN-2	-	ER and cytoplasm (65,69)	[h]WAT > liver > small intestine > brain (68)
LIPIN-3	-	ER and cytoplasm (70)	[h]Intestine > liver > WAT (68)
DGAT1	18:1, 18:2, 16:0, 20:4 (71)	ER (72)	[h]Small intestine > testis > mammary gland (73)
DGAT2	18:1, 18:2, 16:0, 20:4 (71)	ER (41) and LD (74)	[h]Liver > WAT > mammary glands > testis > heart (71)

Tissue distribution; [h]Human, [m]Murine
WAT; White adipose tissue

In the liver, mitochondrial GPAT1 and 2 comprise 30 to 50% of the total activity (75). Liver-specific adenoviral expression of GPAT1 in mice and rats resulted in TG accumulation and hyperlipidemia (76-78). In contrast, *Gpat1*$^{-/-}$ mice had markedly reduced hepatic TG content and increased plasma β-hydroxybutyrate and 3-hydroxy-3-methyl-glutaryl-coenzyme A (HMG-CoA) synthase expression, indicating diversion of acyl-CoA toward β-oxidation (79,80). In other tissues, GPAT3 and/or GPAT4 activity in the ER is 10-fold greater than mitochondrial GPAT activity (75). For example, *Gpat3* mRNA was increased ~60-fold during 3T3-L1 differentiation, and *Gpat3*$^{-/-}$ mice had ~80% and ~40% reductions in total GPAT activity in white adipose tissue and small intestine, respectively (81). When fed a high-fat diet, *Gpat3*$^{-/-}$ mice had decreased weight gain and fat mass. However, the contents of glycerolipids remained unchanged in the liver, perhaps due to a compensatory increase in GPAT1 activity (82). *Gpat4*$^{-/-}$ mice had a 65% reduction in NEM-sensitive GPAT activity in the liver and brown adipose tissue, but normal activity was observed in white adipose tissue due to high levels of GPAT3 expression (52). As a result, oxidation of exogenous oleate was increased and its incorporation into TG was reduced in differentiated primary brown adipocytes from *Gpat4*$^{-/-}$ mice compared to controls, indicating a role in exogenous fatty acid flux into TG synthesis rather than β-oxidation. During fatty acid overload (>0.5 mM oleate) of cultured cells, GPAT4 relocalized from the ER to LDs (40), where it could direct excess acyl-CoAs toward storage pathway, resulting in sufficient amounts of local DG for increased TG synthesis and LD expansion. However, this regulatory response appears to be specific to brown adipose tissue since GPAT4-deficient hepatocytes had normal exogenous fatty acid metabolism

(83), possibly due to the presence of GPAT1. The mechanism by which ER-localized G3P enzymes translocate to LDs is discussed in Section *1.5.3*.

1.3.3 1-Acyl-sn-Glycerol-3-Phosphate Acyltransferases

The second step in the G3P pathway is the CoA-dependent acylation of the *sn*-2 position of lyso-PA by AGPATs, also referred to as lysophosphatidic acid acyltransferases (LPAATs) (43,75). Eleven mammalian AGPATs are classified as members of the pfam01553 family with four highly conserved acyltransferase motifs, and have mitochondria- and ER-localized activities (61,84). While AGPAT1 and 2 show strict acyl acceptor specificity for lyso-PA, other isoforms have a wide range of lysophospholipid specificity (51,55,57,58,85,86).

The mRNA for human and murine AGPAT1 is detected in most tissues, and the protein is localized to the ER (57,58,87). Overexpression of human AGPAT1 in 3T3-L1 adipocytes increased basal and insulin-stimulated [^{3}H]oleate uptake and incorporation into PA and TG (88). AGPAT1 overexpression in 3T3-L1 cells also increased [^{14}C]glucose uptake and conversion to cellular lipids upon insulin stimulation. However, AGPAT1 overexpression in C2C12 myotubes had no effect on [^{14}C]glucose uptake but diverted glucose from glycogen synthesis to lipid synthesis, and increased insulin-mediated [^{3}H]oleate uptake (88), demonstrating a possible tissue-specific function in partitioning energy metabolism.

High levels of human AGPAT2 mRNA have been detected in the heart, liver, and adipose tissue, and it is the only isoform that is associated with a human disease. Mutations or deficiency in AGPAT2 causes severe congenital generalised lipodystrophy

(CGL), an autosomal recessive disorder characterized by an extreme scarcity of adipose tissue (60,89). In cultured adipocytes expressing AGPAT1-5, knockdown of AGPAT2 reduced TG synthesis and increased lyso-PA channeling into phospholipids (59). Thus, these data indicate a critical, non-redundant role of AGPAT2 for TG synthesis and/or PA-dependent signaling pathways during adipogenesis. However, *Agpat2*$^{-/-}$ mice developed hepatic steatosis that was driven by increased fatty acid synthesis and diversion of lyso-PA to TG and phospholipids (89). Since deletion of *Mgat1* did not ameliorate hepatic steatosis in these mice (90), the increase in glycerolipid synthesis is due to an alternate AGPAT-dependent pathway.

While AGPAT1 and AGPAT2 exhibit strict acyl acceptor specificity for lyso-PA, other isoenzymes utilize lyso-PC, lyso-PE and lyso-PS as acyl acceptors. For example, AGPAT3, AGPAT4, and AGPAT5 not only have LPAAT activity with oleoyl-CoA, but also have modest lysophospholipid acyltransferase (LPLAT) activity with a preference for polyunsaturated acyl-CoAs as donors (61-63,81,91), suggesting a dual role in glycerolipid synthesis and phospholipid remodeling. The *sn*-1 position of phospholipids usually contains a saturated or monounsaturated acyl chain, while polyunsaturated acyl-CoAs are esterified at the *sn*-2 position, giving rise to different combinations of acyl chains depending on the phospholipid species (86,92). This highly diverse and asymmetrical distribution of acyl chains is maintained in part by the Lands cycle, in which the *sn*-2 acyl moiety undergoes rapid remodeling by concerted actions of phospholipase A_2 (PLA_2) and LPLATs.

AGPAT9 and AGPAT11 are PC remodeling enzymes known as lyso-PC acyltransferase (LPCAT)1 and 2, respectively. In mice, high levels of *Lpcat1* mRNA

were found in the lung, particularly in alveolar type II cells, (93), and reduced di-palmitoyl-PC levels were observed in the lungs of *Lpcat1*-deficient mice (94). Pulmonary surfactant isolated from LPCAT1 gene-trapped mice failed to reduce surface tension to wild-type levels (95), suggesting that LPCAT1 is required to maintain di-saturated PC levels that are essential for surfactant activity. LPCAT2 catalyzes both platelet-activating factor and PC synthesis in inflammatory cells (96,97). Under resting conditions, the enzyme preferred arachidonoyl-CoA acyltransferase activity to produce membrane lipids.

Recently, LPCAT3 and LPCAT4 were identified in the membrane bound *O*-acyltransferase (MBOAT) family, which possesses acyltransferase activity towards various substrates (98). LPCAT3 is ubiquitously expressed and is the most abundant LPCAT isoform in the liver and small intestine. LPCAT3-mediated incorporation of arachidonic acid at the *sn*-2 position of lyso-PC is essential for neonatal survival and intestinal and hepatic TG-rich lipoprotein production and secretion (99,100). LPCAT4 is highly expressed in epididymis, brain, testis and ovary (101). Interestingly, increased LPCAT4 expression and a high PC to lyso-PC ratio have been identified as a potential biomarker for colorectal cancer (102). However, normal cellular and physiological functions of LPCAT4 is unknown.

1.3.4 Phosphatidic Acid Phosphatases (LIPINs)

The PA synthesized by AGPAT has two fates: dephosphorylation by PA phosphatases (PAPs) called LIPINs to form DG for the synthesis of TG and zwitterionic phospholipids (PC, PE and PS) (103) or conversion to CDP-DG, a substrate for synthesis

of anionic phospholipids (PI, PG and CL) (**Fig. 1.2**). In mammals, PAP enzymes are encoded by three genes (LIPIN-1, LIPIN-2 and LIPIN-3) that have tissue-specific roles in glycerolipid synthesis (68,104). Mammalian LIPINs use PA as a substrate and are inactive toward other lipid phosphate substrates, such as lyso-PA, sphingosine phosphate and ceramide-1-phosphate (68). Murine and human *Lipin-1* mRNA undergoes alternative splicing to generate LIPIN-1α and LIPIN-1β isoforms, which exhibit differences in expression, subcellular localization and cellular function (105). LIPIN-1 is highly expressed in adipose tissue and skeletal muscle and, to a lesser extent, in liver (68). LIPIN-1 deficiency in fatty liver dystrophy mice results in impaired adipose tissue development due to failure to store TG (106,107). In humans, mutations in LIPIN-1 cause acute rhabdomyolysis, but with no evidence of lipodystrophy (108). The discrepancy in adipose tissue-specific phenotypes between species could result from differential compensation by LIPIN-2 or LIPIN-3 in humans (70). The role of LIPIN-2 and LIPIN-3 in the G3P pathway have been studied in tissues with minimal LIPIN-1 expression. For example, PA accumulation was observed in the cerebellum of *Lipin-2* deficient mice, but other phospholipids were unaffected (109).

Two highly conserved regions are important for PAP activity: the C-terminal PAP catalytic motif (DXDXT) (110), and the N-terminal polybasic motif, which is involved in the binding of LIPINs to the negatively charged phospho-monoester head group of PA and nuclear/cytoplasmic shuttling and binding. In addition to PAP activity, LIPIN-1 and LIPIN-2 possess a nuclear localization signal (NLS) and regulate lipid metabolism by interacting with nuclear receptors and transcription factors. They contain a transcriptional co-activator motif that interacts with peroxisome proliferator-activated

receptor (PPAR)γ coactivator-1α (PGC-1α) and PPARα/γ to maintain fatty acid homeostasis by regulating fatty acid flux into oxidation or storage pathways during adipogenesis (111).

1.3.5 Diacylglycerol Acyltransferases

Similar to PA, the DG synthesized by LIPINs can be utilized for the synthesis of phospholipids (PE and PC) or is acylated by DGATs to form TG (112) (**Fig. 1.2**), which is subsequently packed into LDs or incorporated into lipoproteins for secretion (113). Mammalian DGAT1 and DGAT2 are expressed in tissues that have high rates of TG synthesis such as adipose tissue, liver, small intestine, mammary gland, heart and skeletal muscle (71,73).

DGAT1 and DGAT2 contain multiple transmembrane domains and an N-terminus exposed to the cytosol (72,114). The C-termini of DGAT1 and DGAT2, where substrate binding is predicted to occur, face the luminal and cytosolic side of the ER, respectively, suggesting that membrane topology may dictate the site of TG synthesis. Indeed, early studies showed that DGAT activity in liver microsome preparations had cytosolic (overt) and luminal (latent) activities that were involved in TG synthesis for storage in LDs or secretion in very low-density lipoproteins (VLDL), respectively (115). DGAT1-overexpressing mice had 1.6-fold increase in serum VLDL-TG concentrations and enlarged VLDL particle size, which resulted in increased gonadal fat mass weight likely due to increased free fatty acid transport from the liver to adipose tissue (116). In contrast, mice overexpressing hepatic DGAT2 had increased cellular TG but did not increase VLDL secretion or fat mass. These data indicate a differential contribution of DGAT isoforms to

TG storage and secretion. However, a recent study using specific inhibitors of DGAT1 and DGAT2 showed that both isoforms contributed equally to total TG synthesis in hepatocytes, and that TG synthesized by DGAT2 was assembled and secreted in VLDL (117). This could be possible if TG destined for secretion is in equilibrium with a cytoplasmic pool through a hydrolysis and re-esterification pathway in the ER lumen (117,118). Interestingly, TG synthesized by DGAT1 was stored in small LDs and was a preferred source of fatty acids for oxidation, whereas TG synthesized by DGAT2 was stored in large LDs that were used to supply TG for VLDL assembly and secretion (117). In support, DGAT2, but not DGAT1, translocates from the ER to expanding LDs in cultured cells upon exogenous fatty acid loading (40,41). Acyl-CoA synthetase (ACSL)1, ACSL3 and one isoenzyme in each step of the G3P pathway also associate with LDs (40,41,66,67) and could produce TG for storage or secretion.

1.3.6 Targeting Glycerol-3-Phosphate Pathway Enzymes to LDs

GPATs, AGPATs and DGATs are predicted integral membrane proteins and it is not clear how they interact with the phospholipid monolayer of LDs. Membrane topology predictions suggest the *Drosophila* isoenzymes of the G3P pathway that remain in the ER during oleate loading have membrane-spanning helices in the N-terminus that are connected by large hydrophilic loops (40). In contrast, GPAT4 contains two hydrophobic helices that are separated by a short loop of relatively hydrophobic residues, forming a hairpin structure embedded in the monolayer. When this hairpin was replaced with the sequence from ER-localized AGPAT1, GPAT4 failed to relocalize to LDs and remained in the ER, indicating that the hairpin structure in GPAT4 is critical for

translocation from the ER to LDs during oleate loading (40). Thus, the hairpin in GPAT4 does not span the ER membrane bilayer, allowing it to associate with both the ER and the phospholipid monolayer of LDs via ER-LD membrane bridges. *Drosophila* AGPAT3 and DGAT2 (40) and mammalian DGAT2 (119) also contain similar hydrophobic domains with hairpin structure. Moreover, caveolin, a protein that regulates cellular cholesterol homeostasis and localizes to LDs, also contains an intramembrane hairpin that mediates LD targeting (120,121). Thus, hydrophobic hairpins in the proteins that migrate from the ER to LDs might be common LD-targeting motifs. In addition, DGAT2 contains a C-terminal amphipathic α-helix that facilitates interaction with the surface of the LDs during TG synthesis (74).

Unlike these enzymes, LIPINs are cytosolic enzymes that are activated by transient association with membranes enriched in PA (65,110,122), as is the case with LDs upon exogenous fatty acid loading (66,67,123). Alternately, because ER-LD membrane bridges form during initial LD formation and expansion, PA-bound LIPIN-1 on the ER membrane may laterally diffuse onto the surface of LDs. Initial LD formation and expansion, and ER-LD membrane bridges are discussed in Section *1.5.1* and *1.5.2*.

1.3.7 Substrate Channeling in the Glycerol-3-Phosphate Pathway by Enzyme Complexes

In addition to localization of G3P enzymes to LDs, evidence that G3P pathway enzymes form protein complexes in close vicinity to or on the surface of LDs indicate concerted substrate channeling during LD biogenesis. A well-known example is complexes involving seipin, an evolutionary conserved ER membrane protein enriched at

LD formation sites (discussed in Section *1.5.2*) that regulates LIPIN-1 association with the ER (124) and facilitates lipid import into the LDs (125-127). Seipin deficiency is implicated in CGL and impaired LD formation (7,126), possibly due to diminished LIPIN-1 association with the ER and increased PA accumulation (124). Recently, seipin was also co-localized with AGPAT2 and LIPIN-1 at the ER (128), suggesting this multi-protein complex is involved in PA channeling for glycerolipid synthesis at sites of LD formation. Why LIPIN-1 specifically interacts with AGPAT2, but not other isoforms, is unclear. Since AGPAT2 is critical for TG synthesis and other isoforms cannot compensate for its loss (59,60,89), it is possible that LIPIN-1 preferentially binds to AGPAT2-derived PA to efficiently catalyze the conversion into DG during LD biogenesis. In support of this, knockdown of AGPAT2 in cultured adipocytes reduced TG synthesis and increased lyso-PA channeling into PI (59). The reduced conversion of lyso-PA to PA by AGPAT2 could possibly redirect lyso-PA available to other AGPAT isoforms to form a PA pool that is not recognized by LIPIN-1 and preferentially used for PI synthesis. In addition, a recent study showed that mammalian and yeast seipin interact with GPATs (129), indicating other seipin-enzyme complexes may potentiate TG biosynthetic capacity. However, these findings require further investigation since the seipin-interaction results were based on overexpressed proteins.

Several lines of evidence suggest that enzyme complexes containing DGAT2 at the ER and LDs are also involved in substrate channeling. An initial study identified a detergent-solubilized 'TG synthetase' complex composed of DGAT, MGAT, acyl-CoA acyltransferase (ACAT) and ACSL activities from rat intestine (130). DGAT2 association with stearoyl-CoA desaturase-1 (SCD1) was found in the mitochondrial-

associated membranes (MAMs) (131), an ER-organelle contact site that is enriched in enzymes that synthesize TG and phospholipids (132). Furthermore, DGAT2 interacts with MGAT2 in MAMs and LDs (133) and with the fatty acid transport protein (FATP)1 in the ER and LDs (134) to channel fatty acids into TG. Collectively, the association of G3P pathway enzymes with LDs suggest that protein complexes are responsible for substrate channeling in the G3P pathway.

1.4 Enzymes of the CDP-Choline Pathway

1.4.1 Phosphatidylcholine Synthesis

Mammalian cells synthesize PC by successive methylation of the amino head group of PE by *N*-methyltransferase (PEMT) or *de novo* by the CDP-choline pathway (135) (**Fig. 1.3**). Although the PEMT and CDP-choline pathways both produce PC, they have non-overlapping functions in TG metabolism and secretion (discussed in section *1.5.5*). PEMT expression and activity is very low in most tissues (135), and is only quantitatively significant in hepatocytes and differentiated adipocytes (136,137). The CDP-choline pathway begins with uptake of exogenous choline followed by three enzymatic reactions that convert choline to PC (138). This pathway is the focus of this thesis because it is the only route for *de novo* synthesis in all tissues (139).

1.4.2 Choline Transporters

Choline is essential for PC synthesis by the CDP-choline pathway (140), and is also required for the production of other physiologically important molecules such as betaine, an osmolyte that the kidney utilizes to control osmotic pressure (141).

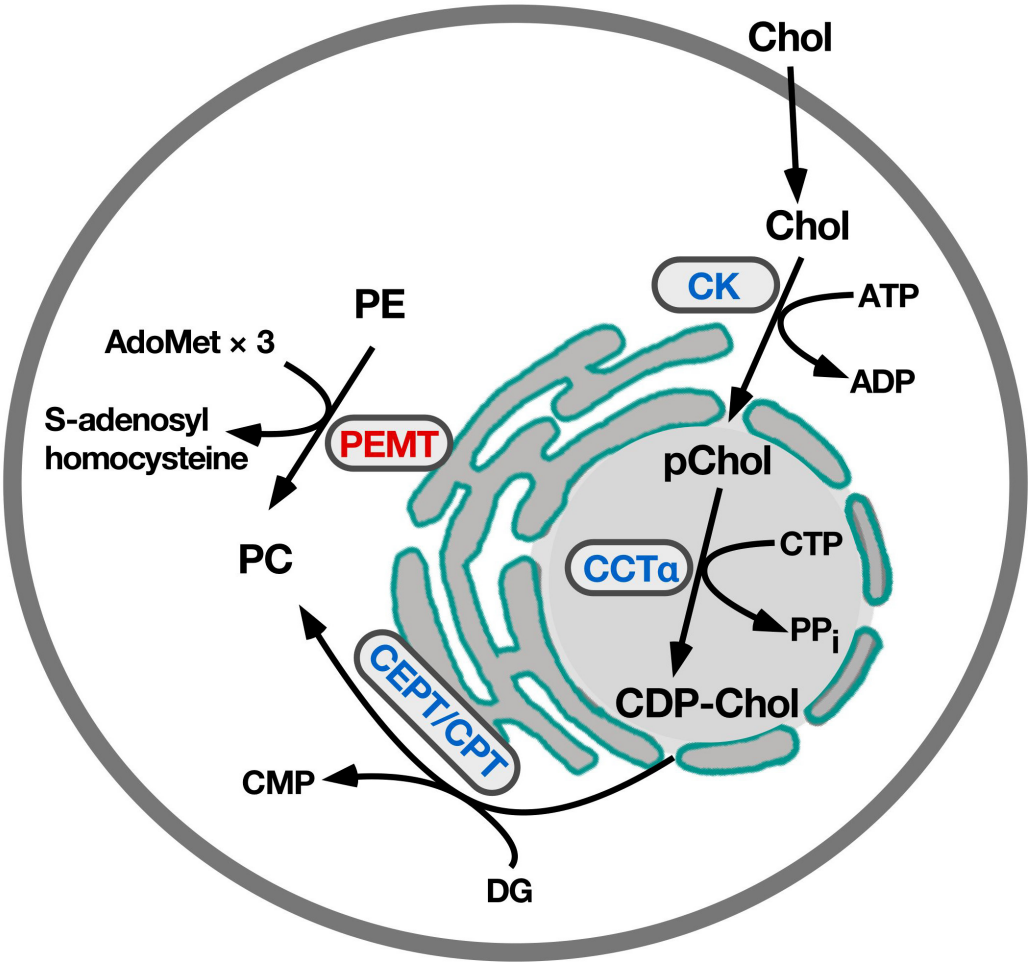

Figure 1.3. PC synthesis by the PEMT and CDP-choline pathways. Schematic of the PEMT and CDP-choline pathways showing intermediates and enzymes with their localization in the cell. PEMT is indicated in red and the CDP-choline enzymes indicated in blue.

Hepatocytes synthesize choline *de novo* via PE methylation (139); however, the majority of choline used for PC synthesis is from the diet and absorbed through facilitated transport (135,139). There are three types of choline transporters with different binding affinities. The low-affinity choline transporters are sodium-independent organic cation transporters (OCTs, SLC22 family) (140). OCTs are highly expressed in intestine, liver, kidney or brain (142-145), however, their physiological role in choline uptake is not clear. The high-affinity choline transporter (CHT1, SLC5A7) is sodium-dependent (8). CHT1 has a K_m of 1-2 μM and is highly expressed in neurons to maintain acetylcholine levels (146). The major choline transporters involved in PC synthesis are the sodium-independent choline transporter-like proteins (CTLs, SLC44 family) (140). CTLs are encoded by five genes, CTL1 to CTL5 (147). CTL1, which has intermediate-affinity for choline (K_m of 70 μM) (147-149), is expressed in most cells and believed to be responsible for choline uptake for PC synthesis. For example, glucocorticoid treatment of human alveolar A549 cells increased CTL1 mRNA expression and PC synthesis (150). Furthermore, an epidermal growth factor receptor antagonist inhibited CTL1 in rat ATII alveolar cells, resulting in compromised PC synthesis and lung surfactant production (151).

1.4.3 Choline Kinase

Choline kinase (CK) catalyzes the ATP-dependent phosphorylation of dietary or endogenous choline to make phosphocholine, the first committed step in the pathway (**Fig. 1.3**). (8). The micromolar affinity of CK for choline ensures rapid conversion to phosphocholine for channeling into PC synthesis. Mammals express three CK isoforms

(CKα1, CKα2 and CKβ) that are encoded by two genes (152). All isoforms are ubiquitously expressed, but significantly higher expression of CKα is found in the liver and testis while CKβ is highly expressed in the heart and liver (152-154). The active enzyme exists as a dimer consisting of subunits encoded by either genes; α/β heterodimers and α/α or β/β homodimers contribute to 60% and 40% of total CK activity, respectively (152).

Although CK does not catalyze the rate-limiting step of the CDP-choline pathway in most tissues, CK activity can be limiting or essential when its expression is reduced. Heterozygous knockout of CKα did not affect PC levels in mice, however homozygous deletion was embryonic lethal at day 3.5-7.5 (139,155). On the other hand, $CK\beta^{-/-}$ mice were viable but developed severe muscular dystrophy in the hind limb as well as bone deformities (156).

1.4.4 Choline/Ethanolamine Phosphotransferase

The final step of the CDP-choline pathway is catalyzed by choline phosphotransferase (CPT) and/or choline/ethanolamine phosphotransferase (CEPT), which share 60% amino acid sequence similarity (157-159). Despite the near identical sequence similarity in the catalytic domains, CPT only utilizes CDP-choline while CEPT recognizes either CDP-choline or CDP-ethanolamine for PC or PE synthesis, respectively (158,159). In this step, phosphocholine is transferred from CDP-choline to DG to generate PC. Both CPT and CEPT are ubiquitously expressed; however CPT is abundantly expressed in the testis and small intestine (159) and CEPT is highly expressed in the testis, colon, heart and spleen (160). CPT is localized to the Golgi apparatus, and

its localization is disrupted by brefeldin A (161). On the other hand, CEPT is primarily localized to the ER and nuclear membranes (157), making it the predominant enzyme of the two in PC synthesis since the rate-limiting enzyme CCT translocates to ER and nuclear membranes upon activation. CPT and CEPT are integral membrane proteins with seven transmembrane segments (158,159), and their enzymatic reaction involving DG and the water soluble CDP-alcohol is thought to occur at the hydrophobic-hydrophilic interface of membranes (8).

The expression level of CPT and CEPT does not influence PC synthesis under normal circumstances. For example, in CHO cells overexpressing CPT, PC biosynthesis was determined by CDP-choline and/or DG availability (162). Interestingly, increased CPT expression, activity and PC synthesis was observed in X-box binding protein 1 (XBP1)-transduced NIH3T3 cells (163). However, the increase in PC synthesis might have resulted from a 30% increased CCT activity and thus increased substrate CDP-choline availability.

1.4.5 CTP:Phosphocholine Cytidylyltransferase

The rate-limiting step of the CDP-choline pathway is catalyzed by CCTα and CCTβ encoded by the *Pcyt1a* and *Pcyt1b* genes, respectively (164). These enzymes catalyze the transfer of the CMP moiety from CTP to phosphocholine to form CDP-choline in a nucleophilic displacement reaction (165). Structural analysis of rat CCTs revealed a common domain structure (166). Both CCTα and CCTβ have highly conserved catalytic (C), membrane binding (M) and phosphorylation (P) domains (**Fig. 1.4)**. The two isoforms share high sequence similarity in the catalytic (C) and membrane

binding (M) domains (167). The main structural difference between the two isoforms is the presence of a 21 amino acid NLS at the N-terminus of CCTα, giving rise to nuclear localization via α-importin pathway (168,169). Alternate splicing produces three isoforms of CCTβ, which all localize to the cytoplasm due to the absence of the NLS (164,170). CCTβ1 lacks significant portion of the C-terminal domain and contains three potential phosphorylation sites of the sixteen present in CCTα (164), suggesting its activity may not be regulated by reversible phosphorylation (discussed in Section *1.4.4.4*). CCTβ2 has a unique N-terminal sequence (170,171). CCTβ3 is identical to CCTβ2, but its amino terminus is 28 amino acids shorter resulting from an alternate exon (171).

In mammals, CCTβ isoform expression is highest in the brain and gonadal tissue and is developmentally regulated (171). CCTβ2 mRNA expression, activity and PC synthesis were increased during differentiation of neuronal PC12 cells and Neuro2a cells. CCTα activity was unaffected suggesting that the β2 specifically contributes to membrane expansion during neuronal differentiation (172). Supporting this conclusion, suppressing CCTβ2 expression during PC12 cells and Neuro2a cell differentiation reduced cell division, growth and proliferation (173). Similarly, nerve growth factor increased CCTβ2 mRNA and protein levels, but not CCTα, in cultured mouse neurons, and the neuronal axons of CCTβ2-deficient had reduced PC synthesis and axon branching (174). Interestingly, loss of CCTβ2 did not influence fetal maturation or brain development but caused gonadal dysfunction and reduced fertility (175).

Gene disruption of the ubiquitously expressed CCTα in mice is embryonic lethal (176), indicating an essential role for PC and its products that cannot be compensated by

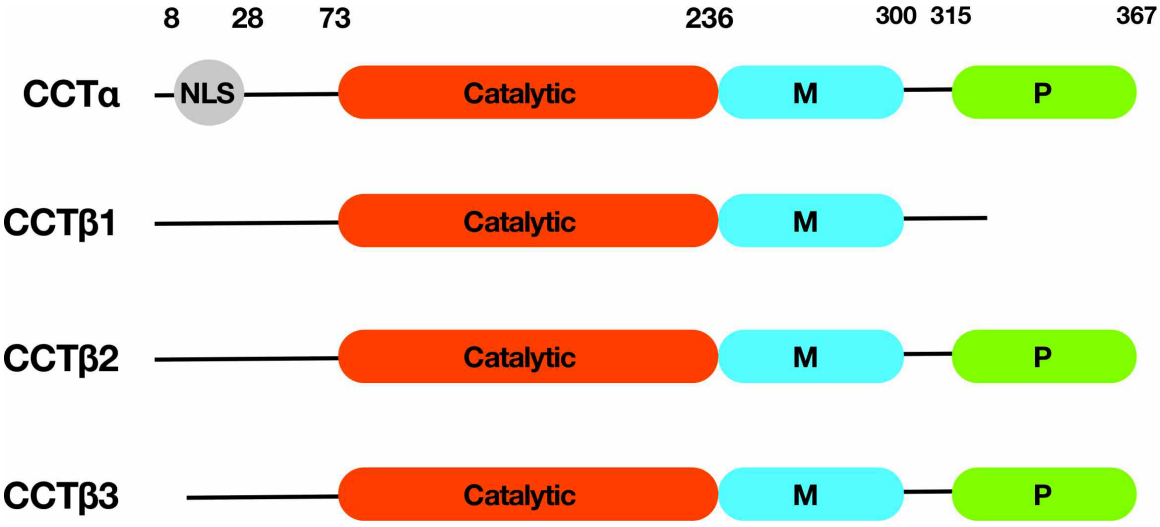

Figure 1.4. Domain structure of CCT isoforms. CCT isoforms have highly conserved catalytic (C), membrane binding (M) and phosphorylation (P) domains. The main difference between the two isoforms is the absence of the nuclear localization signal (NLS) in the β isoforms. CCTβ1 does not contain a significant portion of the C-terminal domain. The N-terminus of CCTβ3 is 28 amino acids shorter compared to other isoforms. The numbers at the top correspond to amino acid positions.

CCTβ during early development. Macrophage-specific CCTα knockout mice were viable but cells had a compensatory induction of CCTβ and were sensitized to cholesterol-induced cell death (177). CCTα is expressed at higher levels in the lung compared to other tissues (173), and is localized to cytoplasm (178), possibly to facilitate the increased PC synthesis required for the production and secretion of surfactant. In pulmonary epithelial type II cells, CCTα is cytoplasmic and synthesizes dipalmitoyl-PC for the production of lung surfactant (178). Lung-specific disruption of the CCTα gene did not affect *in utero* development but reduced dipalmitoyl-PC synthesis and caused respiratory failure at birth (179). Infection with *Pseudomonas aeruginosa* caused caspase cleavage and reduced CCTα mRNA levels, resulting in decreased PC synthesis and surfactant secretion and respiratory distress (179). Collectively, these data indicate a lung-specific function of CCTα related to surfactant production.

1.4.5.1 Nuclear Localization of CCTa

The N-terminal domain of CCTα contains NLS (amino acids 8 to 28) that is sufficient to promote nuclear import of reporter proteins, such as β-galactosidase in CHO cells (168). Within the NLS is a RKRRK sequence that when mutated prevented nuclear import of CCTα (168). The yeast homolog Pct1p also contains an NLS and is localized to the nucleus (180).

CCTα is localized to the nucleus in most primary and immortalized cells. However, CCTα is in the cytoplasm of cells with high PC demand for secretion or rapidly proliferating membranes, such as pulmonary epithelial cells (178) and differentiating B-cells (181) and adipocytes (2). In murine epithelial cells, CCTα was retained and

degraded in the cytoplasm when its interaction with α-importin was inhibited by mono-ubiquitination of a lysine residue adjacent to the NLS (182). Studies that monitored mammalian CCTα distribution indicated that the enzyme reversibly translocated to nuclear envelope (NE) and is exported to the cytoplasm in response lipid activators such as farnesol or oleate (2,30,183). Furthermore, the insect homolog CCT1 also cycled between the nucleus and cytoplasm in oleate-treated *Drosophila* S2 cells (12). Mutational analysis demonstrated that the membrane-binding domain M is required for nuclear export in response to farnesol or oleate (discussed in section *1.4.5.3*) (183). These data suggest that CCTα distribution between the nucleus and cytoplasm is regulated by the strength, duration and location of the lipid activation signal.

1.4.5.2 The Catalytic Domain

Domain C (aa 73-236) is conserved in other members of the cytidylyltransferase superfamily (184), between mammalian CCT homologues (185), and has 61% sequence similarity between the yeast and human enzymes (10). CCTα is a homodimer as determined by cross-linking experiments and the site of dimerization has been mapped to amino acids 139-145 (186). Crystal structure of rat CCTα suggests that the interface between the monomers is stabilized by the interactions between three helices in domain C (187).

The conserved catalytic motif in cytidylyltransferase superfamily (HXGH; aa 89-91) is required for CTP binding and transition state stabilization (188). Mutations of either histidine residue resulted in loss of CCTα activity. Another conserved motif that is important for catalytic activity is RTEGISTS (aa 196-203), where an R196K mutation

compromised CTP binding by 23-fold and the maximal velocity (V_{max}) by 3-fold (189). Mutation of K122, which recognizes the substrate phosphocholine, to alanine or arginine dramatically increased the K_m for phosphocholine (189). Finally, the temperature-sensitive CCTα in CHO MT-58 cells has an R140H mutation in domain C but has normal membrane binding activity and cellular localization, suggesting that catalytic activity does not affect domain M (190).

1.4.5.3 The Membrane Binding Domain

Domain M (aa 236-300) forms an amphipathic α-helix upon membrane binding (191) that has a polar face primarily composed of acidic amino acids, a non-polar face composed of hydrophobic residues and 15 basic amino acids at the membrane interface (192). A reporter protein composed of two copies of domain M fused to GFP was sufficient for nuclear membrane recognition and binding under activating conditions (183). CCTα activity is regulated by reversible membrane binding; it assumes an active, membrane-associated form and an inactive, soluble form. When CCTα associates with membranes, domain M undergoes a conformational change into an extended a-helix that embeds into the membrane surface, resulting in approximately 80-fold increase in catalytic activity (189). CCTα mutant lacking domain M was insensitive to lipid stimulation and constitutively active.

Domain M binding to membranes depends on the lipid composition and membrane curvature of membranes (189). The overall charge of domain M is weakly positive. However, upon folding into an α-helix, most of the basic residues are positioned at the interface between the polar and non-polar faces, making it electrically

positive and recognizable by membranes enriched in Type I lipids (anionic phospholipids and fatty acids) via ionic interactions (189,191,192). Additionally, the packing defects induced by Type II lipids (DG and PE) enhance CCTα-binding by creating hydrophobic insertion sites for the non-polar face of the helix. Insertion of domain M relieves the curvature stress through intercalation into the lipid bilayer (193). When a membrane contains both types of lipid activators, the ionic interactions and packing defects synergistically induce CCTα association and activity. For example, activation of CCTα in the presence of liposomes containing PE and oleic acid was greater than the sum of the activations resulting from the individual molecules (194). Accumulation of free fatty acids, such as oleic acid, exhibit both negative charge and packing strain, and can recruit CCTα for PC synthesis (195). Notably, PLC and PLA_2 generate DG and fatty acids, respectively, indicating that phospholipases can also influence CCTα binding through remodeling of membrane composition (196,197). Lastly, mutations in the lysine residues at the interface between the polar and non-polar face to glutamine eliminated nuclear export of CCTα in response to fatty acids, suggesting that domain M is also responsible for the nuclear/cytoplasmic distribution of CCTα (183). Collectively, the membrane-sensing properties of domain M is responsible for CCTα localization, translocation and catalytic activity.

1.4.5.4 The Phosphorylation Domain

CCTα activity is also regulated by reversible phosphorylation of the C-terminal phosphorylation domain (domain P, aa 315-367). Domain P is enriched in acidic residues and contains 12-16 serine, threonine and tyrosine phosphorylation sites depending on the

species (198). The precise kinases and phosphatases involved in domain P phosphorylation are not known, but consensus sequences and *in vitro* studies implicated casein kinase II (198,199), proline-directed kinases (200), PKC and mitogen-activated protein kinase (MAPK) (201).

CCTα phosphorylation shifts the membrane-binding equilibrium towards the inactive, soluble form. Inactive, soluble CCTα is heavily phosphorylated but underwent dephosphorylation upon translocation to membranes (198,199). Notably, CCTα was dephosphorylated during G1 phase of cell cycle, when demand for PC synthesis is increased. Increased phosphorylation was correlated with less activity during G_0 and M phases (202), suggesting that phosphorylation is inversely correlated with enzyme activity and PC synthesis. Furthermore, membrane localization of a constitutively dephosphorylated mutant (16 serine phosphorylation sites mutated to alanine) was increased 10-fold (198). In contrast, a phosphomimetic mutant with all serine residues in domain P mutated to glutamate could bind to membranes enriched in oleate, indicating that a strong lipid activation signal can overcome the inhibitory effects of domain P phosphorylation. Although the exact mechanism is not understood, it is conceivable that competition between the negatively charged phosphates on domain P and membrane anionic lipids may interfere with interaction of domain M resulting in the inhibition of CCTα membrane association. Overall, the consensus is that phosphorylation 'fine-tunes', rather than dictates, the translocation of CCTα to membranes.

1.4.5.5 Transcriptional Regulation of CCTα

While CCTα is primarily regulated post-transcriptionally by changes in membrane composition and phosphorylation status, regulation also occurs at the transcriptional level. For example, the binding of three transacting nuclear factors, Sp1, Sp2 and Sp3, to the promoter region of *Pcyt1a* has been implicated in CCTα expression (203). During S and G_1 phases of the cell cycle, phosphorylation of Sp1 by cAMP-dependent protein kinases and cdk2 upregulated CCTα expression and PC synthesis (204). siRNA-mediated knockdown of Sp1 decreased CCTα expression, indicating Sp1 as a positive regulator (205). Inhibition of histone deacetylase, which downregulates Sp1, also resulted in upregulation of CCTα expression (206). Increased phosphorylation of Sp3 by p42/44 MAPK upregulated the expression of CCTα in H-Ras transformed fibroblasts (207), which may be important for oncogenic H-Ras to increase PC synthesis.

Sterol response element binding proteins (SREBPs), transcription factors that activate many lipogenic genes including fatty acid synthase (FASN), GPATs and HMG-CoA reductase (208,209), also regulate CCTα transcription. Under conditions of low ER sterol content, SREBPs exit the ER in complex with SREBP cleavage-activating protein (SCAP), are cleaved by site 1 and 2 proteases at the Golgi apparatus and enter the nucleus for their transcription activating functions (210). *Pcyt1a* contains a sterol response element (SRE), but SREBP-mediated upregulation of CCTα mRNA expression is minor (211). Transcriptional induction of fatty acid synthesis by SREBP could indirectly post-transcriptionally activate CCTα (212).

1.5 Phosphatidylcholine and Triglyceride Storage and Secretion

1.5.1 Lipid Droplet Formation

Formation of LDs occurs in the ER when newly synthesized neutral lipids are deposited between the luminal and cytosolic leaflets of the ER (**Fig. 1.5**). As their concentration increases, TG and CE eventually coalesce to form a 'lens' or a 'blister' of at least 17 nm in diameter at the LD nucleation sites (213,214). The reason for this aggregation is not clear, but could be explained by simple biophysical properties. Individual neutral lipid molecules dispersed in the bilayer may condense to form an oil phase in order to minimize the energy costs for the interaction with phospholipids or proteins of the membrane (31).

Whether cells have preferential sites for LD nucleation and the determinants for such sites are unclear. In a uniform bilayer, TG molecules can freely diffuse and nucleation would occur at random sites (31). However, the ER is a complex structure with morphologically and biochemically distinct regions, suggesting that nucleation may favor specific sites. Protruding tips of the ER could be energetically favored sites because part of the energy required for membrane deformation during LD formation is already supplied by the highly-curved surface of the ER membrane. In addition, recent studies indicate that enzymes involved in TG synthesis localize to specialized subdomains of the ER. For example, ACSL3 is recruited to nucleation sites and is essential for TG storage (215). GPAT4 and DGAT2 accumulate in subdomains of the ER in close vicinity to nucleation sites (40,134). Indeed, there is increasing evidence that G3P pathway enzymes and other proteins form protein complexes at the ER and LDs that are responsible for efficient substrate partitioning for LD nucleation and expansion

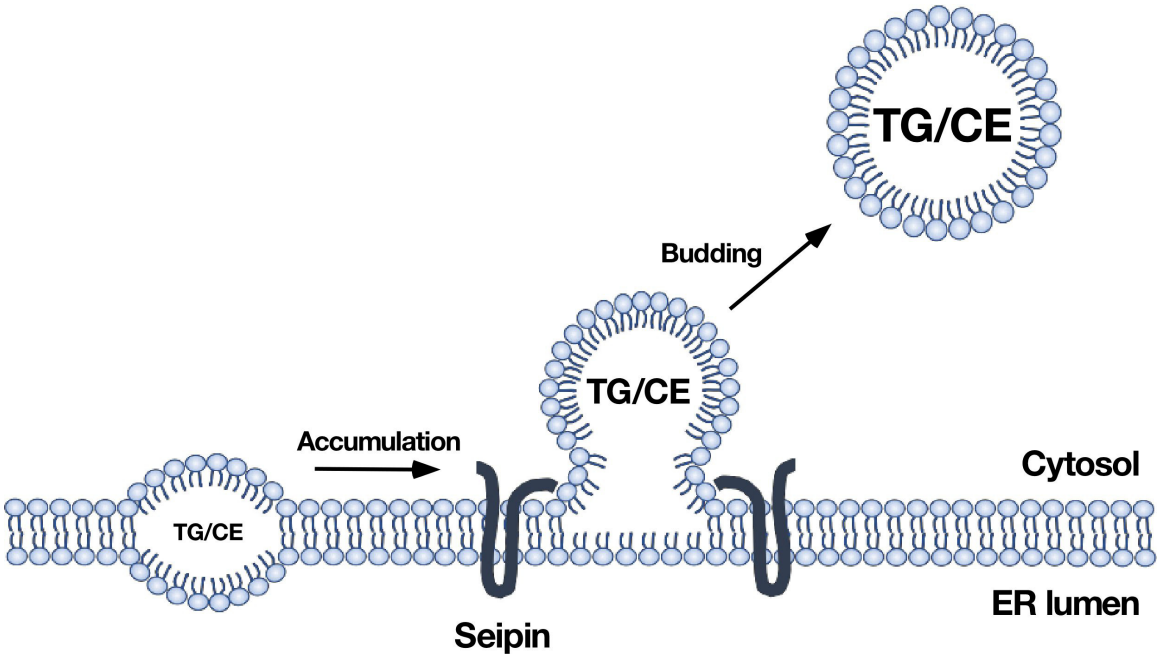

Figure 1.5. Formation of LDs in the ER membrane. Neutral lipids (TG and CE) synthesized in the ER membrane accumulate between the luminal and cytosolic leaflets. As the local concentration of neutral lipids increases, they coalesce and form a lens at the nucleation site. When sufficient amount of the lipids accumulates, the bilayer deforms and a nascent LD buds into the cytoplasm by taking phospholipids from the cytosolic leaflet of the ER. The nascent LDs may remain connected with the ER via seipin-stabilized ER-LD membrane bridge or separate completely.

(discussed in Section *1.3.7*). Taken together, these data indicate that the complex morphology and biochemical composition heterogeneities of the ER may play an important role in determining TG accumulation and LD nucleation sites.

Sufficient accumulation of neutral lipids results in the budding of LDs from the ER into the cytoplasm, forming a nascent LD composed of the cytosolic monolayer of the ER. Defining the limit of budding size at which LDs detach from the ER is challenging with current microscopy techniques due to temporal and spatial resolution limits. Furthermore, it is unclear whether budding occurs for all LDs or some remain connected with the ER via a membrane bridge. In yeast, a substantial fraction of newly formed LDs appear to remain connected with the ER (216). In mammalian cells, at least some LDs are completely separated from the ER (40).

Whether LD budding is protein-mediated is not clear since no single protein has been identified and the step is proposed to occur spontaneously when sufficient TG accumulates and adequate phospholipids are available to lower surface tension (31). However, the size and protein compositional heterogeneities of LDs may result from processes facilitated by proteins (213). A candidate for such a function is seipin, an evolutionary conserved ER membrane protein enriched at LD formation sites (**Fig. 1.5**) (7,126). Biochemical studies showed that seipin deficiency results in dramatically aberrant LD morphology due to reduced incorporation of lipids and proteins into the nascent LDs. In yeast and mammalian cells, seipin mutations lead to abnormal ER-LD membrane bridges, suggesting that seipin stabilizes the membrane bridges during LD budding (7,126). Alternately, seipin may form protein complexes with TG synthetic

enzymes to facilitate the initial growth of nascent LDs and their conversion to larger initial LDs (Section *1.3.7*).

1.5.2 Lipid Droplet Expansion

After budding, a subset of the newly formed LDs can expand by two general mechanisms: local synthesis of TG at the surface of LDs or the generation of a large LDs from two smaller LDs by ripening (diffusion-mediated transfer of core lipids) or fusion (coalescence) (31). For local TG synthesis at the surface of LDs, the enzymes necessary for TG synthesis must be recruited to LDs from the ER. Recently, Wilfling et al. found that at least one isoenzyme for each steps of the G3P pathway (GPAT4, AGPAT3 and DGAT2) relocalize from the ER to the surface of LDs upon oleate treatment of cultured cells (40). This protein targeting to LDs can occur via ER-LD membrane bridges established by the action of Arf/COP-I machinery (217), indicating that the detachment of LDs from the ER is reversible. A current model is that Arf/COP-I machinery on the surface of LDs promotes the budding of very small droplets which depletes phospholipids from the monolayer of the existing 'mother' droplet (218). The phospholipid depletion results in increased surface tension and promotes LD fusion to the ER membrane. Once ER-LD membrane bridges are established, specific isoforms of the G3P pathway enzymes rapidly migrate to LDs for expansion. In addition, because lipids can undergo lateral diffusion in membranes and transfer at contact sites between organelles, it is also possible that the newly synthesized TG molecules in the ER may diffuse through the bridge to the expanding LDs by a mechanism similar to initial LD formation. During the initial budding, nascent LDs may acquire TG synthetic enzymes along with

phospholipids from the cytoplasmic leaflet of the ER membrane. However, this is unlikely since these enzymes fail to target LDs and LDs do not expand without functional Arf/COP-I machinery (219,220).

LD expansion in adipocytes is mediated by ripening that involves fusion of two individual LDs (31,221,222). During this process, the cell death-inducing DEFA-like effector (CIDE) family of proteins localizes to contact zones between two LDs and dimerizes to facilitate the transfer of lipid molecules from smaller LDs to larger LDs (31). As a result, depletion of CIDE proteins or disruption of dimerization increases small LDs, whereas overexpression causes accumulation of large LDs (222-224). Recently, perilipin 1 (Plin1), a key adipocyte-specific LD-associated protein that regulates lipolysis, was identified as an activator of CIDE protein (224,225). Plin1 interacts with the CIDE at the contact sites between droplets and its overexpression markedly increases lipid transfer and LD growth, possibly by modulating CIDE dimerization. It is unclear whether CIDE proteins promote similar LD growth in cell types other than adipocytes. CIDE-B is found in the liver and has been implicated in TG secretion (226), suggesting its possible involvement in LD growth prior to VLDL secretion.

LD growth by fusion of smaller LDs to form large LD is rare under normal circumstances, but can be induced by the monolayer phospholipid composition. A prominent example is the fusion of PC-deficient LDs. Our lab and others have shown that conditions that result in PC deficiency lead to LD fusion in yeast and mammalian cells (2,12,30). During PC deficiency, LD monolayers become enriched in PE, which induces negative membrane curvature due to its conical shape arising from the small polar head group (19). This increases surface tension in the monolayers, and LDs come

in close proximity and fuse to decrease the surface tension (31). Thus, the surface phospholipid composition of LDs is important for interaction with other LDs and size regulation.

1.5.3 Lipid Droplet Catabolism

During times of energy scarcity, lipolysis mediates the sequential hydrolysis of TG stored within LDs to glycerol and free fatty acids (227). Adipose TG lipase (ATGL) catalyzes the first step of lipolysis by hydrolyzing an ester bond in TG to generate DG and fatty acid (227,228). *Atgl*$^{-/-}$ mice accumulated excess TG in most tissues and developed cardiac dysfunction which led to premature death (228). In addition, liver-specific ablation of ATGL promoted steatosis (229,230), whereas overexpression in the liver of obese mice reduced TG levels and alleviated steatosis (231,232). ATGL activity is regulated by interaction with co-activator LD-associated protein called comparative gene identification-58 (CGI-58) (233). Interestingly, mutations of human CGI-58 were identified as a cause of Chanarin-Dorfman Syndrome (CDS), which is characterized by increased TG deposition in most tissues (234). In cultured cells, mutant forms of CGI-58 associated with CDS were not recruited to LDs (235) and failed to activate ATGL (236).

Hormone-sensitive lipase (HSL) is a cytosolic enzyme that is activated and translocated to the LDs upon cAMP-induced phosphorylation by protein kinase A (PKA), which also phosphorylates and dissociates perilipin from LDs for HSL docking (227). HSL was initially believed to be the rate-limiting enzyme for the first step of lipolysis (227). However, *Hsl*$^{-/-}$ mice were not obese but accumulated DG in adipose tissue and non-adipose tissues (237), and ATGL exhibited higher affinity for TG than HSL (227-

230,232), indicating that HSL primarily catalyzes the second step of TG hydrolysis. Whether HSL deficiency is associated with human disease is not clear. However, a recent clinical study identified a 19-bp frameshift deletion in exon 9 of HSL-encoding gene *LIPE* that was associated with diabetes, hepatic steatosis and insulin resistance (238).

In the final step of lipolysis, MG is hydrolyzed to glycerol and fatty acid by MG lipase (MGL) (227). *Mgl*-deficient mice had massive MG accumulation in most tissues. These mice were either leaner or of similar body weight with improved glucose tolerance and insulin sensitivity, potentially due to blunted intestinal TG secretion (239,240). However, unlike ATGL and HSL, little is known about the regulation of MGL activity (227).

In addition to lipolysis, cells break down TG stored in LDs by lysosomal degradation pathway of macroautophagy through a process called lipophagy (232). Lipophagy was initially described in cultured hepatocytes in response to fatty acid exposure (241). Pharmacological or genetic inhibition of autophagy in rat hepatocytes increased TG content and LD size and number, resulting in diminished free fatty acid supply for β-oxidation. Since these findings of autophagy-mediated lipid mobilization, subsequent studies reported the presence of lipophagy in diverse cell types, including neurons (242), brown adipocytes (243), macrophages (244) and enterocytes (245). A current model of LD degradation through lipophagy proposes that the autophagosomal protein microtubule-associated protein light chain 3 (LC3) conjugates with PE on the surface of LDs and initiates the formation of limiting membrane of autophagosome to sequester LDs (241). LD-sequestering autophagosome then fuses with lysosome to form

autolysosome in which the contents of autophagosome and lysosomal acid lipase (LAL) are mixed for degradation and release of fatty acids into the cytoplasm.

Since lipolysis and lipophagy share functional similarities, an important question is what are the relative contributions of these distinct pathways to LD catabolism. ATGL possesses LC3-interacting motifs that block ATGL-mediated lipolysis when mutated (243), suggesting an interplay between ATGL-mediated lipolysis and autophagy. Interestingly, recent studies showed that ATGL acts as an important upstream to regulate lipophagy via SIRT1/PGC-1α/PPAR signaling pathway (232,246), and ATGL or lysosomal inhibition resulted in accumulation of large or small LDs in hepatocytes, respectively (247). Consistently, ATGL was enriched in large LDs while lipophagic vesicles were restricted to small LDs (247). These findings provide a novel insight into the coordination of lipolysis and lipophagy in TG metabolism.

1.5.4 Function and Structure of Chylomicrons

Instead of budding into the cytoplasm, LDs can also bud into the ER lumen to form the precursors for assembly of TG-rich lipoprotein VLDL and chylomicrons (**Fig. 1.6**). TG and CE are water-insoluble and must be assembled into lipoproteins in order to be transported in the bloodstream to different tissues (248). Lipoproteins are similar to LDs in their structure, consisting of a hydrophobic core surrounded by an outer monolayer of phospholipids, cholesterol and proteins. The surface of lipoproteins also has associated apolipoproteins that stabilize the lipoprotein and direct uptake and clearance by interacting with specific lipoprotein receptors and lipid transport proteins (248,249). For example, apolipoprotein apoB-100 is a ligand for the LDL receptor (249).

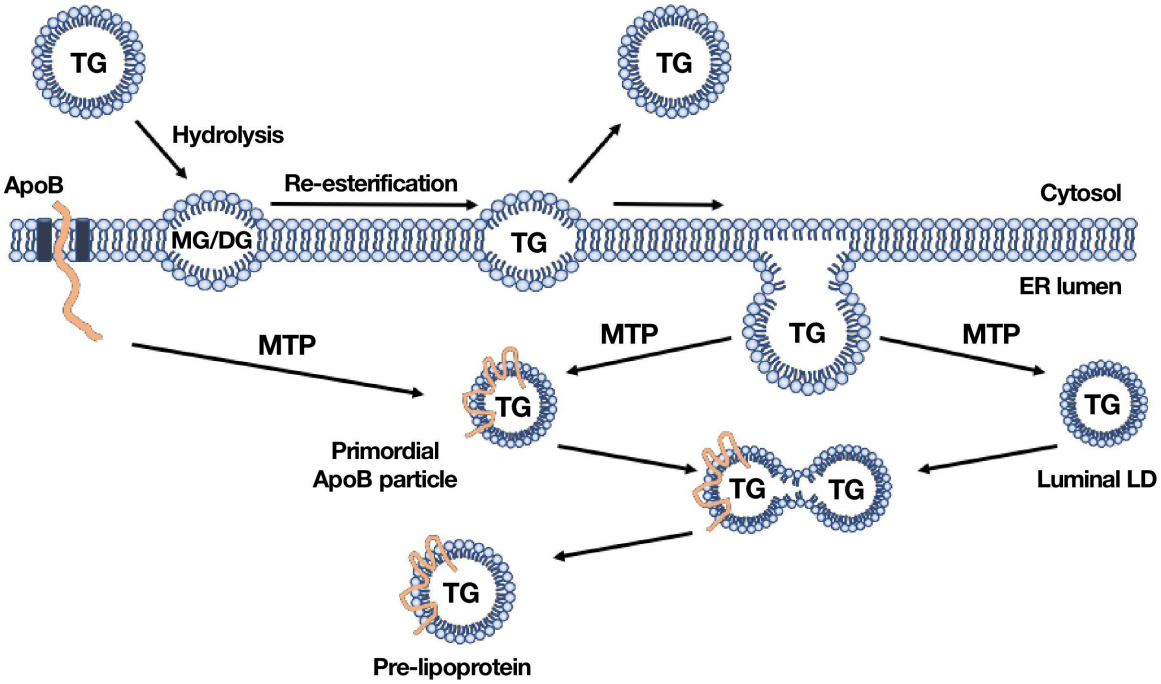

Figure 1.6. TG-rich lipoprotein assembly. TG stored in LD in the cytoplasm is hydrolyzed to MG and DG, which are re-esterified to form TG in the ER. TG is then destined for storage in LD in the cytoplasm or for chylomicron assembly in the ER lumen. MTP mediates bulk lipidation of apoB polypeptide to form primordial apoB particle which is further lipidated by MTP-independent fusion with apoB-free luminal LD to form pre-lipoprotein.

Finally, apolipoproteins also serve as activators or inhibitors of enzymes that metabolize lipoprotein lipids (250).

Lipoproteins are generally divided into five classes based on size, lipid composition and apolipoproteins: chylomicrons, VLDL, intermediate-density lipoprotein (IDL), LDL and HDL. Chylomicrons are TG-rich low-density ($d<0.95$ g/mL) particles produced by the intestine (251). The neutral lipid core is predominantly composed of TG and the particle size varies (diameters 75-1200 nm) depending on the amount of ingested fat. A high-fat diet leads to the formation of large TG-rich particles while fasting produces small particles (248). Chylomicrons contain apolipoproteins A-I, A-II, A-IV, A-V, B-48, C-II, C-III and E. ApoB-48 is the major structural component and its synthesis and lipidation are essential for the assembly, secretion and subsequent metabolism of chylomicrons (discussed in Section *1.5.5*). ApoA-IV, which is incorporated into chylomicrons at an early stage in the ER, has also been implicated in TG secretion *in vitro* (252). ApoA-IV overexpression (253) or knockout (254) *in vivo*, however, did not affect fat absorption or chylomicron production. In the circulation, lipoprotein lipase hydrolyzes chylomicron TG, releasing free fatty acids that are taken up by adipose, cardiac and skeletal muscle tissues (251,255). When a large amount of TG has been hydrolyzed, phospholipids are rapidly transferred to HDL (256), and the chylomicron becomes enriched in ApoE, forming remnants (diameters 30-80 nm) that are subsequently taken up by hepatic LDL receptor-related protein (255).

1.5.5 Chylomicron Formation and Secretion

TG-rich lipoprotein formation begins with hydrolysis of neutral lipids stored in LDs, mobilization of fatty acids to the ER, and re-synthesis of TG and CE at the ER (257,258) (**Fig. 1.6**). The enzymes and co-activator involved in mobilization of fatty acids from LDs are present in enterocytes, and their mRNA levels are increased in response to dietary fat challenge (259). Mice with intestine-specific knockout of ATGL had reduced TG hydrolase activity and increased TG storage in LDs (260). However, these mice had similar TG secretion with reduced mRNA levels of PPAR target genes compared to wild-type mice, suggesting that fatty acids released by ATGL were partitioned towards oxidation pathway. Similarly, intestine-specific knockout of HSL had no effect on TG secretion (261). Lipophagy is also active and regulates intestinal TG metabolism (245,262,263), however, whether it is a key player in TG secretion is not clear as genetic or pharmacological inhibition had no effect on chylomicron secretion (245,263). In contrast, intestinal CGI-58 deficiency led to massive TG storage in enterocytes of mice fed chow or high fat diet, resulting in reduced intestinal oxidation activity and plasma TG levels (264). Additionally, whole body knockout of MGL markedly reduced intestinal TG secretion in mice oral fat challenge (239). These suggest that CGI-58 and MGL could be involved in mobilization of fatty acids from LDs for TG secretion by the intestine.

Neutral lipids in the ER membrane can either be incorporated back into cLDs for storage or partition toward the ER lumen for lipoprotein assembly (118,265). Current model of chylomicron assembly proposes a two-step process: 1) co-translational lipidation of newly synthesized apoB-48 to form primordial particles and 2) bulk transfer

of core lipids from luminal LDs to the primordial apoB-48 particles to form pre-chylomicrons. The transport of neutral lipids into the ER lumen requires microsomal triglyceride transfer protein (MTP) activity, which catalyzes the transfer of TG, CEs and PC (266). MTP is expressed in the inner leaflet of the ER of the cells that synthesize and secrete apoB-containing lipoproteins. MTP physically interacts with the newly synthesized apoB to catalyze lipidation, resulting in the formation of small primordial apoB particles. These primordial apoB particles get further lipidated by fusion with apoB-free luminal LDs and form pre-chylomicrons. Of note, MTP activity has been shown to be crucial for the formation of luminal LDs that lack apoB (118).

Pre-chylomicrons synthesized in the ER are packaged in special transport vesicles termed pre-chylomicron transport vesicle (PCTV) and transported to the Golgi for further maturation (267). Transport of pre-chylomicrons in PCTV is mediated by the soluble NSF attachment protein receptor (SNARE) protein complex, which directs the vesicles to the *cis*-Golgi and facilitates the fusion with the Golgi membrane to release vesicle contents. Mature chylomicrons are released into the cytosol in a large vesicle by unknown mechanisms and transported to the basolateral membrane for secretion into the lamina propria by exocytosis (267).

1.5.6 The Requirement of Phospholipids for Lipid Droplet and Lipoprotein Assembly

As described in previous sections, TG and phospholipids are synthesized from shared precursors (PA and DG) which must be diverted into the competing pathways to optimize the balance between membrane biogenesis and energy storage. An important example is LD biogenesis and expansion, where the synthesis of TG and PC is

coordinated to maintain membrane stability and prevent particle coalescence. In the early stages of nascent LD formation, phospholipids are acquired from the cytosolic leaflet of the ER (2). However, the composition and molecular species of phospholipids in LDs are distinct from the bulk ER, and it is unclear how phospholipids are added to an expanding cytosolic LD. LDs do not exchange membrane phospholipids with cell membranes via vesicle transport (212,268). Interestingly, ER-mitochondria contact sites are enriched in phospholipid biosynthetic enzymes, including PEMT and PS synthases. Similarly, these enzymes may also be present at ER-LD contact sites and provide newly synthesized phospholipids to the expanding LDs. Alternately, ER phospholipids may laterally diffuse into the surface monolayer at the contact sites.

The most abundant phospholipids in mammalian LDs are PC (60%) and PE (25%) (2), and PC content is a key determinant of LD morphology and lipid storage capacity. To accommodate the increased need of PC on the surface of LDs during expansion, some PC biosynthetic and remodeling enzymes localize to the surface of expanding LDs. For example, ectopically expressed PEMT localizes to the surface of LDs during adipocyte differentiation to convert PE to PC (269). Knockdown of PEMT in 3T3-L1 preadipocytes was correlated with reduced LD formation and stability. LPCAT1 and 2 also localize to LDs in various cell lines where it could acylate lyso-PC (270).

PC synthesis is also an important regulator for luminal TG metabolism and lipoprotein assembly. Rats fed a choline-deficient diet for 3 days had TG accumulation in the liver and reduced plasma TG (271). Hepatocytes from these animals had reduced TG and apoB-100 containing VLDL when cultured in medium lacked both choline and methionine, and the secretion was rapidly stimulated upon the addition of either choline

or methionine to the culture medium. Subsequent studies using mouse models showed that attenuation of PC synthesis by PEMT knockout resulted in diminished secretion of apoB-100 containing VLDL and TG by the liver (272,273). Similarly, mice with a liver-specific knockout of CCTα had reduced plasma PC and TG levels (11). However, these mice had two-fold increased PEMT activity, suggesting that induction of PEMT was not sufficient to normalize hepatic VLDL secretion and/or PC synthesized by the CDP-choline pathway has non-redundant role in TG metabolism and secretion.

1.5.7 The Role of CCTα in Lipid Droplet Biogenesis and Lipoprotein Secretion

During LD biogenesis in mammalian cells exposed to excess fatty acids, CCTα is present in the nucleus, NE and cytoplasm (2). Our lab showed a strong induction of CCTα mRNA and protein expression, and translocation to the NE and cytoplasm during differentiation of 3T3-L1 cells, with a concurrent increase in PC synthesis that is required for normal LD biogenesis (2). In another study using a contrasting model of CCTα regulation, the *Drosophila* homologue CCT1 was exported from the nucleus to the surface of LDs when S2 cells were exposed to oleate (12). RNAi silencing of CCT1 reduced PC content of the LD monolayer and caused coalescence of small LDs, which was abolished by adding PC to the cells. As mentioned previously, the importance of CCTα for hepatic lipoprotein secretion has also been demonstrated in both cellular and animal models (11). Collectively, these data highlight that CCTα is an essential regulator of PC synthesis required for LD biogenesis and hepatic lipoprotein secretion.

The contribution of PC biosynthesis by the CDP-choline pathway to the regulation of intestinal TG storage and secretion has not been addressed and is a major

focus of this thesis. Disruption of the Lands pathway for PC acyl-chain remodeling by *Lpcat3*-knockout reduced the levels of arachidonyl-PC that is critical for chylomicron secretion and lipid absorption (100). Furthermore, rats fed a choline-deficient diet had reduced circulating and increased intestinal neutral lipids (274) and intestine-specific CCTα knockout mice had reduced plasma TG when fed a high-fat diet (275), suggesting that TG homeostasis in the intestine is also regulated by PC availability. Our results showing that CCTα and the CDP-choline pathway are required for intestinal TG storage in LDs and secretion in chylomicrons are presented in **Chapter 3**.

1.6 Lipid Synthesis and Storage in Nuclear Lipid Droplets

1.6.1 Nuclear Lipid Composition and Function

The presence of lipids in the nucleus was first demonstrated in 1958 by La Cour et al. (276). Subsequent studies showed that NE lipids account for only about 16% of nuclear mass (277,278). Phospholipids make up 62% of total nuclear lipid mass (279) and PC is the most abundant fraction (55%) (280,281). Lesser amounts of PE (23%), PI (8%) and PS (6%) were also detected. Cholesterol comprises approximately 10% of total nuclear lipids, and higher cholesterol content was detected in the outer nuclear membrane (ONM) compared with the INM (282). Interestingly, comparison with microsomes showed that the NE has more cholesterol per mg protein. Neutral lipids were also detected, but at lesser amounts than cholesterol (278,281).

Nuclear lipids are important components of the NE that is supported by the underlying nuclear lamina (277,278), but other lipid-specific functions or the presence of nuclear lipid metabolic pathways was thought to be of minor significance (283).

However, there is an increasing recognition that the nucleus contains important lipid metabolic activities. For example, PLC-mediated hydrolysis of PIP_2 produces inositol 1,4,5- IP_3 to regulate intranuclear Ca^{2+} levels (284), which is responsible for transcription of genes by a mechanism that is distinct from gene regulation by cytoplasmic Ca^{2+} signaling (285). The other PIP_2 hydrolysis product DG recruits PKC to the nucleus and regulates cell proliferation and differentiation (286,287).

1.6.2 Nuclear Lipid Droplet Composition and Function

Recently, nuclear TG and CE were shown to be organized in discrete compartments similar to cLDs. These nLDs are observed in many eukaryotic cells and liver sections (13,14,278,288,289). Because cLDs are formed at the ER membrane, which is contiguous with the outer NE, it was initially suggested that nLDs observed by confocal microcopy could be cLDs trapped within invaginations of the NE. However, subsequent studies using electron microcopy revealed that nLDs are on the INM, invaginations of the INM or are free in the nucleoplasm (14,289). As well, nLDs from rat liver have a very different lipid composition from cLDs (278). nLDs were composed of 19% TG, 39% CE, 27% cholesterol and 15% phospholipids, whereas cLDs contained 91% TG and 0.6% phospholipids. Consistently, nLDs from rat hepatocytes and HepG2 cells were smaller in size than cLDs, and comprise approximately 2-10% of total cellular LDs. Furthermore, nLDs are composed of 38% lipids and 62% protein while cLDs are composed of 78% lipids and 22% protein by weight.

Like their cytoplasmic counterparts, nLDs are dynamic organelles whose number and size increase or decrease following fatty acid treatment or removal, respectively (13).

Although nLDs contain relatively less lipids than cLDs, they may constitute a new subnuclear domain for neutral lipid storage that is involved in lipid homeostasis to protect the cells from lipotoxicity. As well, nLDs may serve as a buffer system capable of providing lipid components for signaling or synthesis. For example, fatty acids released by nLD lipolysis could interact with transcription factors, such as PPARs or hepatocyte nuclear factor (HNF)4α, to regulate cell proliferation (290,291). nLDs have lipid and protein composition different from cLDs, implying a novel nuclear-specific function (278). The cLD proteins Plin1 and ACAT1 were not identified in rat liver nucleus. Furthermore, in oleate-treated Huh7, PML-NBs and CCTα, which do not localize to cLDs in mammalian cells, were associated with nLDs (14) (discussed in Section *1.6.4*). Identification of other proteins that associate with nLDs could identify the cellular processes in which nLDs are involved as well as how they are formed.

1.6.3 Nuclear Lipid Droplet Formation at the Inner Nuclear Membrane

While detailed mechanisms for cLD formation in the ER membrane have been proposed (discussed in Section *1.4.2*), the mechanisms by which nLDs form and expand are unclear. The ER is contiguous with the ONM and INM and is punctuated by nuclear pores. In yeast, nLDs appear to form on the INM, possibly by localized TG and lipid synthesis (292). Given that lipids can undergo lateral diffusion within membranes, the INM could receive lipids from the ER for nLD synthesis (**Fig. 1.7A**). Recently, nLDs in hepatocytes were shown to originate from apoB-free ER luminal LDs, which are precursors for VLDL generated by MTP activity (288). It was proposed that continuous growth of the luminal LDs that are trapped in type I nucleoplasmic reticulum (NR) eventually rupture the membrane to release the nascent nLDs into the nucleoplasm (**Fig.**

1.7B). However, cells that do not express MTP or secrete TG also contain nLDs, suggesting that nLDs may form by an alternative pathway.

As proposed for yeast (292), nLDs could form on the INM of mammalian cells by local *de novo* TG and phospholipid synthesis. Indeed, enzymes for TG and phospholipid biosynthesis localize to the INM and nLDs, for example, ectopically expressed human AGPAT3 and AGPAT5 have been detected in the NE (61). The yeast Lipin1 homologue Pah1 has also been localize to the INM, and PA levels in the INM were increased in cells lacking *Pah1* (293). Ectopically expressed DGAT2 was localized to the surface of nLDs, and exogenous fluorescent-labeled fatty acid analog BODIPY558/568-C_{12} was incorporated into nLDs (14). Seipin, which has been implicated at the ER-cLD contact sites for substrate partitioning and membrane bridge stability, was detected in the INM and was required for the formation of proper membrane bridges between INM and nLDs in yeast (292). However, microsomal GPAT3 or GPAT4 have not been localized to the INM or nLDs.

Similar to cLDs, PC synthesis is expected to be required to make the surface monolayer of nLDs. GFP-tagged Pct1, the yeast ortholog of CCTα, resides on the INM in rapidly proliferating cells (293). With choline supplementation, Pct1-GFP was released from the INM into the nucleoplasm, suggesting that the enzyme senses INM packing defects caused by PC deficiency. In human hepatocytes, endogenous CCTα translocated to the surface of nLDs in response to oleate (14). A recent study using split-GFP reporter screen identified the yeast homologues of CPT and CEPT (Cpt1p and Ept1p) in the INM (294). Additionally, epitope-tagged CEPT expressed in CHO cells was localized to the NE (183) and co-localized with CCTα in the presence of exogenous

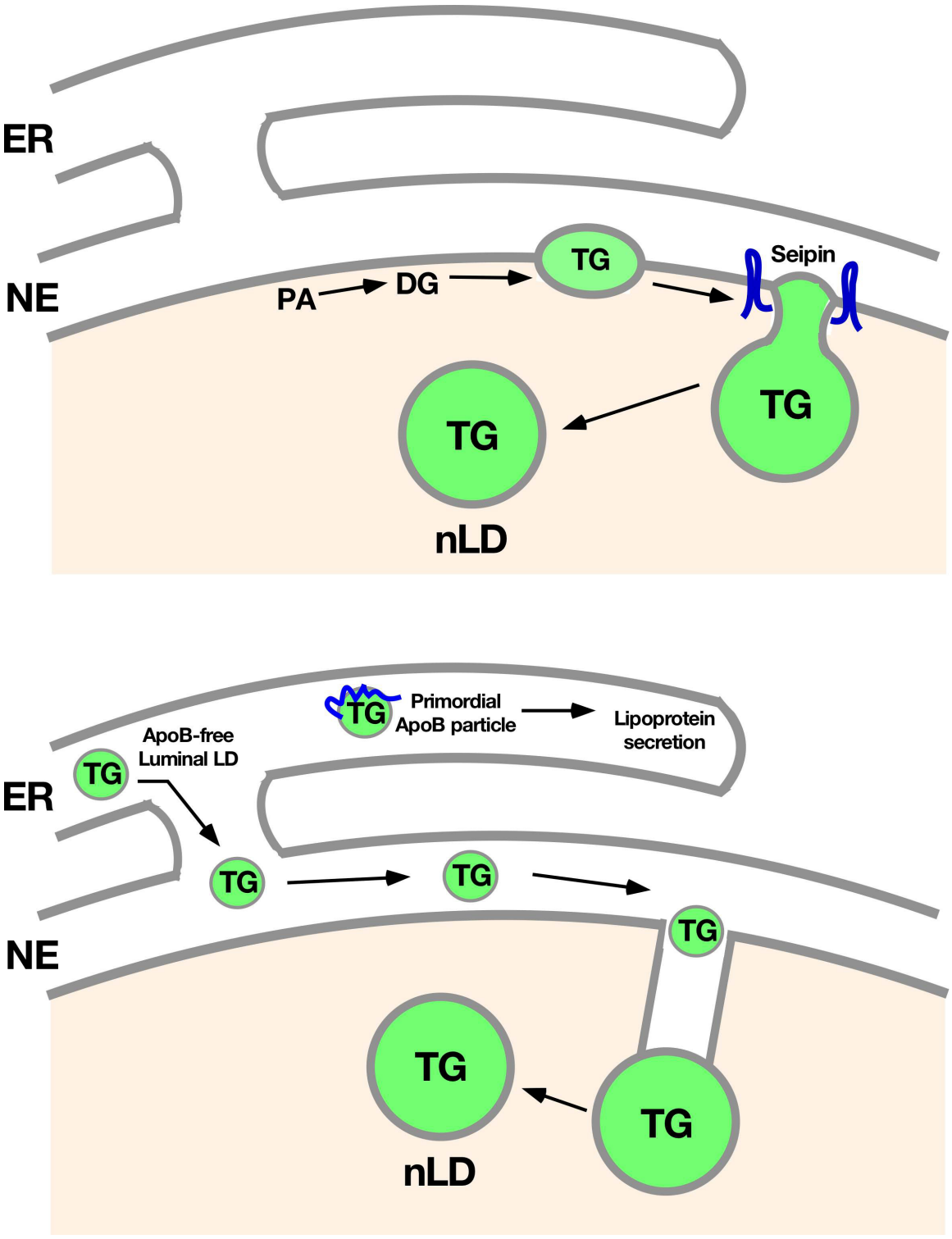

Figure 1.7. Formation of nLDs. In yeast or mammalian non-TG secreting cells, lipids in the ER can diffuse into the INM where nLDs form and bud into the nucleoplasm by seipin-dependent mechanism **(A)**. In hepatocytes, apoB-free ER luminal LDs migrate and grow in type I NR. These LDs relocate to the nucleoplasm by rupturing NR membrane **(B)**.

oleate (161). However, it is not clear whether CHO cells are capable of forming nLDs. Nevertheless, these data suggest that INM could be metabolically active for *de novo* lipid synthesis, and that nLDs may be formed in the INM by a mechanism similar to cLD biogenesis in the ER.

1.6.4 Promyelocytic Leukemia Nuclear Bodies, Nuclear Lipid Droplets and Lipid Homeostasis

PML is a tumor suppressor protein that was originally identified in acute promyelocytic leukemia due to a reciprocal chromosomal translocation between chromosomes 15 and 17 (295). The PML gene encodes 6 nuclear-localized splice variants (PML-I to -VI) that polymerize to form subnuclear structures known as PML-NBs (296). The polymerization of PML isoforms to PML-NBs requires sumoylation, which is enhanced under stress conditions (297). PML-NBs are present in most cell lines (298) and have been implicated in a wide variety of important cellular processes such as transcriptional regulation, apoptosis, DNA repair and the replication of viral and cellular DNA (299,300). Although PML-NBs have received much attention in the past decade, the mechanisms by which they contribute to various nuclear activities remain to be elucidated. To date, it has been estimated that PML-NBs functionally interact directly or indirectly with more than 160 proteins and physically interact with 120 proteins (297), and serve as sites for post-translational modifications (sumoylation, phosphorylation or ubiquitination) of sequestered proteins under stress conditions. For example, p53 is phosphorylated and acetylated by HIPK2 and CBP, respectively, in PML-NBs in response to DNA damage caused by ultraviolet radiation (301).

Several studies have indicated that PML plays important role in lipid homeostasis. PML deficiency in haematopoietic stem cell reduced PPAR signaling and fatty acid oxidation, resulting in impaired cell maintenance which was ameliorated by enhancing PPARδ activity (302). PML involvement in fatty acid oxidation was also shown in breast cancer cells where it unexpectedly inhibited anoikis by affecting PGC-1α acetylation and activating PPARδ signaling (303). In another study, knockdown of PML in mice infected with hepatitis B prevented lipolysis and accumulated saturated fatty acid, which resulted in obesity and steatosis (304)

Recently, Ohsaki et al. showed that nLDs associate with PML-NBs and CCTα in oleate-treated human hepatoma Huh7 cells (14). Knockdown of PML-II decreased nLDs whereas overexpression of PML-II, but not other isoforms, increased nLDs. Interestingly, the same group also showed that inhibition of MTP activity reduced nLD formation and PC synthesis without affecting CCTα expression, indicating that nLDs are sites for CCTα activation (288). As described in previous sections, nLDs may provide a platform for a lipid-dependent stress response. In this regard, these studies suggest that the interaction of PML-NBs, specifically those containing PML-II, with nLDs and CCTα could play an important role in regulating cellular lipid homeostasis. Our results demonstrating the significance of PML for the association of LIPIN-1 and CCTα with nLDs and TG and PC metabolism in response to fatty acid overload are presented in **Chapter 4**.

1.7 Aims of This Study

A) Does CCTα Control PC Synthesis Required for Intestinal TG Storage and Secretion?

Despite evidence that PC biosynthesis by the CDP-choline pathway is essential for LD biogenesis in mammalian cells and VLDL secretion by the liver, the precise mechanisms and role of CCTα in intestinal lipid metabolism has not been addressed. To investigate this, **human epithelial colorectal carcinoma Caco2 cells with knockout of CCTα were utilized to establish the contribution of the CDP-choline pathway to the regulation of intestinal TG storage in LDs and secretion in chylomicrons**.

B) Are nLD-PML-NBs Important Centers for Control of Cellular Lipid Metabolism?

The biological significance of nLDs is poorly understood. The association of nLDs with PML-NBs and CCTα suggested to us that assembly of PML-NBs on nLDs may provide a protective response against the lipotoxic effects of fatty acid overload. To test this, **human osteosarcoma U2OS cells with knockout of PML and human epithelial colorectal carcinoma Caco2 cells with knockout of CCTα were utilized to show that the assembly and composition of nLDs is a critical determinant of lipid metabolic activity of cells**.

CHAPTER 2: Materials and Methods

Table 2.1. Materials

Name	Source	Catalog number
Albumin bovine serum, fraction V, ≥96%	Sigma, St. Louis, MO	A9647
[^{3}H]Acetic acid	Perkin-Elmer, Waltham, MA	NET003H025MC
Alexa- Fluor® 488 goat anti-mouse	Thermo Scientific, Rockford, IL	A11029
Alexa- Fluor® 594 goat anti-mouse	Thermo Scientific, Rockford, IL	A11032
Alexa- Fluor® 647 goat anti-rabbit	Thermo Scientific, Rockford, IL	A32733
Anti-β-actin antibody, mouse monoclonal	Sigma, St. Louis, MO	A5441
ApoB antibody, mouse monoclonal	Dr. Roger McLeod, Dalhousie University, Halifax, NS	Gift
BODIPY™ 493/503	Thermo Scientific, Rockford, IL	D3922
CCTα antibody, rabbit polyclonal	GenScript, Piscatawa, NJ	Made on contact
CCTβ2 antibody, rabbit polyclonal	Dr. Suzanne Jackowski, St. Jude Children's Research Hospital, Memphis, TN	Gift
[^{3}H]Choline chloride	Perkin-Elmer, Waltham, MA	NET109001MC
Complete EDTA-free protease inhibitor cocktail tablets	Roche Diagnostics, Indianapolis, IN	04 693 132 001
DL-Dithiothreitol	Sigma, St. Louis, MO	051M18701V
Dulbecco's Modified Eagle Serum (DMEM)	Invitrogen, Burlington, ON	12800-082
Emerin antibody, rabbit polyclonal	Santa Cruz Biotechnology, Missisauga, ON	FL-254
Fetal bovine serum (FBS)	Sigma, St. Louis, MO	F1051
[^{3}H]Glycerol	Perkin-Elmer, Waltham, MA	NET022L001MC

Table 2.1. Materials (continued)

Name	Source	Catalog number
Glycine and acrylamide/bis solution (40%)	Bio-Rad, Hercules, CA	1610146
Hoechst 33258	Invitrogen, Burlington, ON	H1398
Lipofectamine 2000	Invitrogen, Burlington, ON	11668-019
LMNA/C antibody, mouse monoclonal	Cell Signaling, Danvers, MA	4C11
Mowiol® 4-88 reagent	EMD Biosciences, La Jolla, CA	475904
Nitrocellulose membrane	Bio-Rad, Hercules, CA	
Odyssey blocking buffer	LI-COR Biosciences, Lincoln, NE	927-40000
Oleic acid	Sigma, St. Louis, MO	O1630
Phosphphomolybdic acid hydrate	Sigma, St. Louis, MO	221856
Plasmid purification kit	Qiagen, Missisauga, ON	163029415
PML antibody, mouse monoclonal	Santa Cruz Biotechnology, Missisauga, ON	sc-377390
PML antibody, rabbit polyclonal	Bethyl Laboratories, Montgomery, TX	A301-167A
Puromycin	Invitrogen, Burlington, ON	A1113803
Stannous chloride	Thermo Scientific, Rockford, IL	T141
SurfactAmps® X-100	Thermo Scientific, Rockford, IL	TH266403
TEMED	Bio-Rad, Hercules, CA	210011953
Thin-layer chromatography (TLC) silica gel G	Analtech, Newark, NJ	5719800
Thin-layer chromatography (TLC) silica gel HL	Analtech, Newark, NJ	02419
TG mass quantification kit	Biovision, San Francisco, CA	K622
Tween-20	Bio-Rad, Hercules, CA	1706531
Polypropylene membrane insert Transwell plates	Corning Costar, Cambridge, MA	3450
1-stearoyl-2-hydroxy-sn-glycero-3-phosphocholine (18:0-lyso-PC)	Avanti Polar Lipids, Alabaster, AL	855775P
1-oleoyl-2-hydroxy-sn-glycero-3-phosphocholine (18:1-lyso-PC)	Avanti Polar Lipids, Alabaster, AL	845875P
V5 antibody, mouse monoclonal	Bio-Rad, Hercules, CA	MCA1360

Table 2.2. Plasmids

Plasmids	Source	Description
pLIPIN-1α-V5	Dr. Zemin Yao, University of Ottawa, Ottwa, ON	
pLIPIN-1β-V5	Dr. Zemin Yao, University of Ottawa, Ottwa, ON	
pEGFP-PML isoforms	Dr. Graham Dellaire, Dalhousie University, Halifax, NS	
pCCTα-mCherry	Ridgway Lab	
pGFP-nes-2xPABP	Sergio Grinstein, University of Toronto, Toronto, ON	
pGFP-C1(2)δ	Dr. Tobias Meyer, Stanford University, Stanford, CA	Addgene #21216
pGFP-C1(2)δ-2xNLS	Prepared by subcloning a x2 GFP cassette into the BsrGI-AflII site of pGFP-C1(2)δ	

2.1 Cell Culture

Caco2, Caco2 CCTα-KO (CCTα-KO), U2OS and U2OS PML-KO (PML-KO) cells (305) were cultured in DMEM containing 10% FBS (medium A) at 37°C in a 5% CO_2 incubator. Caco2 and CCTα-KO cells were differentiated into polarized epithelial monolayers by culturing on polypropylene membrane inserts of 35 mm Transwell plates for 21 days in medium A. The integrity of epithelial Caco2 monolayers was determined by measuring transepithelial resistance (TER) in an Ussing chamber with an aperture size of 0.12 cm^2. Each hemichamber contained 1.2 ml Krebs solution (117 mM NaCl, 4.6 mM KCl, 20 mM $NaHCO_3$, 6 mM glucose, 1 mM $MgCl_2$, 1.5 mM $CaCl_2$ and 10 mM hydroxyethyl piperazineethanesulfonic acid (HEPES), pH 7.4). The buffer inside the chambers was continuously stirred with magnetic stir bars, gassed with 95% O_2/5% CO_2, and the temperature was maintained at 37°C with water circulated on the outside surface of the chambers. Ag/AgCl electrodes were connected to the apical and basolateral side of the membrane inserts with agar bridges (3 M KCl-2% agar) to measure transepithelial potential difference (TPD). Electrode asymmetry was corrected at the beginning and end of experiment with fluid resistance compensation. TER was determined by the change in the TPD generated by a brief 10 μA pulse controlled by a high-impedance automatic dual voltage clamps (DVC 4000; World Precision Instruments, Sarasota, FL). Resistance data was collected and analyzed using a PowerLab 28T and LabChart software (ADInstruments, Colorado Springs, CO).

2.2 Preparation of Oleate/BSA Complex

Oleate was conjugated to fatty acid-free BSA at molar ratio of 6:1 as previously described (306). The sodium salt of oleic acid was made by titrating with 5 N NaOH in ethanol, drying under N_2 and resuspension in 150 mM NaCl. BSA was dissolved in 150 mM NaCl solution over 4 h at room temperature and stored at 4°C. The oleate and cold-BSA solutions were then rapidly combined and stirred for 10 min at room temperature and stored at -20°C.

2.3 Plasmid Transfection

In 35 mm dishes, 30% confluent Caco2 and CCTα-KO cells were transiently transfected with 2 μg DNA and 6 μl Lipofectamine 2000. For U2OS and PML-KO cells, transfection was performed at 60% confluency using 2 μg DNA and 4 μl Lipofectamine 2000. Double transfections were performed using 1 μg DNA of each DNA plasmid and 4 μl Lipofectamine 2000. DNA and transfection reagent were incubated separately in 0.5 ml DMEM for 5 min. The DNA solution was then added to the Lipofectamine solution, mixed, and incubated at room temperature for 30 min. Subsequently, the mixture was added to the cells cultured in DMEM dropwise and incubated at 37 °C. After 6 h, cells received fresh medium A and incubated for 16-18 h at 37 °C prior to experiments.

2.4 CRISPR/Cas9 Knockout of CCTα

A deletion was introduced into *PCYT1a* in Caco2 cells by CRISPR/Cas9 gene editing (Ran et al., 2013). A guide RNA (sgRNA) was designed (http://crispr.mit.edu/) to target exon 3 (5'-GCGCCCGGACCCAAC-3') and cloned into pX459. After transfection,

cells were selected with 10 μg/ml puromycin for 7 days. Puromycin was also added to non-transfected cells (canary dishes) of equal density to ensure complete killing. Clonal cell lines were isolated by limiting dilution and knockout was confirmed by SDS-PAGE and immunoblotting for CCTα

2.5 Isolation of Chylomicrons by Ultracentrifugation

Polarized Caco2 and CCTα-KO cells were incubated with medium A in the apical chamber containing 400 μM oleate/BSA complex and/or of 25 μM lyso-PC. Basolateral medium (0.8 ml) was collected into polycarbonate tubes (11 × 34 mm; Beckman Instruments, Inc.) and lipoproteins were isolated by sequential ultracentrifugation. The d=1.006 g/ml fraction was isolated by overlaying with 0.2 ml of 0.15 M NaCl, 0.3 mM EDTA (pH 7.4) and centrifugation using a Beckman Optima^{TM} TLX tabletop ultracentrifuge and TLA-120.2 fixed-angle rotor (Beckman Instruments, Inc.) at 480,000 *g* for 2.5 h. After removal of the d=1.006 g/ml fraction, the medium was then adjusted to d=1.21 g/ml using NaBr, overlayed with a d=1.21 g/ml NaBr solution and centrifuged for 4 h at 480,000 *g*. The two lipoprotein fractions were subjected to 5% SDS-PAGE and immunoblotted for apoB-100 and apoB-48.

2.6 Immunoblotting

Cells were washed twice with ice-cold PBS before lysis with 2x SDS buffer (12.5% SDS, 30 mM Tris-HCl, 12.5% glycerol, and 0.01% bromophenol blue, pH 6.8). Lipoprotein fractions were adjusted in 2x SDS buffer. Cell lysates and lipoprotein fractions were heated at 95°C for 5 min, equal amounts of samples were separated by

sodium dodecyl sulphate-polyacrylamide gel electrophoresis (SDS-PAGE) in SDS-running buffer (3 mM SDS, 200 mM glycine, 25 mM Tris-base). Following electrophoresis, proteins were transferred to nitrocellulose membranes in transfer buffer (25 mM Tris, 192 mM glycine, 20% methanol) at 100 V for 1 h for cell lysates or 1.5 h for lipoprotein fractions. After transfer, membranes were briefly stained in Ponceau S to confirm protein loads and washed three times with TBS. The membranes were then incubated in TBS (20 mM Tris-HCl and 500 mM NaCl (pH 7.4)):Odyssey blocking solution (5:1, v/v) for 1 h at room temperature. Primary antibodies were applied for 1 h at room temperature or 4°C overnight. Antibody titers were as follows: CCTα, 1:1,000; apoB, 1:1,000; PML (rabbit polyclonal), 1:1,000; CCTβ2, 1:1,000; V5, 1:2,000; β-actin, 1:1,5000 . The membranes were then washed three times with TBS-Tween-20 for 5 min each, followed by application of IRDye 800CW and 680LT secondary antibodies (1:15,000) for 1 h at room temperature. The membranes were washed three times with TBS-Tween-20 and proteins were visualized at scanning at 680 or 800 nm using an Odyssey imaging system and fluorescence intensity was quantified using application software (v3.0; LI-COR Biosciences).

2.7 Immunofluorescence Microscopy

Cells were seeded on sterile coverslips (0.15 mm thickness) in 35 mm dishes. At the end of experiments, cells were fixed in 4% (w/v) paraformaldehyde for 15 min at room temperature and permeabilized for 10 min in 0.05% (w/v) Triton X-100 at 4°C. In the case of polarized cells, Transwell membrane inserts were fixed in 4% (w/v) paraformaldehyde for 15 min at room temperature and permeabilized with 0.2% (w/v)

Triton X-100 at room temperature for 30 min. Following permeabilization, cells on glass slides or Transwell filters were blocked in PBS (10 mM sodium phosphate [pH 7.4], 225 mM NaCl and 2 mM $MgCl_2$) supplemented with 1% BSA (w/v) for 1 h at room temperature or 4°C overnight. Primary antibodies were diluted in PBS/BSA as follows: CCTα, 1:1,000; LMNA/C, 1:500; PML (mouse monoclonal), 1:200; PML (rabbit monoclonal), 1,1000; emerin, 1:200; V5, 1:1,000. All antibodies were incubated with cover slips at room temperature for 1 h or with Transwell filters at room temperature for 1.5 h. The samples were then washed three times with PBS/BSA for 10 min each. Secondary AlexaFluor-conjugated antibodies were diluted 1:4,000 in PBS/BSA and were incubated at room temperature for 1 h. To visualize LDs, BODIPY 493/503 or LipidTox Red was diluted 1:1,000 or 1:500, respectively, and incubated with the secondary antibodies. Samples were then washed three times with PBS/BSA for 10 min each. For nuclear staining marker, Hoechst 33258 was diluted 1:2,000 in PBS and incubated for 10 min at 4°C. Coverslips were then mounted onto glass slides with 10 µl Mowiol 4-88. Transwell filters were mounted onto glass slides with 10 µl Mowiol 4-88 followed by another 10 µl Mowiol 4-88 and fresh coverslips. Confocal imaging was performed using a Zeiss LSM510/Axiovert 200M microscope (0.6 µm sections) with a Plan-Apochromat 63×/1.40 numerical aperture oil immersion objective. LD size distribution was quantified using ImageJ software, version 1.47 (National Institues of Health, Bethesda, MD). Images were converted to 8-bit, threshold was adjusted, and the "analyze particle" command was used to exclude cells at the edges. The area distribution was binned according to droplet particle size. nLDs were measured by selecting the LMNA/C- or

Hoechst-stained nucleus using "Region of Interest" command. cLDs were measured by subtracting nLDs from total LDs.

2.8 Choline Transport Assay

Caco2 and CCTα-KO cells were 80% confluent in 12-well plates prior to the start of the experiment. Cells were rinsed twice in 500 µl of Krebs-Ringer buffer [130 mM NaCl, 1.3 mM KCl, 2.2 mM $CaCl_2$, 1.5 mM $MgCl_2$, 1.2 mM K_2HPO_4, 10 mM D-glucose, and 10 mM HEPES (pH 7.4)] and incubated in 500 µl of the same buffer for 30 min at 37°C. Cells were then incubated with 500 µl of Krebs-Ringer buffer containing 1–25 µM [^{3}H]choline for 10 min at 37°C. Cells were placed on ice, washed three times with ice-cold Krebs-Ringer buffer, and solubilized in 250 µl of 0.1% SDS/0.2 N NaOH for 10 min at room temperature. Radioactivity in 50 µl of sample was measured by liquid scintillation counting (LSC) and expressed relative to total cell protein. Cells were washed three times with the buffer and solubilized in 100 µl of NaOH (0.5 N) at room temperature and protein was quantified by the Lowry method (307).

2.9 Measurement of [^{3}H]Choline Incorporation into PC and Choline Metabolites

Cells at 80% confluency in 35 mm dishes were washed twice with choline-free medium A prior to the start of the experiment. Cells were incubated with choline-free medium A containing [^{3}H]choline (2 µCi/ml) for the indicated times in figure legends. After labeling, cells were rinsed once with cold PBS, harvested in 1 ml methanol:water (5:4, v/v). Two hundred µl was taken for Lowry protein quantification. Chloroform (3 ml) was added and the samples were centrifuged at 2,000 rpm for 5 min to separate the aqueous and organic phases. The aqueous phase was collected by aspiration. The

organic phase was washed twice with 2 ml of ideal upper phase (chloroform:0.58% NaCl:methanol; 45:47:3, v/v), dried under nitrogen, resuspended in 500 µl chloroform and the radioactivity in 100 µl was quantified by LSC. The aqueous phase was also dried under nitrogen, resuspended in 50 µl of water and 10 µl was spotted onto TLC plates along with standards for phosphocholine, CDP-choline and GPC. The TLC plate was resolved using water:ethanol:ammonium hydroxide (50:95:6, v/v). The plates were then sprayed with 1% phosphomolbydate in choloroform:methanol (1:1, v/v) followed by 1% (w/v) stannous chloride in 3N HCl. Samples were collected by scraping and the radioactivity was measured by LSC.

2.10 Measurement of TG Mass

TG mass in undifferentiated Caco2 and CCTα-KO cells (80% confluency) incubated in the presence or absence of 400 µM oleate/BSA for 12 h was quantified using a TG quantification colorimetric kit (**Table 2.1**) according to the manufacturer's instructions. In this assay, the glycerol released enzymatically from cellular TG is oxidized to generate a product which reacts with the probe to generate color. Cell lysates were solubilized in 100 µl of NP-40 (5%, v/v), heated at 100°C for 5 min, subjected to centrifugation at 10,000 g for 2 min, and the supernatant was diluted 10-fold with distilled water before the assay. Samples (50 µl) were added to each well in a 96-well plate and incubated with 2 µl of lipase for 20 min at room temperature to convert TG to glycerol and fatty acids. In the meantime, a reaction mix was prepared by mixing 46 µl of TG assay buffer, 2 µl of TG probe and 2 µl of TG enzyme mix. After 20 min, the

reaction mix was added to each well containing the samples and incubated for 30 min at room temperature, and absorbance was measured at 570 nm.

2.11 Analysis of TG Synthesis using [^{3}H]Glycerol or [^{3}H]Oleate Incorporation

TG synthesis by cells (80% confluency) was measured by incubation with 2 μCi/ml [^{3}H]glycerol with or without oleate/BSA at 37°C. TG and CE synthesis from exogenous fatty acid was determined by incubation with [^{3}H]oleate/BSA. Concentrations and incubation periods are indicated in figure legends. Cells were rinsed twice with cold Buffer B (150 mM NaCl, 50 mM Tris-HCl (pH 7.4) and 2 mg/ml BSA) and once with cold Buffer C (150 mM NaCl, 50 mM Tris-HCl (pH 7.4)). The [^{3}H]glycerol- or [^{3}H]oleate-labeled lipids were extracted with hexane:isopropanol (3:2, v/v). Samples were dried under nitrogen, resuspended in hexane containing TG or CE standard and spotted onto TLC. The TLC plate was resolved using hexane:diethyl ether:acetic acid (90:30:1, v/v). Samples were collected by scraping and the radioactivity was measured by LSC and normalized to total cellular protein determined by Lowry protein quantification.

TG and CE synthesis and secretion in polarized Caco2 and CCTα-KO cells were determined by incubation of the apical chamber with medium A containing 200 or 400 μM [^{3}H]oleate/BSA for 12 h at 37°C. Cells and medium in the basolateral chamber were extracted with hexane:isopropanol (3:2, v/v) and [^{3}H]oleate incorporation into TG and CE was determined as described above.

2.12 Analysis of TG and Phospholipid Metabolism using [^{3}H]Glycerol Pulse-Chase Incorporation into TG and PC and PE

TG and phospholipid metabolism in polarized Caco2 and CCTα-KO cells was also monitored by pulse-chase labeling with [^{3}H]glycerol. Cells were incubated with apical medium A containing [^{3}H]glycerol (2 μCi/ml) and 400 μM of oleate/BSA. After 12 h, basolateral medium was collected, cells were rinsed with medium A, and incorporation of [^{3}H]glycerol into intracellular and secreted TG, PC and PE was determined after extraction with hexane:isopropanol (3:2, v/v) (pulse, time 0). The mobilization and secretion of [^{3}H]glycerol-labeled lipids was monitored by incubation in medium A and extraction of [^{3}H]glycerol-labeled TG, PC and PE from the cells and basolateral medium at 3 and 6 h. Samples were divided into two fractions (one for TG and one for PC and PE determination) and dried under nitrogen. Samples were resuspended in hexane and chloroform for TG and phospholipid, respectively, and spotted onto TLC with standards. TG was separated by TLC in hexane:diethyl ether:acetic acid (90:30:1, v/v) and phospholipids were separated by TLC in chloroform:methanol:acetic acid:water (60:40:4:1, v/v). Radioactivity was measured by LSC and normalized to total cellular protein.

2.13 Measurement of [^{3}H]Acetate Incorporation into Cholesterol and Fatty Acid Synthesis

U2OS and PML-KO cells (60% confluency) were cultured in medium A or LPDS medium for 16 h prior to incubation with 2.5 μCi/ml [^{3}H]acetate for 4 h at 37°C to measure *de novo* cholesterol and fatty acid synthesis. Cells were then rinsed cold-PBS and dissolved

in 0.1M NaOH. Lipid extracts were saponified in ethanol and 50% potassium hydroxide (w/v) for 1 h at 60°C, extracted with hexane, were resolved by TLC in hexane/diethyl ether/acetic acid (60:40:1, v/v), and radioactivity in cholesterol and lanosterol was measured by LSC. The hydrolysate was acidified with HCl (pH <3) and radiolabeled fatty acids were extracted with hexane and quantified by LSC. Incorporation of [^{3}H]acetate into lipids was normalized to total cellular protein.

2.14 LC-MS/MS Analysis of PC and PE Molecular Species

A Dionex Ultimate 3000 UHPLC system coupled to a Thermo Scientific LTQ-Orbitrap Velos Pro mass spectrometer equipped with an electrospray ionization (ESI) source was used. Lipids were separated on a Waters BEH C8 UPLC column (1.7 μm, 2.1 x 50 mm) using a 0.01% formic acid in water and acetonitrile-isopropanol (1:1)-0.01% formic acid as the mobile phases for binary-solvent gradient elution. The column flow rate was 0.4 mL/min and the column temperature was 60ºC. For metabolite detection and relative quantitation, the instrument was run in the survey scan mode with FTMS detection at a mass resolution of 60,000 FWHM at 400 m/z. The mass scan range was m/z 150 to 1800. For LC-MS/MS, collision induced dissociation was applied at normalized collision energies of 28% to 35% in a data-dependent analysis way. Metabolite assignments were carried out by searching against the lipid and metabolome databases with the measured m/z values within an allowable mass error of <3 ppm). LC-MS/MS using collision-induced dissociation in the ion trap was performed to provide confirmation of the assigned lipid identities. The survey scan was performed in a mass range of m/z 200 to 1800 and the top 6 most intensive ions on each survey scan were selected for subsequent fragmentation at

normalized collision energies of 28% to 35%. MS/MS spectra were manually interpreted to confirm the lipid classes and identified by the observed fragment ions.

2.15 Statistical Analysis

Unless otherwise stated in the figure legend, data are presented as mean and standard error of the mean (SEM) of at least three experiments. Results for LD number per cell, area and size distribution are presented as box and whisker plots showing the mean and 5th to 95th percentile for analysis of indicated number of cells. Statistical significance was determined using two-tailed Student's t-test or one way analysis of variance (ANOVA).

CHAPTER 3: Regulation of Intestinal Triglyceride Storage and Secretion by the CDP-Choline Pathway

3.1 Results

3.1.1 CCTα Deficiency Increases TG Storage in Caco2 Cells

CCTα has been reported to regulate PC synthesis for LD biogenesis in various cell lines as well as hepatic TG storage and secretion in VLDL, but its role in intestinal TG metabolism has not been addressed. To investigate this, the CRISPR/Cas9 gene editing system was used to knockout CCTα expression in Caco-2 cells using a single guide RNA targeting exon 3 of PCYT1A in Caco2. A CCTα-KO cell line that was devoid of CCTα was isolated and had no compensatory change in the expression of CCTβ2 isoform (**Fig. 3.1A**). LD formation was stimulated by acute oleate treatment and visualized with the neutral lipid dye BODIPY 493/503, and immunostained for the NE marker LMNA/C and CCTα. Immunofluorescence microscopy of undifferentiated Caco2 cells showed that CCTα was exclusively nuclear and partially localized with LMNA/C (**Fig. 3.1B**). Both control and CCTα-KO cells had no LDs in the absence of oleate (**Fig. 3.1B and C**). Exposure of Caco2 cells to 400 μM oleate/BSA for 12 h resulted in the formation of LDs but did not affect nuclear localization of CCTα (**Fig. 3.1B**). CCTα-KO cells treated with oleate also accumulated LDs that appeared larger in size and fewer in number compared to Caco2 controls (**Fig. 3.1C**).

To assess the effect of CCTα knockout on PC synthesis, Caco2 and CCTα-KO cells were incubated in medium containing [^{3}H]choline for up to 8 h, and isotope incorporation into PC, metabolites of CDP-choline pathway and the PC degradation

product glycerophosphocholine (GPC) was measured (**Fig. 3.2**). [^{3}H]Choline incorporation into PC in CCTα-KO cells was lower compared to control values during the 8 h labeling period and reduced by 50% at 6 h (**Fig. 3.2A**). Unexpectedly, [^{3}H]choline incorporation into pCholine, the substrate of CCTα, was not affected in CCTα-KO cells (**Fig. 3.2B**). However, a significant reduction in isotope incorporation into the enzyme product, CDP-choline, was observed at 4 and 6 h (**Fig. 3.2C**). Isotope incorporation into GPC was reduced throughout the experiment, and was significantly lower at 4 h (**Fig. 3.2D**). The lack of effect of CCTα-KO on [^{3}H]choline incorporation into pCholine (**Fig. 3.2B**) suggested a potential defect in choline uptake due to reduced PC levels or altered phospholipid composition of the plasma membrane. To test this, the uptake of choline (1-25 μM) into the cells was measured (**Fig. 3.2E**). Saturable choline transport and the K_d for control (138 ± 36 pmol/min/mg and 16 ± 8 μM) and CCTα-KO cells (146 ± 36 pmol/min/mg and 17 ± 8 μM) were similar, indicating that the reduced incorporation of [^{3}H]choline incorporation into the metabolites was not due to defective uptake. To monitor the effect of CCTα knockout on PC turnover, cells were pulse-labelled with [^{3}H]choline for 12 h, followed by a chase period up to 72 h (**Fig. 3.2F**). The degradation of [^{3}H]choline-labeled PC in control and CCTα-KO cells was similar during the chase period. However, there was a 30-40% reduction in the proliferation of CCTα-KO compared with controls when measured by total amount of protein (**Fig. 3.2G**). Thus, these data indicate that knockout of CCTα reduced choline flux through the CDP-choline pathway, and that synthesis and degradation are not linked in CCTα-KO cells, resulting in PC deficiency and reduced proliferation of the knockout cells.

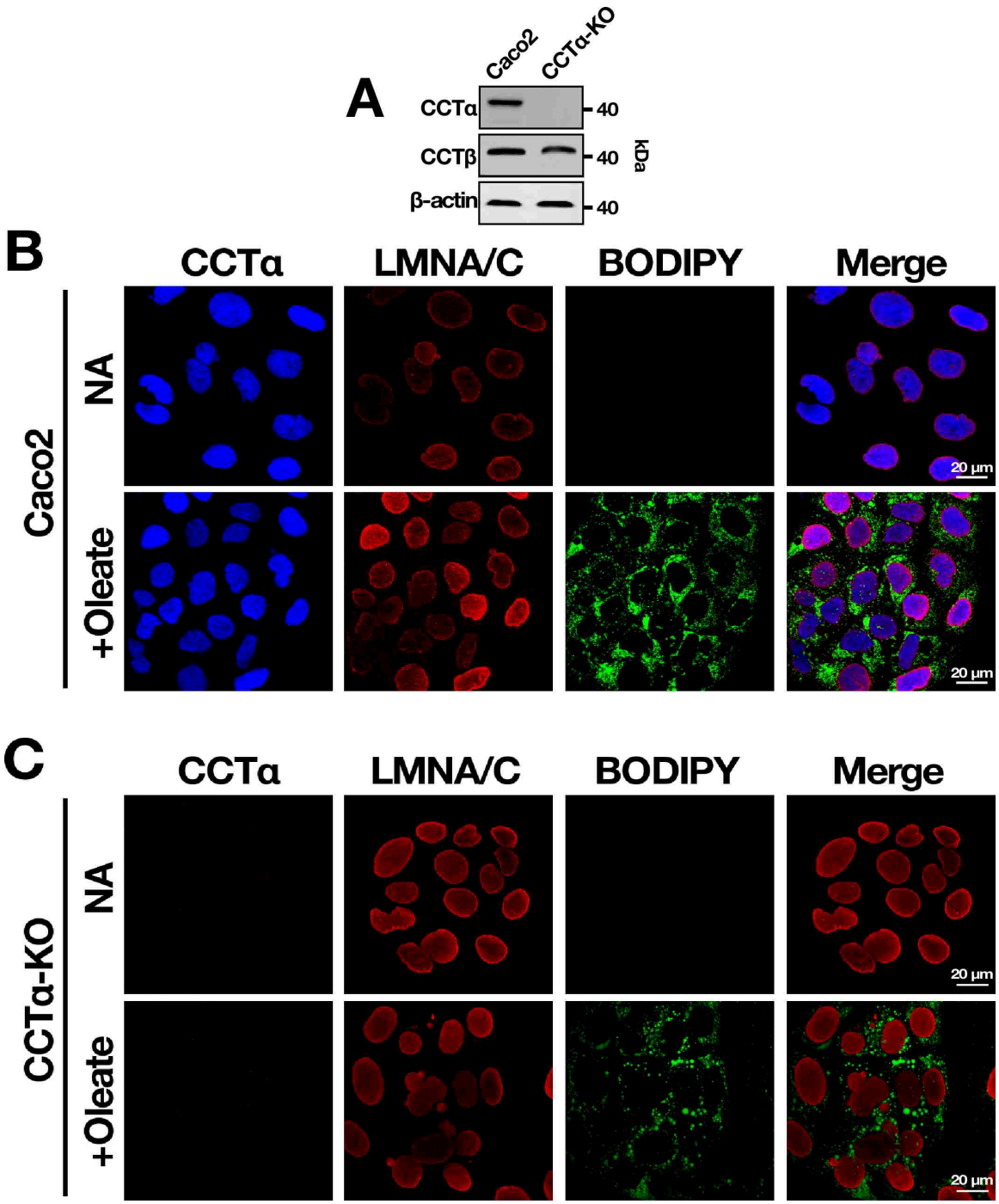

Figure 3.1. CRISPR/Cas9-mediated knockout of CCTα expression in Caco2 cells. Expression of CCTα and CCTβ2 isoforms in whole cell lysates of Caco2 and CCTα-KO cells was determined by SDS-8% PAGE and immunoblotting **(A)**. Caco2 **(B)** and CCTα-KO cells **(C)** were treated with or without oleate/BSA (400 μM) for 12 h. Cells were immunostained with CCTα polyclonal and LMNA/C monoclonal antibodies followed by AlexaFluor-647 and -594 secondary antibodies, respectively. LDs were visualized with BODIPY-493/504. Cells were imaged using confocal microscopy.

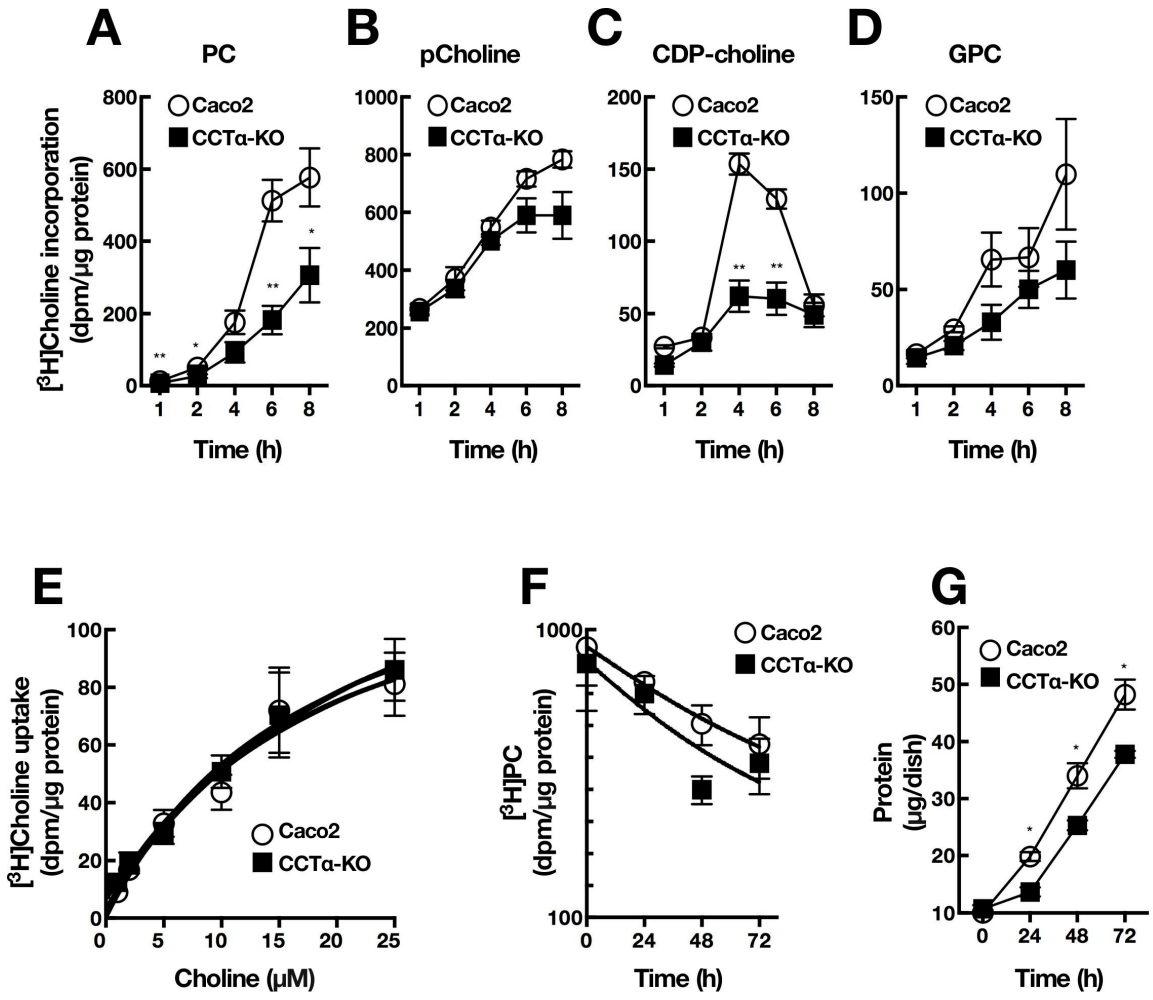

Figure 3.2. Reduced PC synthesis in CCTα-KO cells. Caco2 and CCTα-KO cells were cultured with [^{3}H]choline (2µCi/ml) and incorporation into PC **(A)**, pCholine **(B)**, CDP-choline **(C)**, and GPC **(D)** were measured up to 8 h. Results are the mean and SEM of three experiments. **P*<0.05, ***P*<0.005 compared with Caco2 controls. Transport of [^{3}H]choline into Caco2 and CCTα-KO cells. B_{max} and K_d values were determined by Scatchard analysis using a one-site specific binding model. Results are the mean and SEM of triplicate measurements from three experiments **(E)**. Caco2 and CCTα-KO cells were incubated with [^{3}H]choline (2µCi/ml). After 12 h, isotope-free medium was exchanged and the decay of radioactivity in [^{3}H]PC was measured during 72 h chase period **(F)**. Cellular protein concentrations during the 72 h chase period. Results are the mean and SEM of three experiments. **P*<0.005 **(G)**.

LC-MS/MS analysis was performed to determine whether CCTα knockout affected PC and/or PE molecular species composition. The major PC species in undifferentiated (**Fig. 3.3A**) or differentiated (**Fig. 3.3B**) CCTα-KO cells were similar to controls. However, differentiation of Caco2 and CCTα-KO cells into monolayers shifted the distribution of PC to long-chain unsaturated species (i.e. 36:3, 38:4 and 38:5), with a decrease in shorter-chain species (i.e. 32:1 and 34:2). CCTα knockout also did not affect the mass of PE molecular species in undifferentiated (**Fig. 3.3C**) or differentiated cells (**Fig. 3.3D**). Unlike PC, the distribution of PE species was not affected by differentiation, however, a slight increase in the 38:4 species was observed.

Reduced PC synthesis is reported to increase size and decrease number of LDs in mammalian cells. Exposure to oleate resulted in noticeable change in the morphology of BODIPY-493/503 stained LDs in CCTα-KO cells (**Fig. 3.4A**). Quantification of cross-sectional area of LDs revealed a significant reduction in small LDs (<0.2 μm^2) and an increase in large LDs (>1 μm^2) in CCTα-KO cells (**Fig. 3.4B**). CCTα knockout also reduced the total number of LDs per cell by 60% (**Fig. 3.4C**). In the absence of oleate, CCTα-KO cells had 1.9-fold higher TG mass compared with control cells (**Fig. 3.4D**). TG mass in CCTα-KO cells exposed to oleate was 3.8-fold higher, suggesting that the shift toward large LDs in knockout cells was accompanied by an increase in TG mass. Lack of CCTα may divert DG away from the last step of PC synthesis and toward TG synthesis and increased TG mass. To investigate this, cells were pulse-labeled with [^{3}H]glycerol or [^{3}H]oleate to measure TG synthesis (**Fig. 3.5**). Interestingly, [^{3}H]glycerol (**Fig. 3.5A**) or [^{3}H]oleate (**Fig. 3.5B**) incorporation into TG in CCTα-KO cells was similar to control cells, suggesting that the increase in TG mass in CCTα-KO cells was

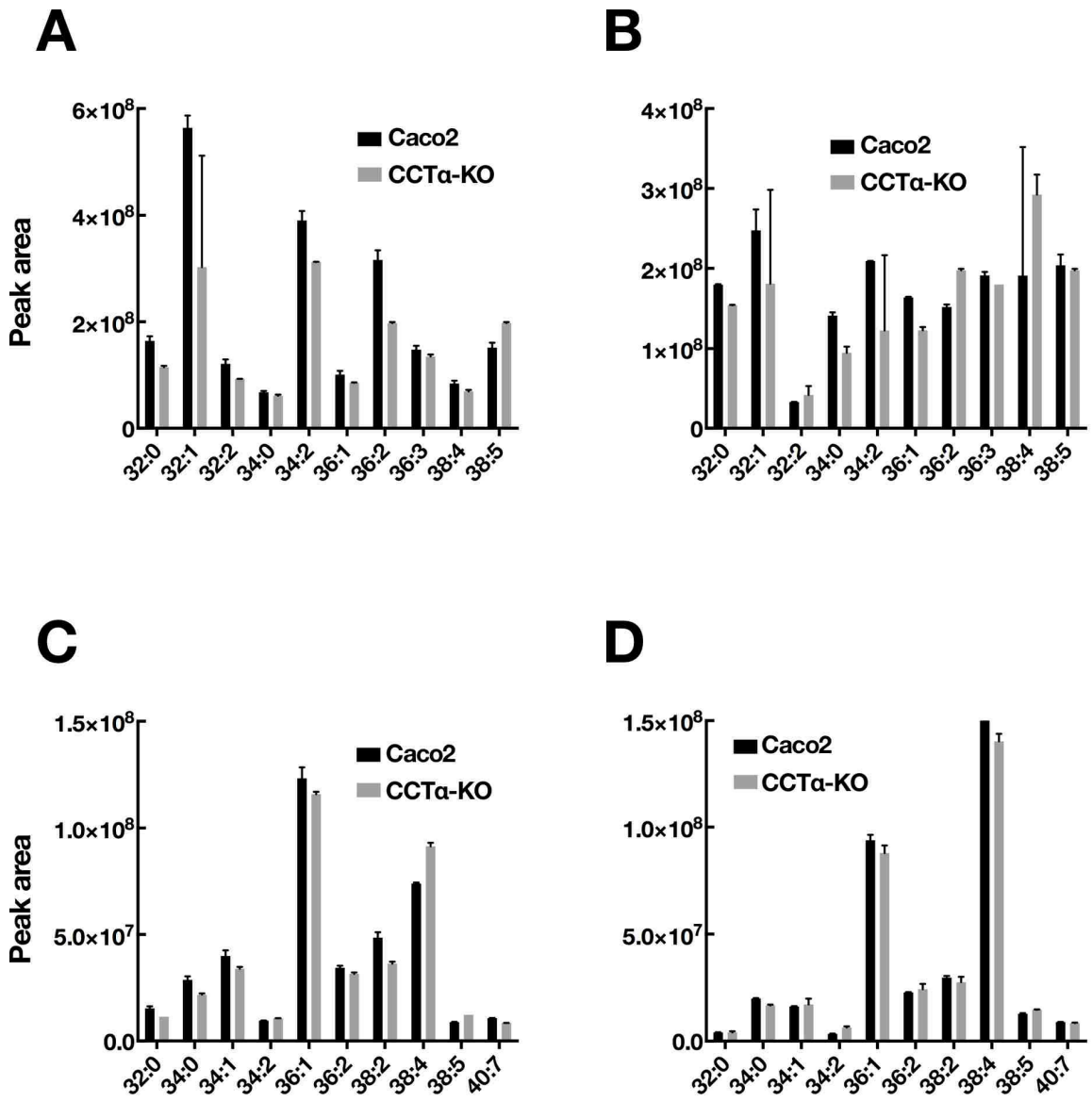

Figure 3.3. Mass of PC and PE molecular species in Caco2 and CCTα-KO cells. PC molecular species distribution in undifferentiated **(A)** and differentiated **(B)** Caco2 and CCTα-KO cells. PE molecular species distribution in undifferentiated **(C)** and differentiated **(D)** Caco2 and CCTα-KO cells. The molecular species mass distribution was determined by LC-MS/MS as described in Chapter 2. Results are the mean and range of two separate replicates.

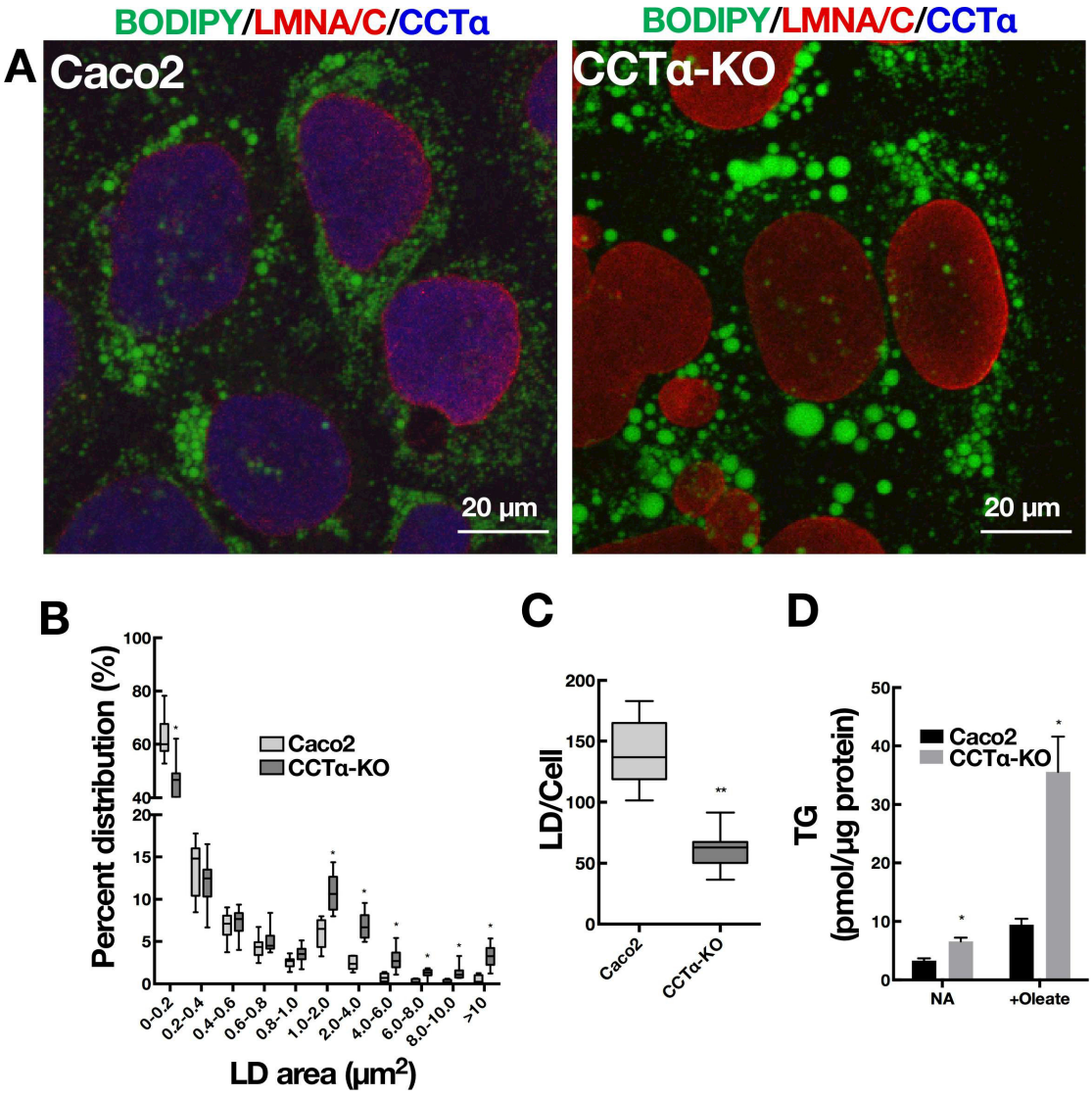

Figure 3.4. Altered LD morphology in CCTα-KO cells. Representative confocal image of Caco2 and CCTα-KO cells treated with oleate/BSA (400 μM) for 12 h. LDs were visualized with BODIPY-493/503 and nuclei were immunostained with LMNA/C-monoclonal and AlexaFluro594-secondary antibodies (**A**). The cross-sectional area of LDs was quantified and binned into ranges. **P*<0.001 **(B)**. The number of LDs per cell **(C)** was quantified from data from **(B)**. **P<0.0005. 3-4 fields of cells from five separate experiments. TG mass was quantified in cells treated with or without oleate/BSA (OA, 400 μM) for 12 h. Results are the mean and SEM of three experiments. **P*<0.01 compared with control cells **(D)**.

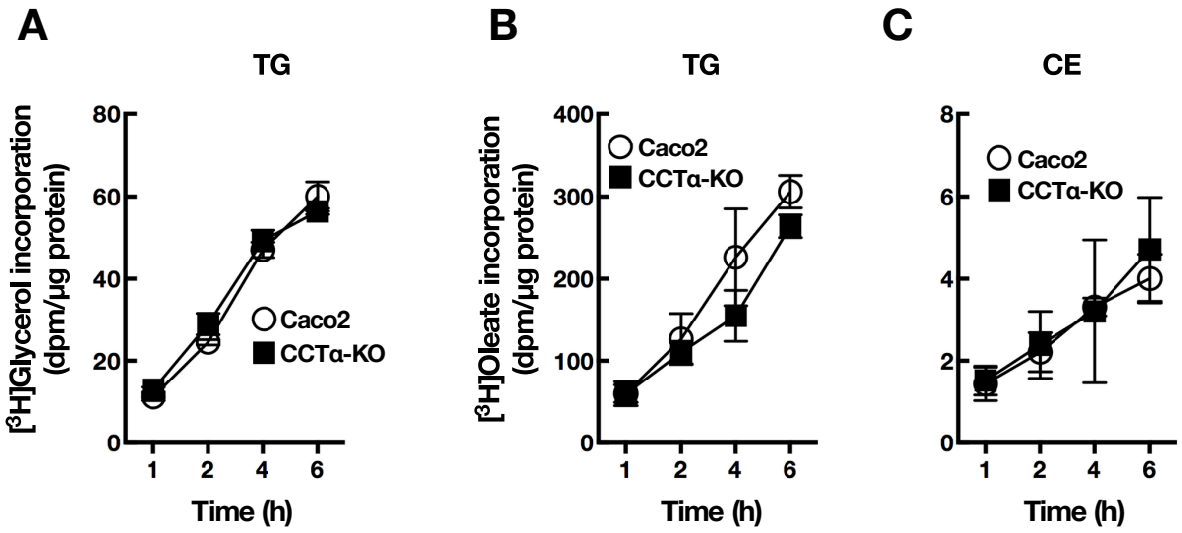

Figure 3.5. Neutral lipid synthesis is not affected by CCTα knockout. Caco2 and CCTα-KO cells pulse-labeled with 200 µM oleate/BSA and [^{3}H]glycerol (2µCi/ml) for the indicated times and incorporation into TG was quantified **(A)**. Cells were pulse-labeled with [^{3}H]oleate/BSA complex (200 µM) for the indicated times, and the incorporation of [^{3}H]oleate into TG **(B)** and CE **(C)** was quantified. Results are the mean and SEM of three experiments.

not due to increased synthesis, but potentially to reduced mobilization from the storage pool. The synthesis of CE was also unaffected by CCTα knockout, as measured by [^{3}H]oleate incorporation (**Fig. 3.5C**).

To verify that the change in LD morphology in CCTα-KO cells was caused by CCTα knockout, a rescue experiment was performed by transient expression of mCherry-CCTα (**Fig. 3.6**). Untransfected or mock-transfected CCTα-KO cells had fewer and larger LDs. Expression of mCherry-CCTα in CCTα-KO cells reverted the size distribution and total number per cell back to the levels in control cells, suggesting that the LD phenotype was caused by CCTα deficiency.

In the intestine, the Lands pathway enzyme LPCATs are involved in PC synthesis and acyl-chain remodeling that is important for TG secretion (100). To examine whether PC synthesized by the Lands pathway could compensate for the loss of CCTα, oleate-treated CCTα-KO cells were supplemented with 25 μM of 18:0-lyso-PC or 18:1-lyso-PC. BODIPY 493/503 staining in lyso-PC supplemented CCTα-KO cells appeared similar to that of Caco2 controls (**Fig. 3.7A**). Quantification revealed that supplementation with 18:0-lyso-PC in CCTα-KO cells partially shifted the size distribution and total number of LDs toward that of control Caco2 cells (**Fig. 3.7B and C**). However, the results were still significantly different from the controls. 18:1-lyso-PC supplementation was more effective in this regard, reverting the size distribution and number of LDs to that of control cells. Thus, defects in LD morphology due to a deficiency in the CDP-choline pathway can be corrected acylation of lyso-PC via the Lands pathway.

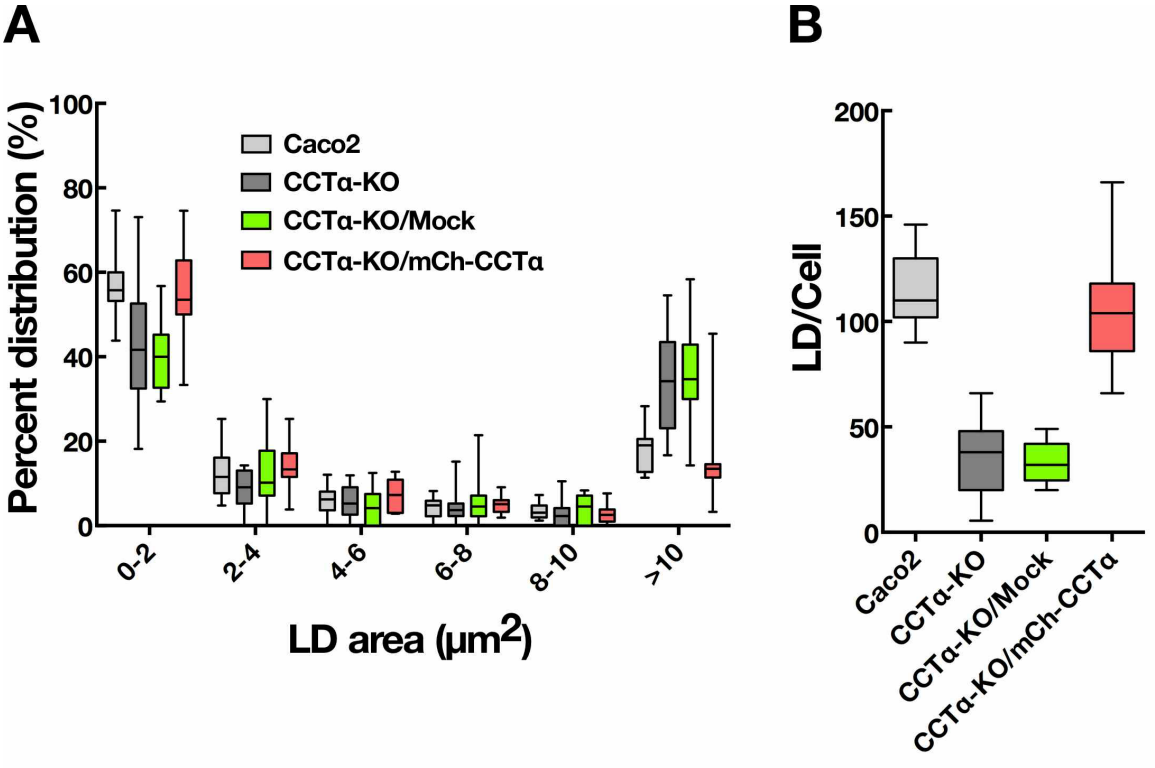

Figure 3.6. Transient expression of mCherry-CCTα in CCTα-KO cells restores the defective LD phenotype. CCTα-KO cells were transiently transfected with pCCTα-mCherry for 36 h using Lipofectamine 2000, followed by platting on glass coverslips for 24 h. Subsequently, cells were incubated with oleate/BSA (400 μM) for 12 h. The cross-sectional area of LDs was quantified and binned into ranges. 15 cells from a representative experiment **(A)**. The number of LDs in each cell was quantified **(B).**

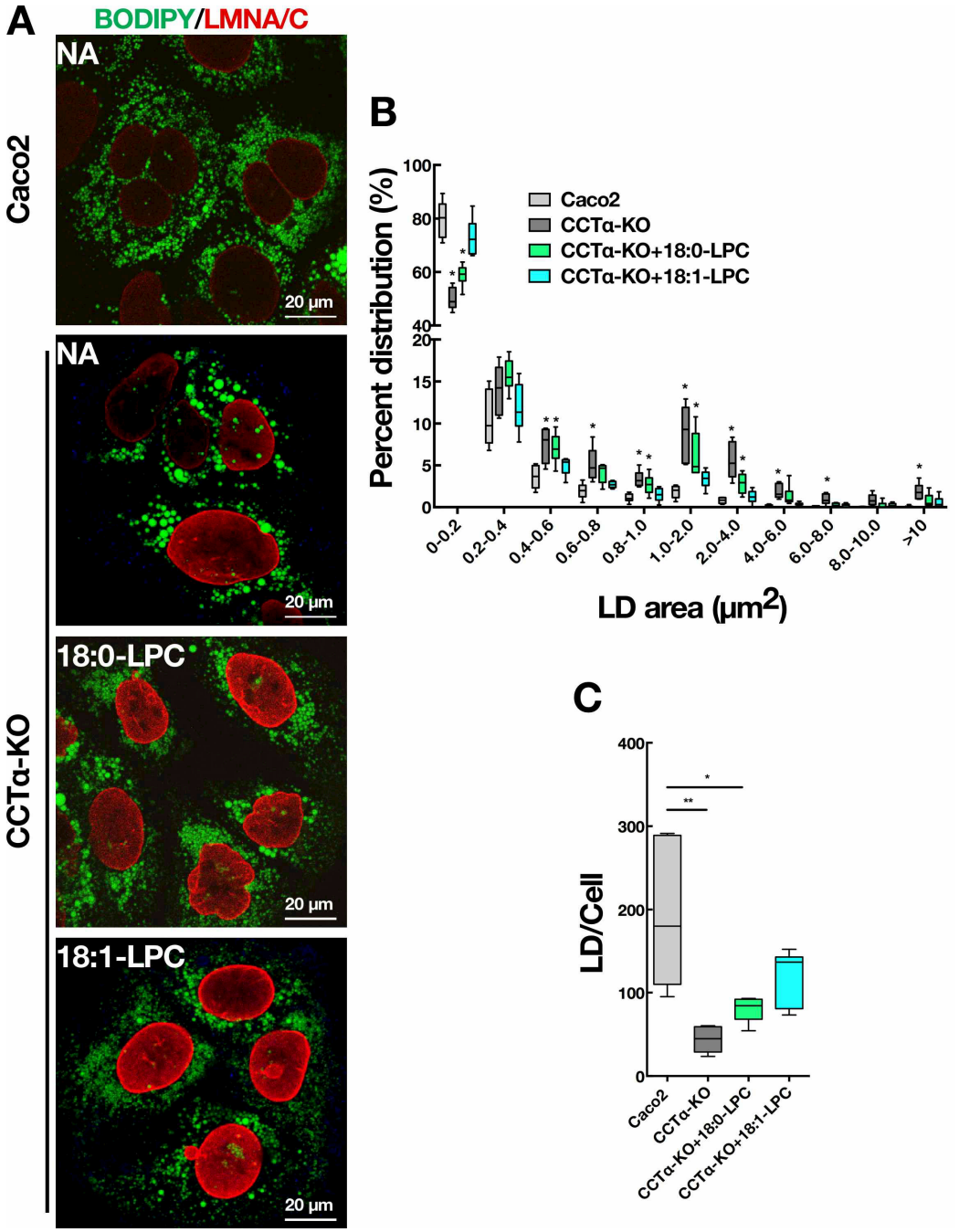

Figure 3.7. Lyso-PC treatment restores LD size and number in CCTα-KO cells. Representative confocal image of Caco2 and CCTα-KO cells cultured in oleate/BSA (400 μM) supplemented without (NA, no addition) or with 18:0- or 18:1-lysoPC (LPC, 25 μM) for 12 h. LDs were visualized with BODIPY-493/503 and nuclei were immunostained with LMNA/C-monoclonal and AlexaFluro594-secondary antibodies (**A**). The cross-sectional area of LDs was quantified and binned into ranges. Six fields of cells from three separate experiments. **P*<0.001 **(B)**. The number of LDs in each cell was quantified **(C)** from data in **(B)**. ***P*<0.01, **P*<0.05.

3.1.2 Differentiation of Caco2 Cells and LD Morphology

Polarized intestinal epithelial cells take up fatty acids at the apical membrane for esterification into TG, which can be stored or secreted in chylomicrons and VLDL-like particles from the basolateral surface. To generate polarized cells, Caco2 and CCTα-KO cells were differentiated into epithelial monolayers on membrane supports for 21 days. TER was measured in an Ussing chamber at the end of differentiation period to confirm the formation of tight epithelial monolayers of Caco2 (316 $\Omega \cdot cm^2$) and CCTα-KO cells (323 $\Omega \cdot cm^2$). Similar to undifferentiated cells, differentiated CCTα-KO cells had more TG compared with control cells, and oleate treatment for 12 h increased TG mass by 2- to 2.5-fold (**Fig. 3.8A**). Notably, untreated differentiated cells had more TG compared with undifferentiated counterparts (compare with **Fig. 3.4D**) as well as more BODIPY-stained LDs (**Fig. 3.8B**). Untreated differentiated CCTα-KO cells had fewer and larger LDs compared with untreated controls, and oleate treatment appeared to exert minimal effect on LD morphology. Furthermore, 18:1-lyso-PC supplementation appeared to partially revert LD distribution in oleate-treated CCTα-KO cells back to that of control cells. Quantification of cross-sectional LD area revealed a significant reduction in small LDs ($<2\ \mu m^2$) and an increase in large LDs ($>10\ \mu m^2$) in CCTα-KO cells (**Fig. 3.8C**). Accompanying the increase in the proportion of large LDs, the total number of LDs per cell was reduced in CCTα-KO cells (**Fig. 3.8D**). Exposure to oleate did not affect LD size or number, but incubation of CCTα-KO cells with oleate and 18:1-lyso-PC shifted the size distribution and number of LDs toward that of control cells (**Fig. 3.8C and D**). Thus, these data indicate that CCTα deficiency in differentiated Caco2 cells also leads to

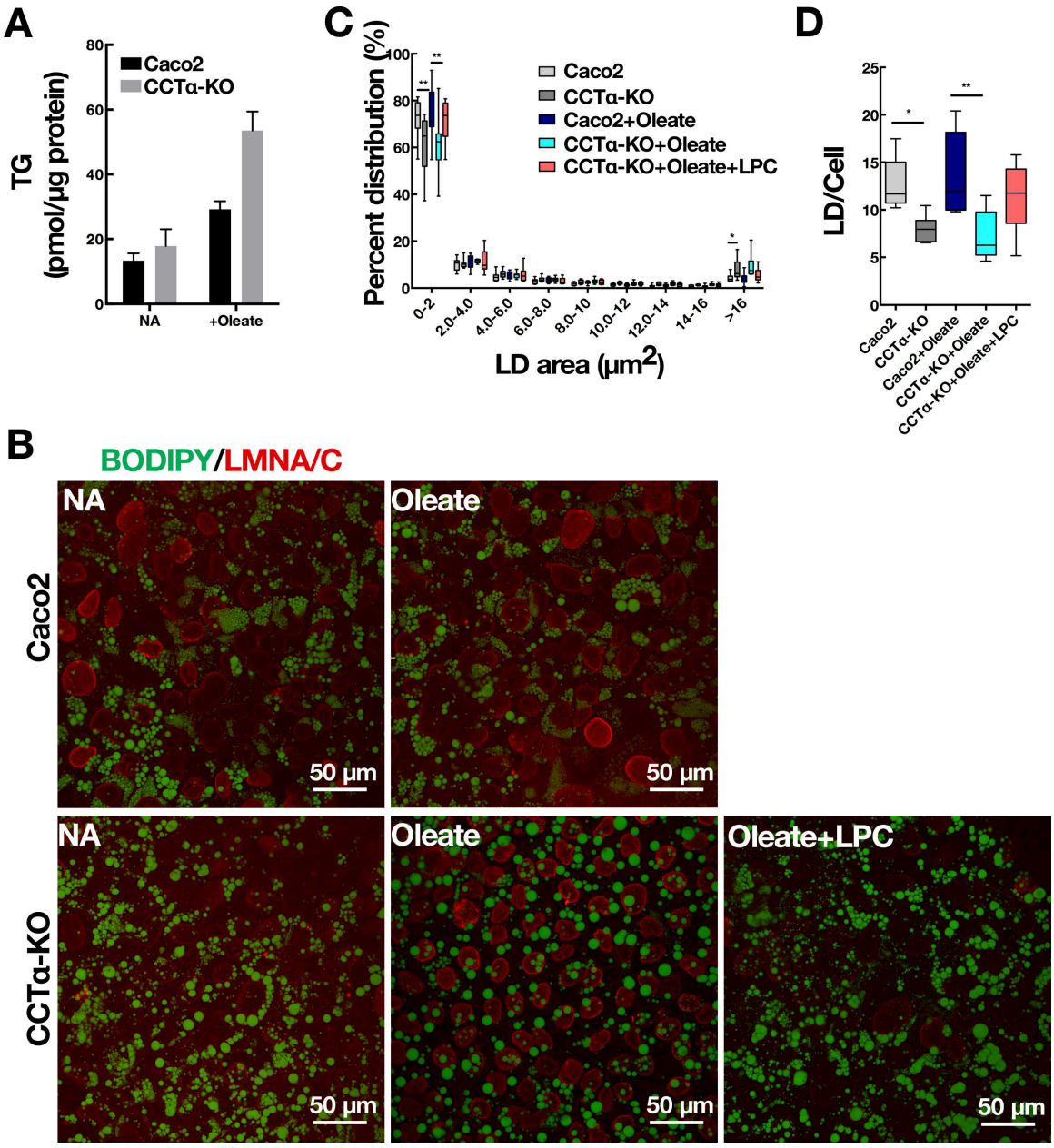

Figure 3.8. Altered LD morphology in differentiated CCTα-KO cells. TG mass in differentiated Caco2 and CCTα-KO cells cultured in the absence (NA, no addition) or presence of oleate/BSA (400 µM) for 12 h **(A)**. Representative confocal image of cells incubated with no addition, OA, or OA plus 18:1-lysoPC (LPC, 25 µM) for 12 h. LDs were visualized with BODIPY-493/503 and nuclei were immunostained with LMNA/C-monoclonal and AlexaFluro594-secondary antibodies (**B**). The cross-sectional area of LDs was quantified and binned into ranges. Six fields of cells from three separate experiments. ANOVA **P*<0.01, ***P*<0.001 **(C)**. The number of LDs in each cell was quantified **(D)** from data in **(C)**. **P*<0.05 compared with Caco2 controls. ANOVA **P*<0.01, ***P*<0.001.

altered LD morphology, and that the Lands pathway can substitute for the CDP-choline pathway when sufficient exogenous lyso-PC is provided.

3.1.3 Reduced TG Secretion in Chylomicrons by CCTα-KO Cells

To assess whether CCTα deficiency affects TG and lipoprotein secretion by differentiated cells, [^{3}H]oleate was added to the apical medium for 12 h and incorporation into cellular and basally secreted TG and CE was quantified (**Fig. 3.9**). Incorporation of 200 and 400 μM [^{3}H]oleate into cellular TG in CCTα-KO cells was significantly increased by 1.8- and 2.9-fold, respectively (**Fig. 3.9A**). On the other hand, secretion of [^{3}H]oleate-labelled TG was reduced by 2.4- and 2.0-fold. Similarly, [^{3}H]oleate incorporation into cellular CE was also increased in CCTα-KO cells but secretion was not affected (**Fig. 3.9B**).

TG metabolism was also monitored by pulse-chase labeling of cells with [^{3}H]glycerol to trace the fate of TG after hydrolysis, re-esterification and secretion in lipoproteins (**Fig. 3.10A**). Cells were cultured in medium containing [^{3}H]glycerol and 400 μM oleate/BSA for 12 h to stimulate chylomicron secretion, and intracellular and basal secretion of radiolabeled TG was quantified at the end of 12 h pulse period. To monitor the mobilization and secretion, cells were culture for up to 6 h in medium without [^{3}H]glycerol or oleate (chase). As expected, there was a significant cellular accumulation of [^{3}H]glycerol-labeled TG in CCTα-KO cells, which was accompanied by a reduction in secretion at the end of pulse period. Interestingly, the level of cellular [^{3}H]glycerol-labeled TG in CCTα-KO cells declined during the 6 h chase period but remained higher relative to controls. It appeared that CCTα deficiency did not affect

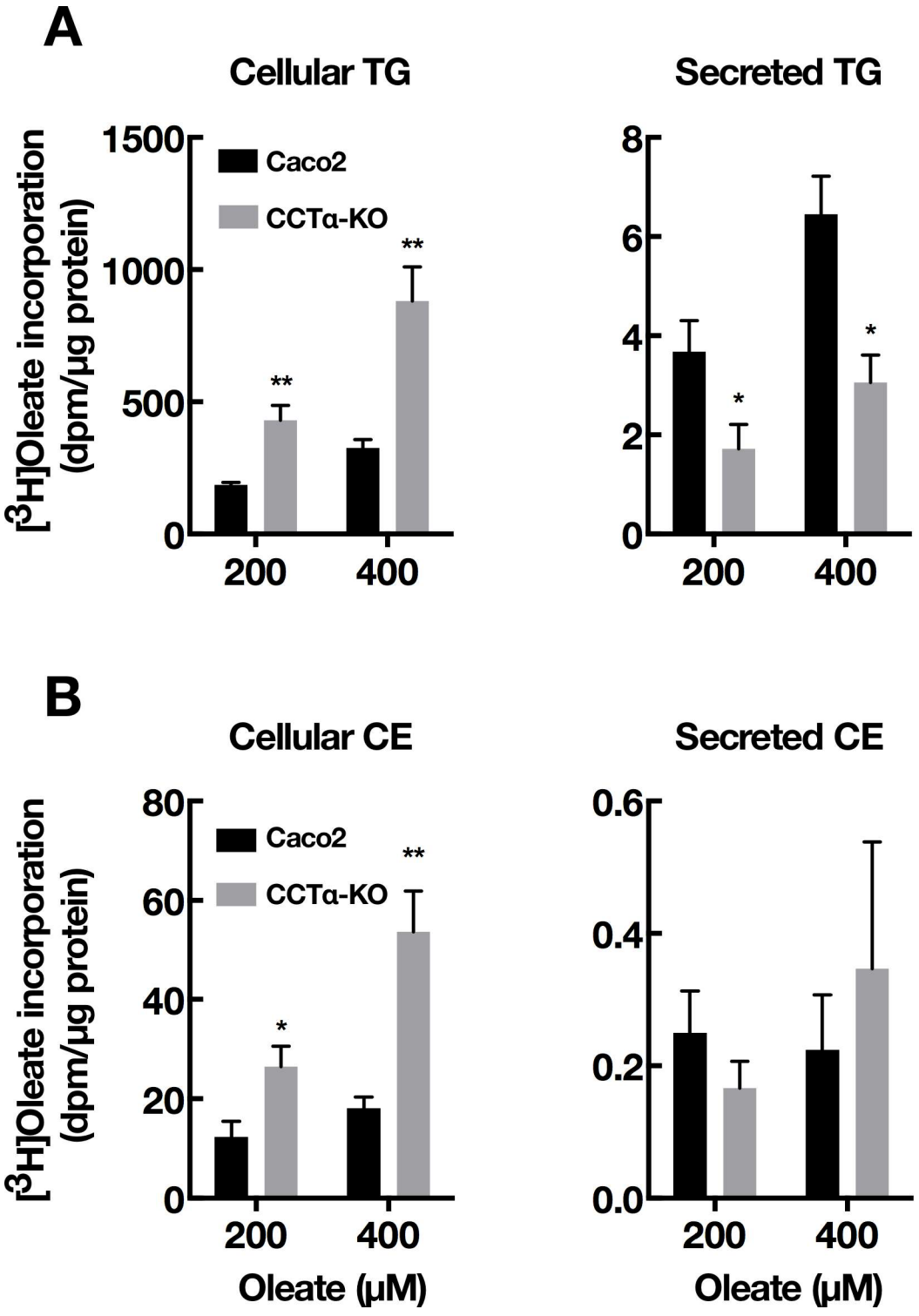

Figure 3.9. Intracellular TG accumulation and impaired TG secretion in CCTα-KO cells. Differentiated Caco2 and CCTα-KO cells were cultured with [^{3}H]oleate/BSA (200 and 400 µM), and incorporation into intracellular and secreted TG **(A)** and CE **(B)** was measured after 12 h. The results are the mean and SEM of three experiments. **P*<0.05, **<0.01 compared with Caco2 controls.

secretion during the chase period but the ratio of secreted to cellular TG revealed an overall 1.8-fold reduction. Collectively, CCTα knockout resulted in intracellular accumulation and reduced secretion of TG.

PC and PE metabolism were also monitored in the same experiment. Cellular [^{3}H]glycerol-labeled PC levels were not affected in CCTα-KO cells, but secretion was diminished at the end of the pulse period (**Fig. 3.10B**). PC secretion in control and CCTα-KO cells was similar during the chase period. The secretion of [^{3}H]glycerol-labeled PE by CCTα-KO was also reduced at the end of pulse period (**Fig. 3.10C**). However, cellular and secreted PE was slightly increased during the chase period.

Increased intracellular TG mass (**Fig. 3.8A**) and reduced secretion of radiolabeled TG (**Figs. 3.9 and 3.10**) by differentiated CCTα-KO cells suggested that CCTα knockout affected chylomicron secretion. To investigate this, basolateral secretion of apoB-48- and apoB-100-containing chylomicrons was measured. CCTα expression in Caco2 cells was not altered during differentiation or in response to 12 h exposure to 200 or 400 μM oleate/BSA (**Fig. 3.11A**). To assess whether CCTα affected lipoprotein secretion, cells were treated with or without 400 μM oleate/BSA for 12 h, and the 1.006 g/mL fraction was isolated from the basolateral medium by ultracentrifugation. Immunoblotting showed that apoB-48 secretion from Caco2 cells was increased >3-fold in response to oleate (**Fig. 3.11B and C**). ApoB-48 secretion by CCTα-KO cells incubated with or without oleate was <10% of control counterparts. Caco2 cells also secreted significant amounts of apoB-100, which was not significantly affected by CCTα knockout or exogenous oleate (**Fig. 3.11B and D**). Furthermore, secretion of apoB-100 into the higher density fraction (1.006-1.21 g/mL) was also unaffected (**Fig. 3.11B**). To assess

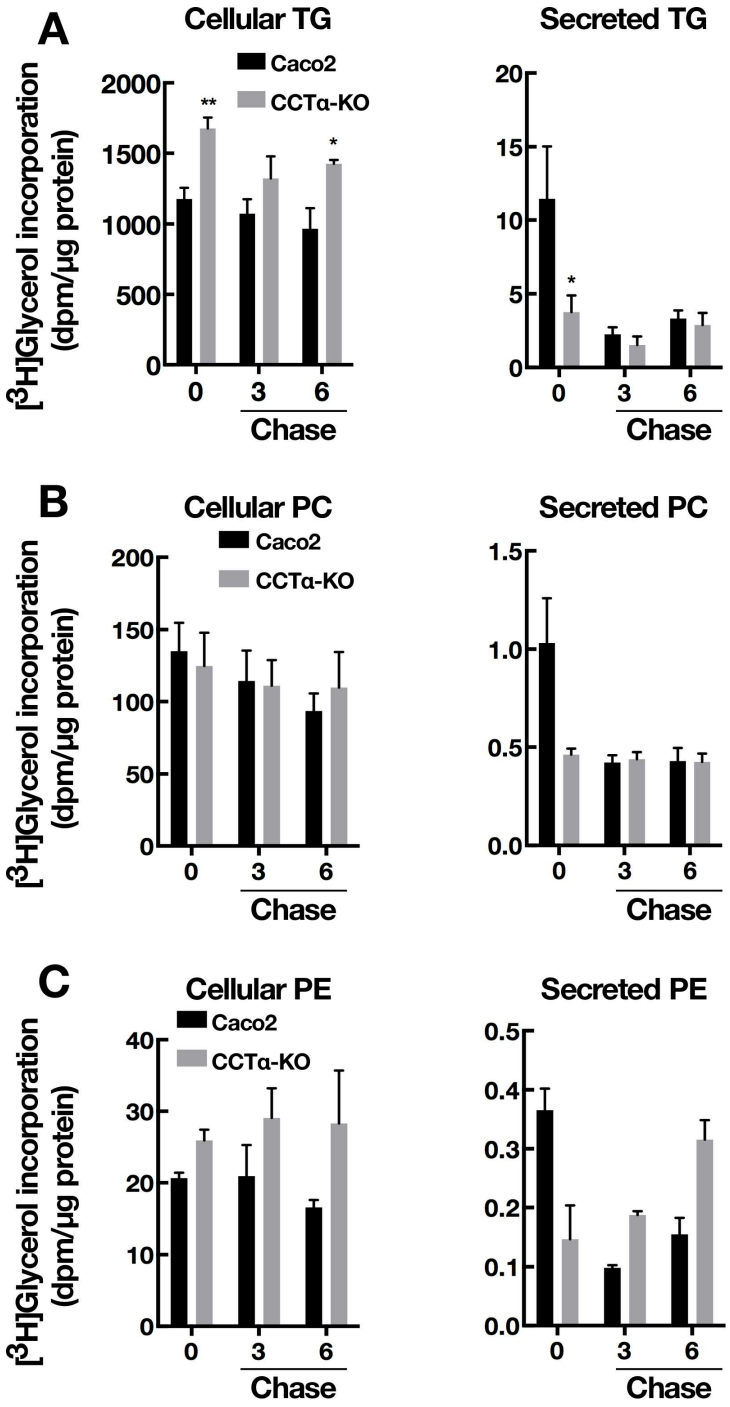

Figure 3.10. Impaired secretion of [^{3}H]glycerol-labeled TG in CCTα-KO cells. Differentiated Caco2 and CCTα-KO cells were cultured with [^{3}H]glycerol (2µCi/ml) and oleate/BSA (400 µM) for 12 h. Cells and basolateral media were collected (0 h), or cells were subjected to an additional 3 and 6 h chase period in isotope-free medium. At the indicated times, [^{3}H]glycerol incorporation into cellular and secreted TG was quantified. The results are the mean and SEM of three experiments. *P<0.05 compared with Caco2 controls **(A)**. Intracellular levels and secretion of [^{3}H]glycerol-labeled PC **(B)** and PE **(C)**. Results are the mean and range of two experiments.

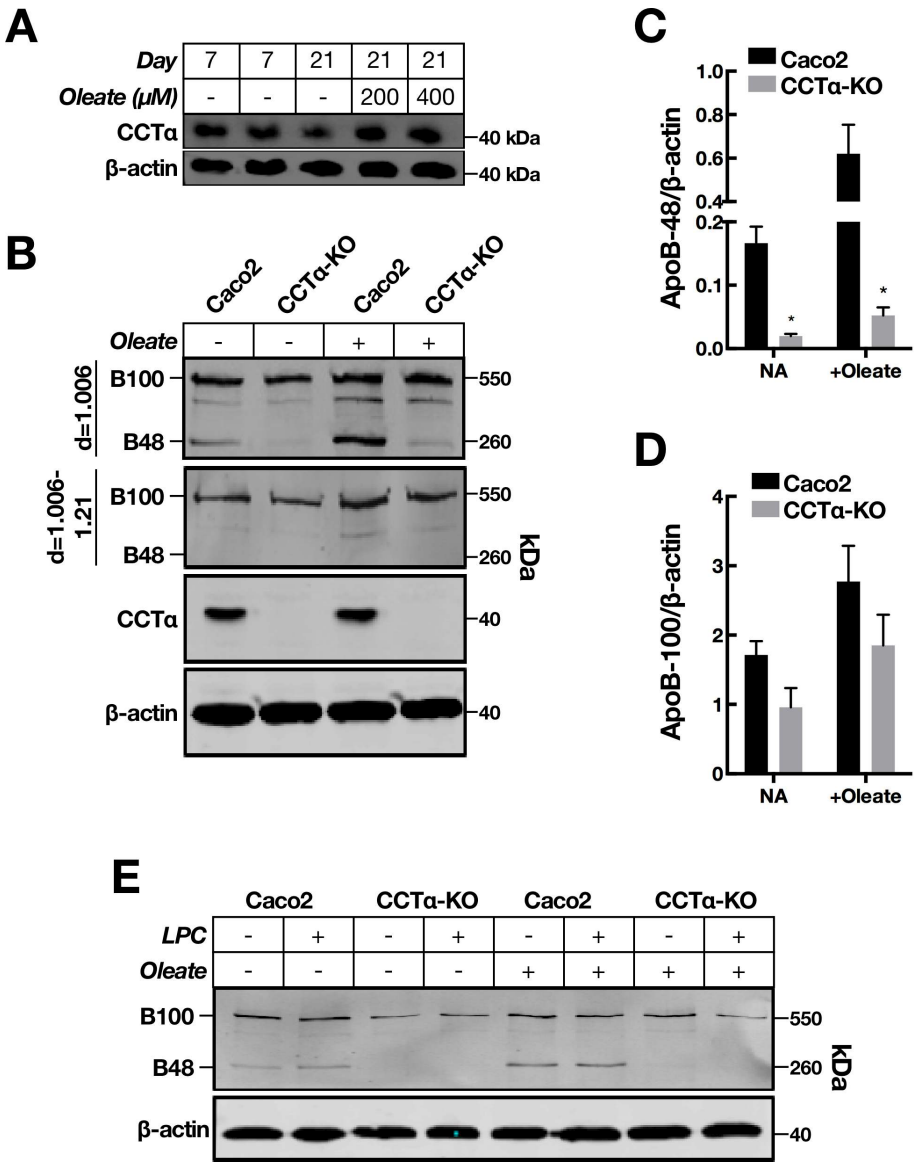

Figure 3.11. Decreased apoB-48 chylomicron secretion by CCTα-KO cells. CCTα expression was monitored in Caco2 cells during a 21-day differentiation period and after exposure to oleate/BSA for 12 h **(A)**. Differentiated Caco2 and CCTα-KO cells were treated with oleate/BSA (400 μM) on the apical surface for 12 h. Basolateral medium was collected and lipoproteins in the 1.006 g/ml and 1.006-1.21 g/ml density fractions were isolated by sequential ultracentrifugation. apoB-48 and apoB-100 was resolved by SDS-5%PAGE and immunoblotting **(B)**. apoB-48 **(C)** and apoB-100 **(D)** in the d = 1.006 g/ml fraction was quantified from immunoblots in **(B)** and expressed relative to cellular actin. The results are the mean and SEM of three experiments. **P*<0.01, ***P*<0.005 compared with Caco2 controls **(C** and **D)**. Cells were treated with indicated combinations of oleate/BSA (400 μM) and 18:1-lysoPC (25 μM) in apical medium for 12 h. Lipoproteins in the 1.006 g/ml fraction were isolated and immunoblotted for apoB as described above **(E)**.

whether apoB-48 secretion by CCTα-KO cells can be restored by lyso-PC supplementation, cells were cultured in the absence and presence of oleate/BSA and 18:1-lyso-PC for 12 h. Immunoblotting revealed that lyso-PC supplementation did not restore the secretion of apoB-48 by CCTα-KO cells (**Fig. 3.11E**). As well, apoB-48 or apoB-100 secretion by control cells was not affected by exogenous lyso-PC. Taken together, these data show that TG secretion in apoB-48 containing chylomicrons by Caco2 cells specifically requires PC synthesis by the CDP-choline pathway.

3.2 Discussion

The assembly and secretion of chylomicrons is essential for delivery of dietary fatty acids to peripheral tissues. The dietary TG is hydrolyzed in the intestinal lumen by lipases to yield fatty acids and MG. These hydrolysis products are efficiently taken up by enterocytes at the brush border membrane, esterified into TG and stored in cytoplasmic LDs or assembled into chylomicrons for secretion. Previous studies showed that CCTα knockdown and inhibition of PC synthesis in mammalian cells resulted in fewer LDs of large size (2), and reduced VLDL secretion by mouse liver (11), suggesting an important role in providing the phospholipid surface monolayer. In this study, Caco2 cells with a knockout of CCTα were used to show a specific requirement of the CDP-choline pathway for intestinal TG storage in LDs and the mobilization of TG for secretion in chylomicrons. Caco2 cells are a human epithelial colorectal carcinoma that undergoes spontaneous differentiation into polarized and columnar monolayers when grown on filter inserts. Differentiated cells display morphological and functional properties of small

intestine enterocytes, making them an excellent *in vitro* model for studying intestinal lipid metabolism.

Consistent with previous reports for other mammalian cells (2), CCTα was exclusively localized to the nucleoplasm of Caco2 cells and did not translocate to LDs formed by oleate exposure (**Fig. 3.1B**), suggesting that the enzyme was active within the nucleus. CCTβ2 is not expressed in adult human intestine but was detected in Caco2 cells (**Fig. 3.1A**). This dissimilarity between adult enterocytes and Caco2 cells could be related to the transformed phenotype of Caco2 cells. However, the expression of CCTβ2 more likely reflects the development state since Caco2 cells have features of fetal tissue (i.e. apoB-100 secretion) and CCTβ mRNA expression in fetal tissues typically decreases or disappears during development.

Metabolic labeling with [^{3}H]choline showed that CRISPR/Cas9-mediated knockout of CCTα resulted in an approximate 50% reduction in PC synthesis (**Fig. 3.2A**). Because CCTβ2 lacks an NLS, the residual PC synthesis would be provided by the cytoplasmic arm of the CDP-choline pathway. [^{3}H]CDP-choline (**Fig. 3.2C**) and [^{3}H]GPC (**Fig. 3.2D**), the product of CCTα and PC degradation, respectively, were also reduced during the labeling period. The incorporation of [^{3}H]choline into CDP-choline is relatively low in comparison to PC, suggesting that the transient decrease in [^{3}H]CDP-choline could be due to a rapid conversion of CDP-choline produced by CCTβ2 to PC by CPT/CEPT. Pulse-chase labeling experiment showed that the turnover of [^{3}H]choline-labelled PC in CCTα-KO cells was not affected (**Fig. 3.2F**). As a result, the proliferation of knockout cells was reduced by 30-40% (**Fig. 3.2G**). Interestingly, [^{3}H]pCholine, the substrate of CCTα, did not accumulate in CCTα-KO cells (**Fig. 3.2B**). This was

surprising because CCTα catalyzes the conversion of pCholine to CDP-choline, and a knockout of CCTα was expected to cause substrate accumulation. Reduced choline transporter activity due to reduced PC levels or altered phospholipid composition in the plasma membrane was discounted as a cause (**Fig. 3.2E**). However, it is feasible that knockout of CCTα also reduces CK expression/activity and pCholine by an indirect mechanism. Taken together, loss of nuclear CCTα did not cause a bottleneck in the CDP-choline pathway but residual PC synthesis provided by cytosolic CCTβ2 was not sufficient to maintain cell proliferation.

Despite a reduction in synthesis and no effect on PC turnover in CCTα-KO cells, the mass of major molecular species of PC and PE was not affected in undifferentiated or differentiated cells (**Fig. 3.3**). Interestingly, differentiated cells contained more long-chain unsaturated PC species compared to undifferentiated controls. Furthermore, this shift in the molecular species was independent of reduced *de novo* PC synthesis caused by CCTα deficiency. Enterocytes and differentiated Caco2 cells contain highly curved microvilli brush border membrane (308). Because the fatty acyl composition of phospholipids is determined by Lands remodeling pathways, one possible explanation for the shift is altered availability of long-chain unsaturated fatty acids or the expression of lipases and LPCATs during Caco2 cell differentiation that would modify PC molecular species.

Imaging of BODIPY-stained LDs showed that loss of CCTα and partial inhibition of PC synthesis resulted in the formation of fewer larger LDs and increased TG mass (**Fig. 3.4**). This could be due to a diversion of DG from the CDP-choline pathway into TG synthesis, leading to TG accumulation. However, this is unlikely because

undifferentiated CCTα-KO cells had reduced [^{3}H]oleate and [^{3}H]glycerol incorporation into TG (**Fig. 3.5**). The most likely reason is that large LDs are formed by fusion of small PC-poor nascent LDs, and the reduced surface to volume ratio of large LDs may reduce TG turnover by preventing the access of lipases to the surface. Interestingly, our previous study using shRNA-mediated knockdown of CCTα showed a similar LD phenotype in rat IEC-18 cells (2). However, these cells displayed decreased TG deposition and cytotoxicity in response to oleate, possibly due to accumulation of unesterified free fatty acid. This discrepancy could relate to the relatively low expression of CCTβ2 isoform in IEC-18 cells, which could result in more profound suppression of PC synthesis and inhibition of TG storage.

Transient expression of mCherry-CCTα in CCTα-KO cells restored LD size distribution and number back to control cells (**Fig. 3.6**), confirming that the LD phenotype was due to loss of CCTα. Because LPCAT1 and LPCAT2 synthesize PC on the surface of LDs when supplied with lyso-PC, and silencing of either enzyme increased LD size that was accompanied by decrease in number (270), it was thought that PC synthesized by the LPCAT activity may substitute for the CDP-choline pathway if sufficient lyso-PC is supplied. As expected, 18:1-lyso-PC supplementation restored LD morphology in CCTα-KO cells (**Fig. 3.7**), indicating that the source of PC is not critical for maintaining LD morphology. However, 18:0-lyso-PC supplementation did not effectively reverse LD phenotype. It is possible that the fatty acyl chain composition of phospholipid monolayer affects membrane properties such as curvature, fluidity, lipid packing and membrane protein function. Thus, 18:0-lyso-PC supplementation could be insufficient to provide membrane stability to avoid LD coalescence. Indeed, artificial

emulsions of TG prepared with unsaturated PC formed smaller droplets than those prepared with saturated PC. These data indicate that not only the polar head group of phospholipids but also the degree of acyl chain unsaturation is important for regulating the size of LDs. The reduced efficacy of 18:0-lyso-PC in CCTα-KO cells could also be due to reduced utilization by LPCATs. However, this is unlikely because LPCAT1 and LPCAT2 have similar substrate preferences (101), and LPCAT1 exhibits only slightly higher enzymatic activity towards 18:1-lyso-PC (270).

Interestingly, CCTα knockout showed a differential effect on apoB-100 and apoB-48 secretion. Secretion of apoB-48 was reduced by 90% in CCTα-KO cells under basal and oleate-treated conditions (**Fig. 3.11B and C**) and apoB-100 secretion was unaffected (**Fig. 3.11B and D**). This was surprising since CCTα knockout in hepatocytes caused a 75% reduction in PC synthesis and inhibited secretion of apoB-100-containing VLDL (11). The lack of effect on apoB-100 secretion is likely due to less severe inhibition of the CDP-choline pathway (50% reduction in PC synthesis, **Fig. 3.2A**) due to CCTβ2 in Caco2 cells and/or a reduced requirement for phospholipids and TG to assemble VLDL. Alternately, it is possible that chylomicrons and VLDL are produced by separate pathways. A previous study using Caco2 cells showed that the secretion of VLDL utilizes preformed TG and is not stimulated by oleate whereas newly synthesized TG was preferentially used for chylomicron secretion (309). This could be explained by the existing pool of LDs in differentiated cells and their abnormal size distribution in differentiated CCTα-KO cells under basal conditions (**Fig. 3.8**). Secretion of apoB-100 by differentiated Caco2 cells was approximately 10-fold higher than apoB-48 (**Fig. 3.11B, C and D**), suggesting that cellular pool of TG in pre-existing LDs could be a

precursor for VLDL, but not for chylomicrons. Incubation with oleate resulted in a >3-fold increase in secretion of apoB-48, but did not significantly affect apoB-100 secretion. This is consistent with a study using complex lipid micelles mimicking post-digestive duodenal micelles, which favored secretion of apoB-48-containing lipoproteins by Caco2 cells (310). In another study, intraduodenal administration of Pluronic L-81, a non-ionic hydrophobic surfactant, in rats, preferentially inhibited chylomicron secretion but not VLDL secretion (311).

Accompanying the blockage in chylomicron and [^{3}H]oleate- or [^{3}H]glycerol-labeled TG secretion (**Fig. 3.9 and Fig. 3.10**), differentiated CCTα-KO cells also had fewer but larger LDs, and stored significantly more TG than controls (**Fig. 3.8**). The accumulation of TG in CCTα-KO cells could be due to inhibition of secretion. However, a comparison of secreted versus intracellular levels of [^{3}H]oleate- or [^{3}H]glycerol-labeled TG indicate that secreted TG would account for such a small fraction of the cellular pool (2-4%) that a 50% blockage in the secretion would have minimal impact on cellular accumulation. It is not clear whether the TG secreted in chylomicrons was initially stored in LDs and then mobilized by lipolysis, or was directly assembled into chylomicrons in the ER. However, since CCTα knockout had no effect on TG synthesis but increased TG mass in undifferentiated cells (**Fig. 3.5C**) and the secretion of [^{3}H]glycerol-labeled TG by differentiated CCTα-KO cells was reduced during a chase period (**Fig. 3.10),** we posit that the mobilization of TG in LDs was partially defective. In support of this, Pluronic L-81 treatment of Caco2 cells enhanced cytosolic TG accumulation and inhibited chylomicron secretion by interfering with the transfer of TG from the cytosol to the ER (312).

Lastly, because 18:1-lyso-PC supplementation of CCTα-KO cells partially shifted the size distribution and number of LDs toward that of control cells (**Fig. 3.7 and 3.8**), it was thought that 18:1-lyso-PC supplementation would induce apoB secretion. However, 18:1-lyso-PC did not affect apoB-48 or apoB-100 secretion by either both Caco2 and CCTα-KO cells (**Fig. 3.11E**). It is possible that exogenous 18:1-lyso-PC was preferentially utilized by LPCAT to form PC on the surface of cytosolic LDs. LPCAT activity would synthesize PC that was available to correct LD morphology in CCTα-KO cells, indicating a redundancy between the Lands remodeling and CDP-choline pathways for PC synthesis for LD biogenesis. However, PC availability for chylomicron assembly could still be limiting due to insufficient PC synthesis by ER-localized enzymes of the CDP-choline pathway. Thus, PC synthesized by the CDP-choline pathway may be preferred for chylomicron assembly.

CHPATER 4: Nuclear Lipid Droplet-associated Factors Regulate Cellular Triglyceride and Phosphatidylcholine Metabolism

4.1 Results

4.1.1 CCTα Deficiency Alters nLD Morphology in Caco2 Cells

Previous studies showed that nLDs associate with PML-NBs and CCTα in Huh7 cells (14). We confirmed that BODIPY-positive nLDs were associated with endogenous PML-NBs and CCTα in 24 h oleate-treated U2OS (**Fig. 4.1A**), Caco2 (**Fig. 4.1B**) and HepG2 cells (**Fig. 4.1C**). To assess the effect of CCTα knockout on nLD formation, Caco2 and CCTα-KO cells were incubated with oleate for 12 and 24 h and immunostained for PML and LDs (**Fig. 4.2**). nLD association with PML (indicated with arrows) became apparent after 24 and 12 h treatment in Caco2 and CCTα-KO cells, respectively. At 12 h, when CCTα does not translocate to nLDs (**Fig. 3.4**), CCTα-KO cells had similar number of nLDs and fewer cLDs per cell (**Fig. 4.2** and **4.3A**). Both nLDs and cLDs were increased approximately two-fold in Caco2 cells but did not change in CCTα-KO cells after 24 h treatment. Quantification of cross-sectional area of LDs revealed a significant shift in the distribution from small LDs (<0.4 μm^2) to large LDs (>1μm^2) in both the cytoplasm and nucleus of CCTα-KO cells (**Fig. 4.3B**). Notably, PML expression on nLDs appeared to increase with the size of nLDs during oleate treatment (**Fig. 4.3C**). These indicate that CCTα is essential for not only cLDs but also nLDs, and its absence leads to increase in size and decrease in abundance of nLDs and increased nLD-PML association.

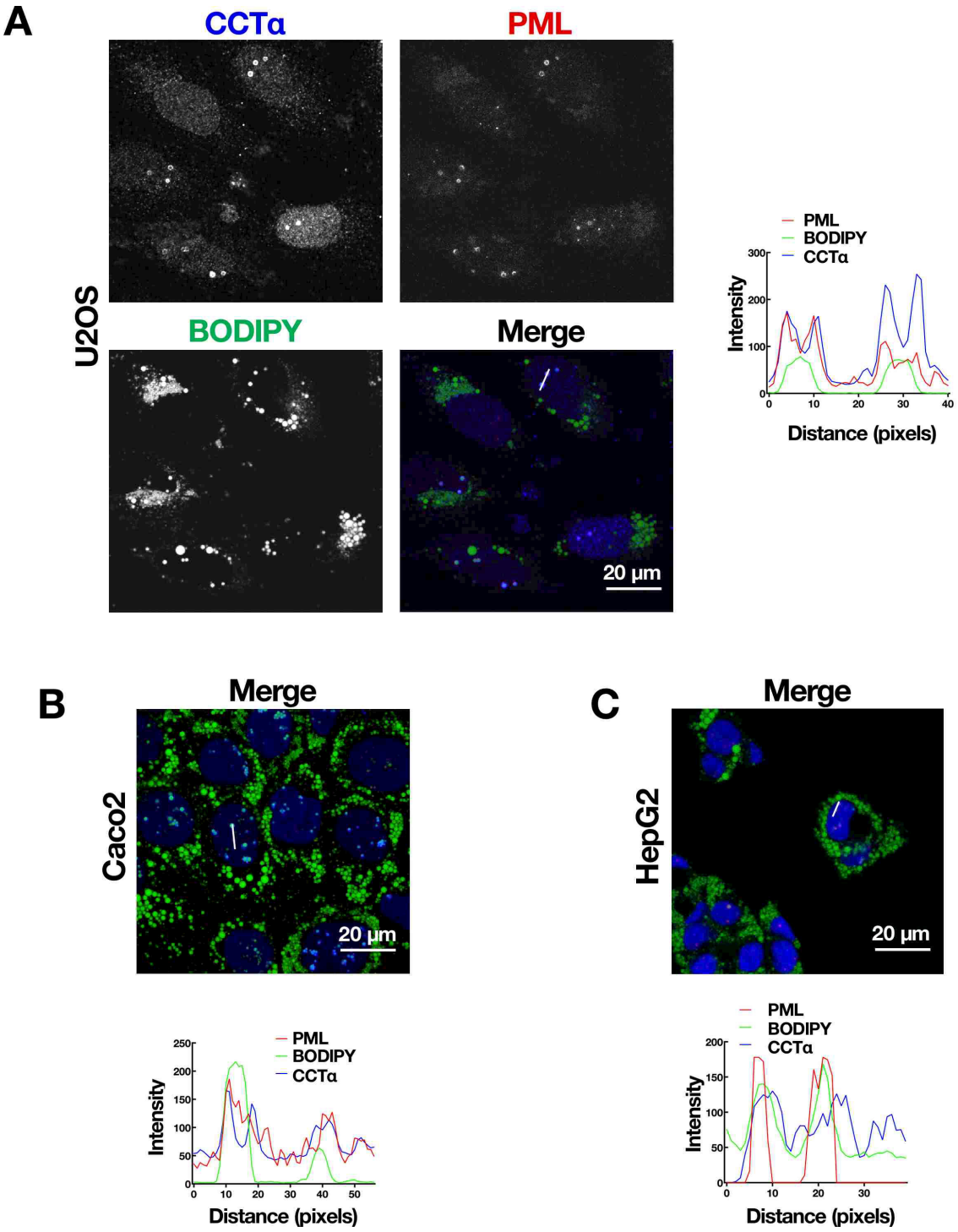

Figure 4.1. Co-localization of CCTα, PML and nLDs. U2OS **(A)**, Caco2 **(B)** and HepG2 **(C)** cells were treated with oleate/BSA (400 μM) for 24 h. Cells were immunostained with CCTα polyclonal and PML monoclonal antibodies followed by AlexaFluor-647 and -594 secondary antibodies, respectively. LDs were visualized with BODIPY-493/504. RGB line graphs show localization of CCTα and PML on the surface of nLDs. Cells were imaged using confocal microscopy.

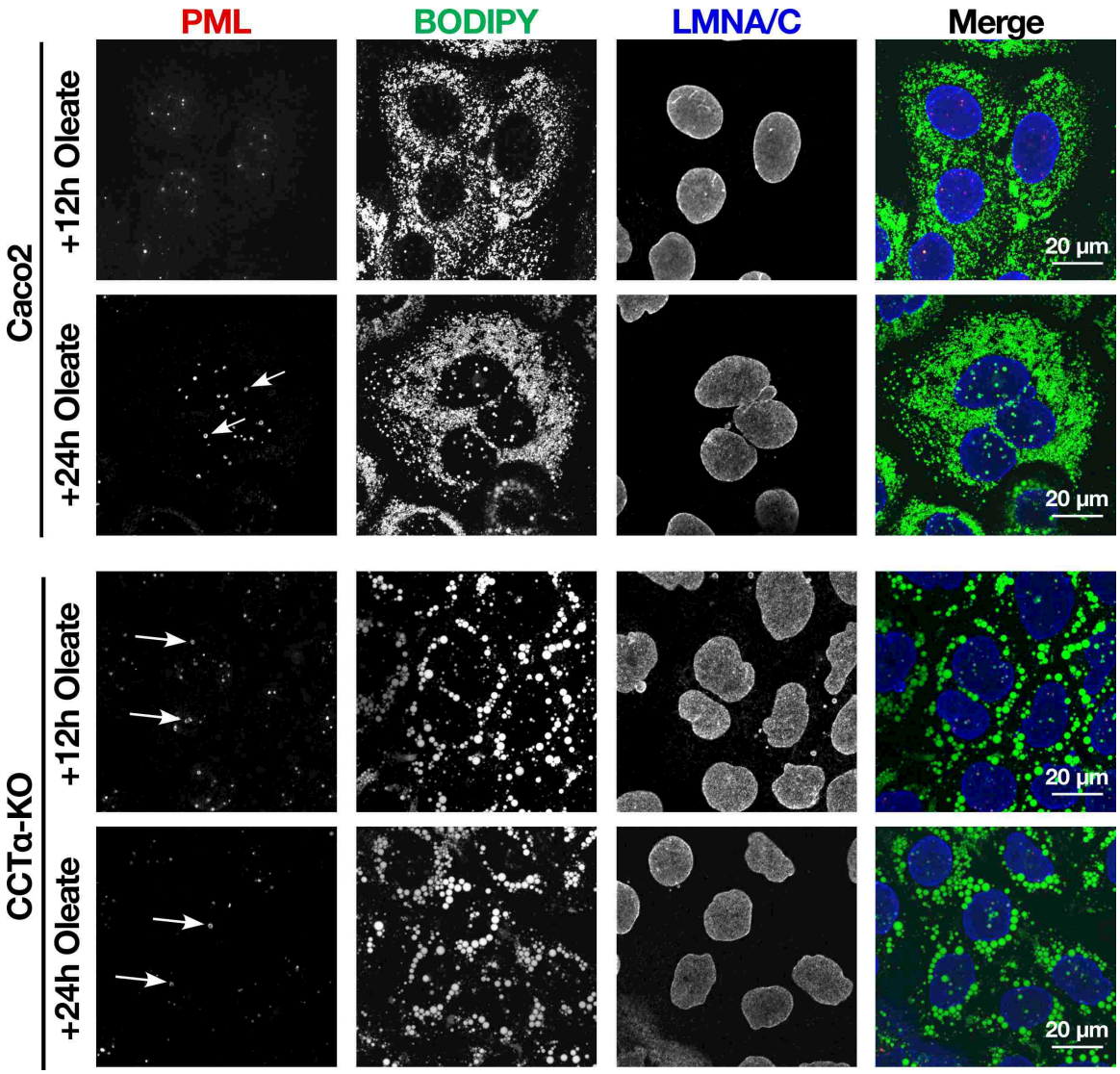

Figure 4.2. Reduced nLD formation and PML-association in CCTα-KO cells. Representative confocal image of Caco2 and CCTα-KO cells treated with oleate/BSA (400 μM) for 12 and 24 h. Cells were immunostained with PML polyclonal and LMA/C monoclonal antibodies followed by AlexaFluor-594 and -647 secondary antibodies, respectively. LDs were visualized with BODIPY-493/504. Arrows indicate PML-associated nLDs.

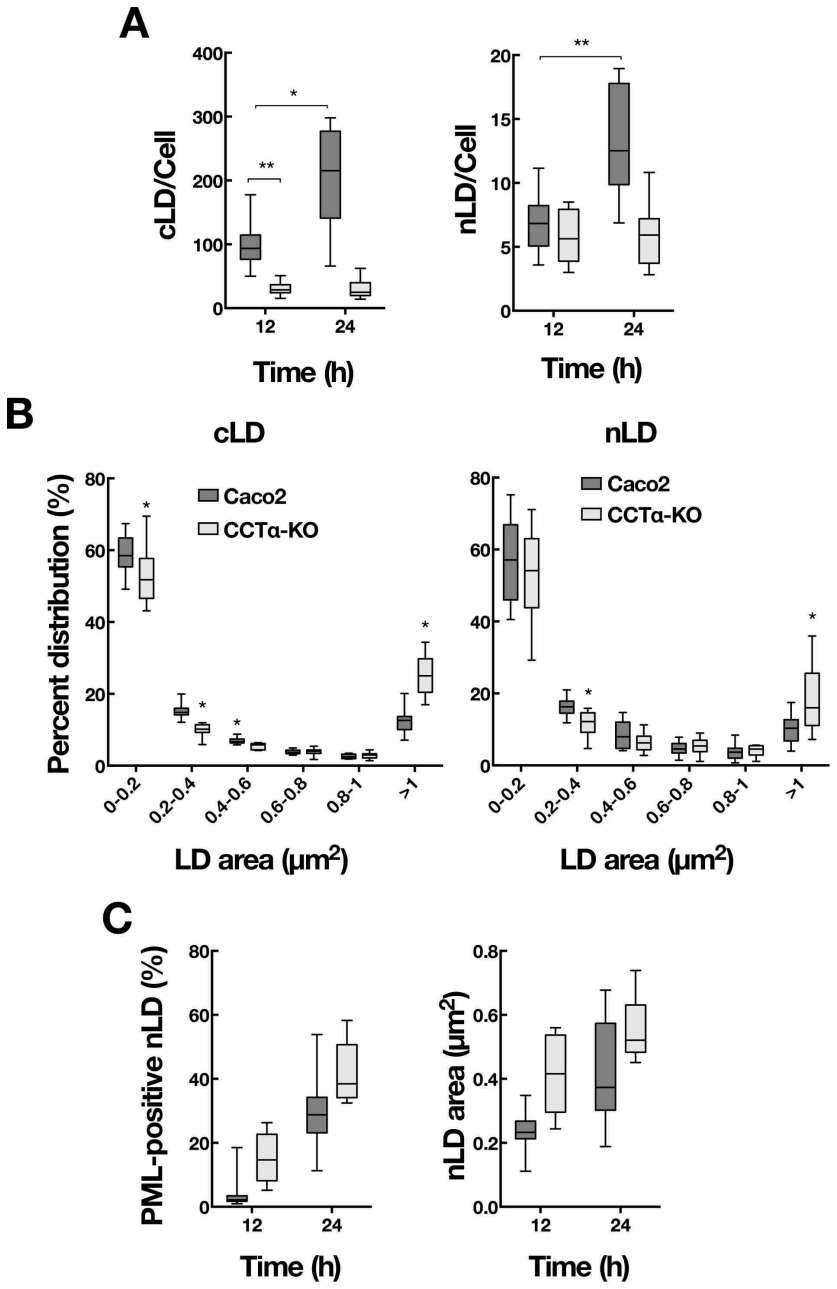

Figure 4.3. CCTα-KO cells have fewer, larger cLDs and nLDs. Quantification of cLDs and nLDs for 3-4 fields of cells from three separate experiments. $^{**}P<0.0005$, $^{*}P<0.005$ **(A)**. The cross-sectional area of cLDs and nLDs in cells (3-4 fields of cells from three separate experiments) treated with oleate/BSA for 24 h was quantified and binned into ranges. $^{*}P<0.05$ **(B)**. Quantification of PML-positive nLDs and cross-sectional area of total nLDs (6-8 fields of cells from two separate experiments) **(C)**.

4.1.2 PML Regulates CCTα Association with nLDs

To investigate the role of PML-NBs in LD biogenesis, U2OS cells with a CRISPR/Cas9 deletion of all PML isoforms were utilized (**Fig. 4.4A**) (305). PML expression in U2OS cells did not change in response to oleate treatment. nLDs in both control U2OS and PML-KO cells had minimal association with the NE protein emerin (**Fig. 4.4B** and **C**; arrows point at the nLDs associated with emerin).

Immunofluorescence microcopy and RGB line plots in cells treated with oleate revealed that CCTα was exclusively expressed in the nucleus and associated with nLDs in U2OS cells whereas PML-KO cells appeared to have fewer BODIPY- and CCTα-positive nLD (**Fig. 4.5A**). PML-KO cells had a significant 41% and 23% reduction in the number of nLDs and cLDs per cell, respectively (**Fig. 4.5B and C**). Compared with control cells, PML-KO cells also had a significant reduction in CCTα-positive nLDs (**Fig. 4.5D**). Quantification analysis of the cross-sectional area of nLDs revealed a significant shift in the distribution from large (> 1μm^2) to small nLDs (<0.5 μm^2) in PML-KO cells (**Fig. 4.5E**), but the area of cLDs in PML-KO cells was similar to controls (**Fig. 4.5F**). The shift toward small nLDs in PML-KO cells resulted in a 40% decrease in average nLD area compared with control cells (**Fig. 4.5G**). However, the size of CCTα-positive nLDs in control and PML-KO cells was comparable.

Consistent with previous studies, GFP-tagged PML-II was associated with LipidTox Red-positive nLDs formed by 24 h oleate treatment of PML-KO cells (**Fig. 4.6A**). The other PML isoforms formed punctate bodies in the nucleus but did not associate with nLDs. Expression of GFP-PML-II also restored the average size of nLDs (**Fig. 4.6C**) and number of both nLDs and cLDs in knockout cells (**Fig. 4.6B**),

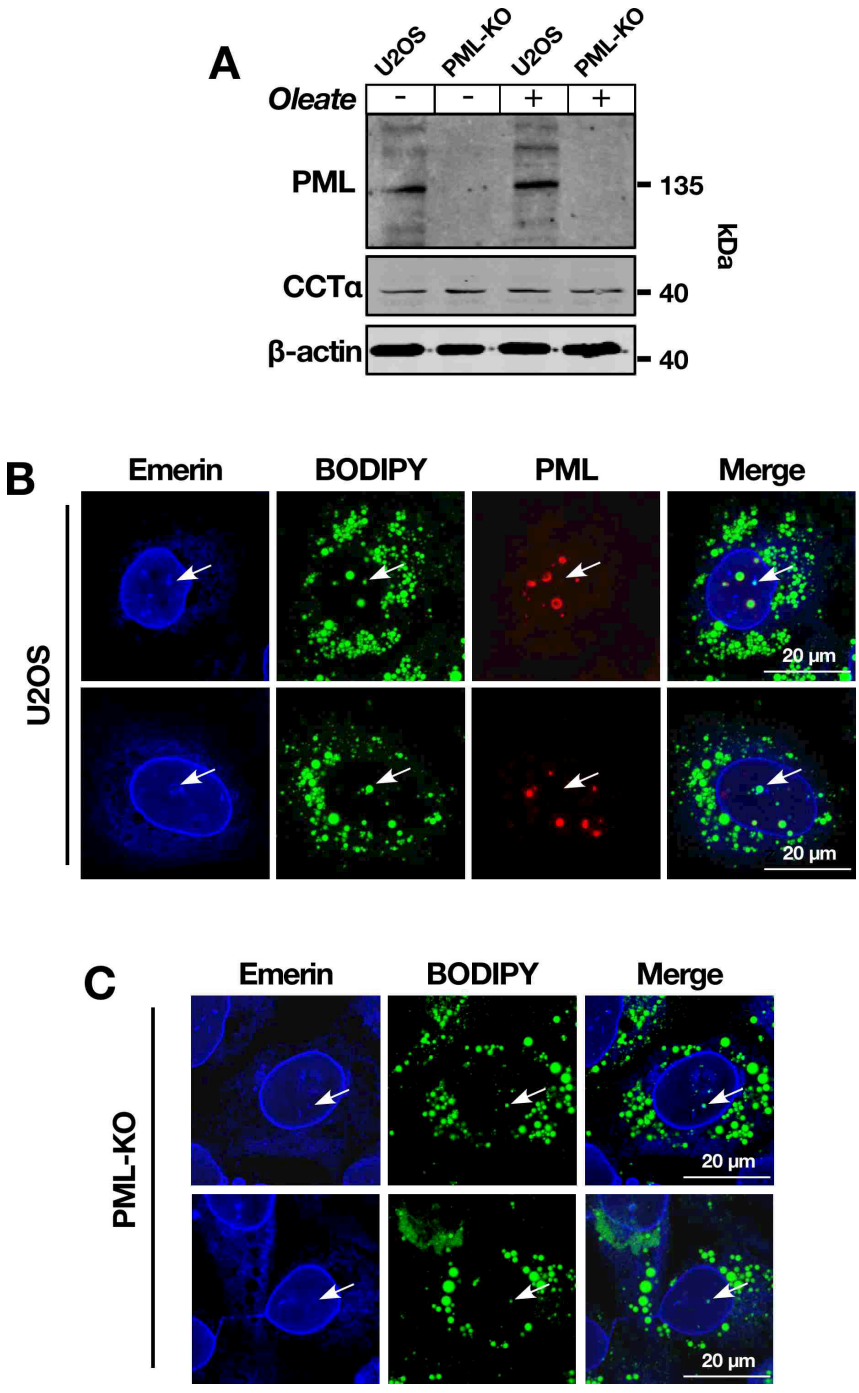

Figure 4.4. **Localization of nLDs with emerin on the nuclear envelope and nucleoplasmic reticulum.** Expression of PML and CCTα in U2OS and PML-KO cells cultured with or without oleate/BSA (400 μM) for 24 h was determined by SDS-PAGE (7%; PML, 8%; CCTα) and immunoblotting **(A)**. U2OS **(B)** and PML-KO **(C)** cells treated with oleate were immunostained with emerin polyclonal and PML monoclonal antibodies followed by AlexaFluor-647 and -594 secondary antibodies, respectively. LDs were visualized with BODIPY-493/504. Arrows indicate the position of PML-negative nLDs that are associated with emerin-positive nucleoplasmic reticulum.

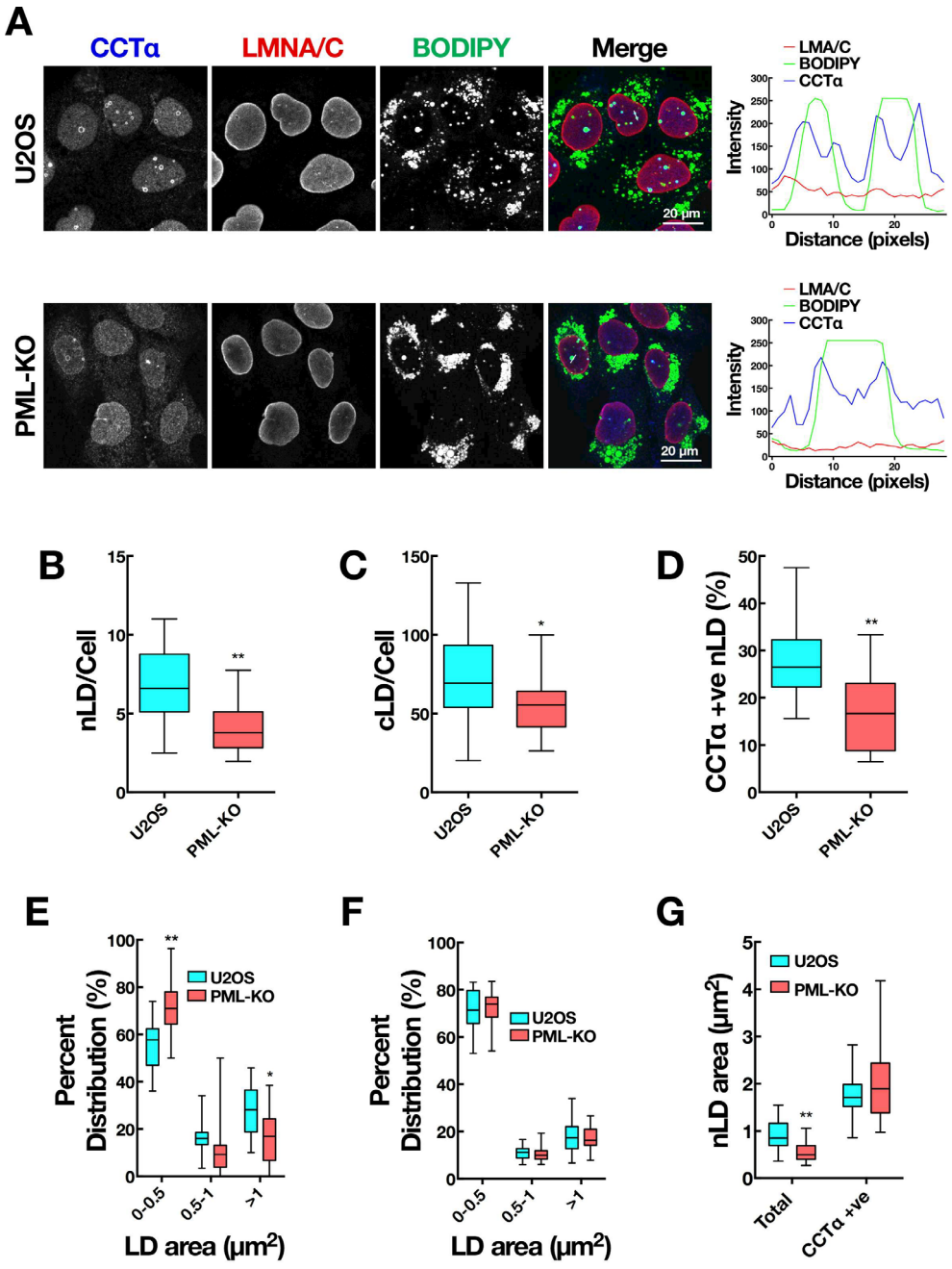

Figure 4.5. **PML regulates the size distribution of nLDs and cLDs.** U2OS and PML-KO cells treated with oleate/BSA (400 μM) for 24 h were immunostained with CCTα polyclonal and LMNA/C monoclonal antibodies followed by AlexaFluor-647 and -594 secondary antibodies, respectively. LDs were visualized with BODIPY-493/504. RGB line graphs show localization of CCTα on the surface of nLDs **(A)**. Quantitation of nLDs **(B)**, cLDs **(C)** and CCTα-positive nLDs **(D)**. The cross-sectional area of nLDs **(E)** and cLDs **(F)** was quantified and binned into ranges. The cross-sectional area of total nLDs and CCTα-positive nLDs was quantified **(G)**. 50-100 cells from three separate experiments. $^{**}P<0.001$, $^{*}P<0.01$ compared with matched control cells.

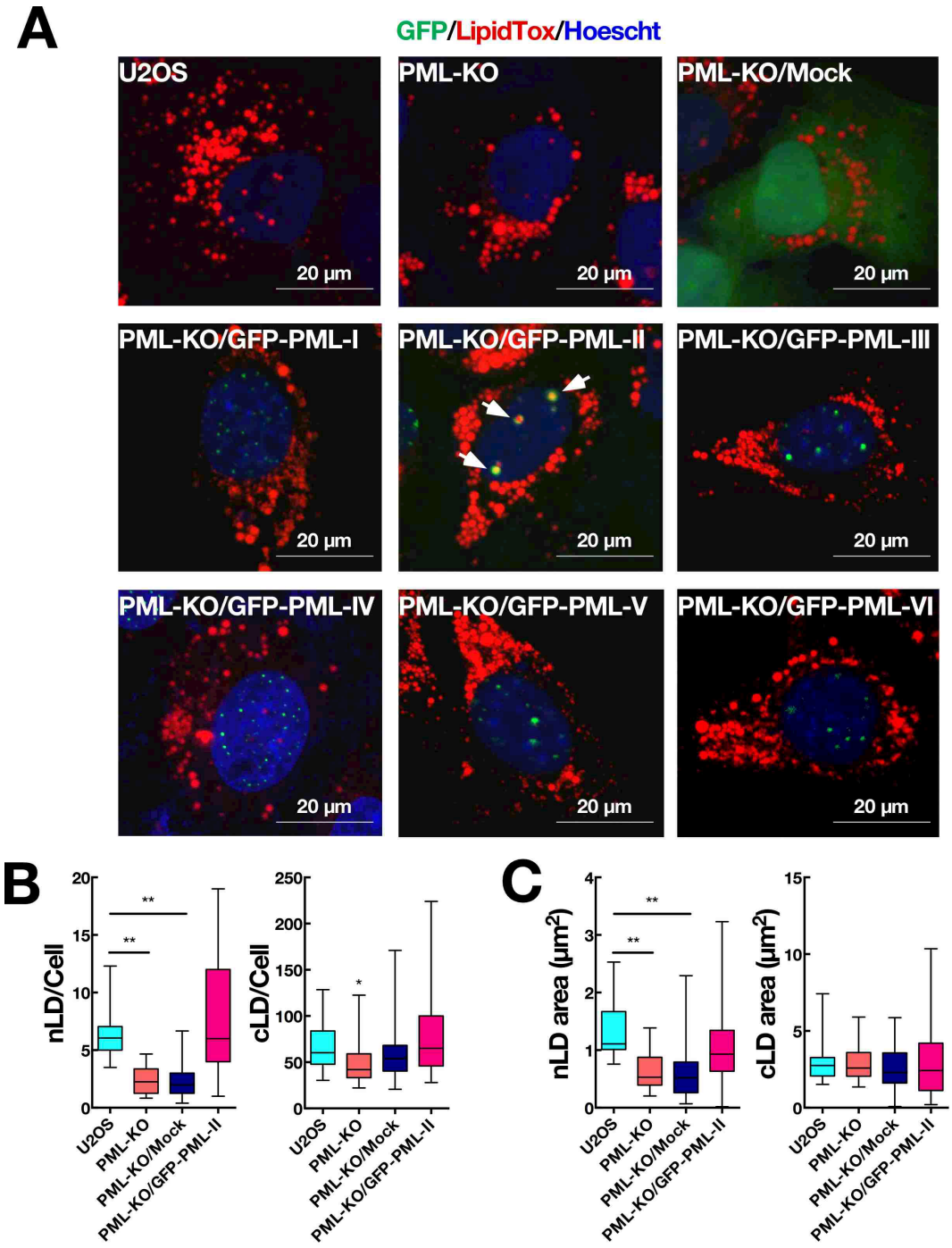

Figure 4.6. Transient expression of GFP-PML-II in PML-KO cells restores number and size of LDs. PML-KO cells were transiently transfected with GFP tagged PML isoforms for 24 h using Lipofectamine 2000. Subsequently, cells were incubated with oleate/BSA (400 µM) for 24 h. LDs and nuclei were visualized with LipidTox Red and Hoechst 33258, respectively. Arrows indicate the association of GFP-PML-II with nLDs **(A)**. The number of nLDs and cLDs in each cell was quantified **(B).** The cross-sectional area of nLDs and cLDs was quantified **(C)**. 25-50 cells from three separate experiments. ***P*<0.001, *P<0.005.

confirming that the LD phenotype shown in Figure 4.4 was caused primarily by PML-II deficiency.

CCTα associates with membranes enriched in DG, which is a substrate shared by the final enzymes of G3P and CDP-choline pathways. To test if PML deficiency affects DG levels on LDs, cells were transiently transfected with the DG biosensor GFP-C1(2)δ (313), and its localization was monitored in cells cultured with or without oleate for 24 h (**Fig. 4.7**). In the absence of oleate, the DG biosensor was present on perinuclear ER and punctate structures in both control and PML-KO cells (**Fig. 4.7A**). In oleate-treated U2OS cells, the biosensor appeared on dispersed cytoplasmic structures that did not correspond to cLDs, and occasionally associated with LipidTox Red-positive nLDs (**Fig. 4.7B, panels a, b and c**). In contrast, the DG sensor was strongly associated with cLDs in PML-KO cells, and there appeared to be few if any DG-positive nLDs (**Fig. 4.7C, panels a, b and c**).

To more efficiently image DG levels on nuclear membranes and nLDs, a tandem NLS was engineered into GFP-C1(2)δ vector, and it was transiently expressed in control and PML-KO cells. This nuclear DG biosensor was detected on two types of structures; small puncta that did not stain with LipidTox Red and larger PML-positive nLDs (**Fig. 4.8A**). For quantification analysis, we divided nLDs into two distinct populations based on the presence or absence of DG. Compared to controls, PML-KO cells had similar number of DG- nLDs but fewer DG+ nLDs (**Fig. 4.8B**), suggesting that PML regulates DG partitioning between the nuclear and cytoplasmic LD populations.

To investigate further, co-localization of the DG biosensor with endogenous PML was monitored in U2OS cells (**Fig. 4.9A**), and nLDs were divided into four distinct

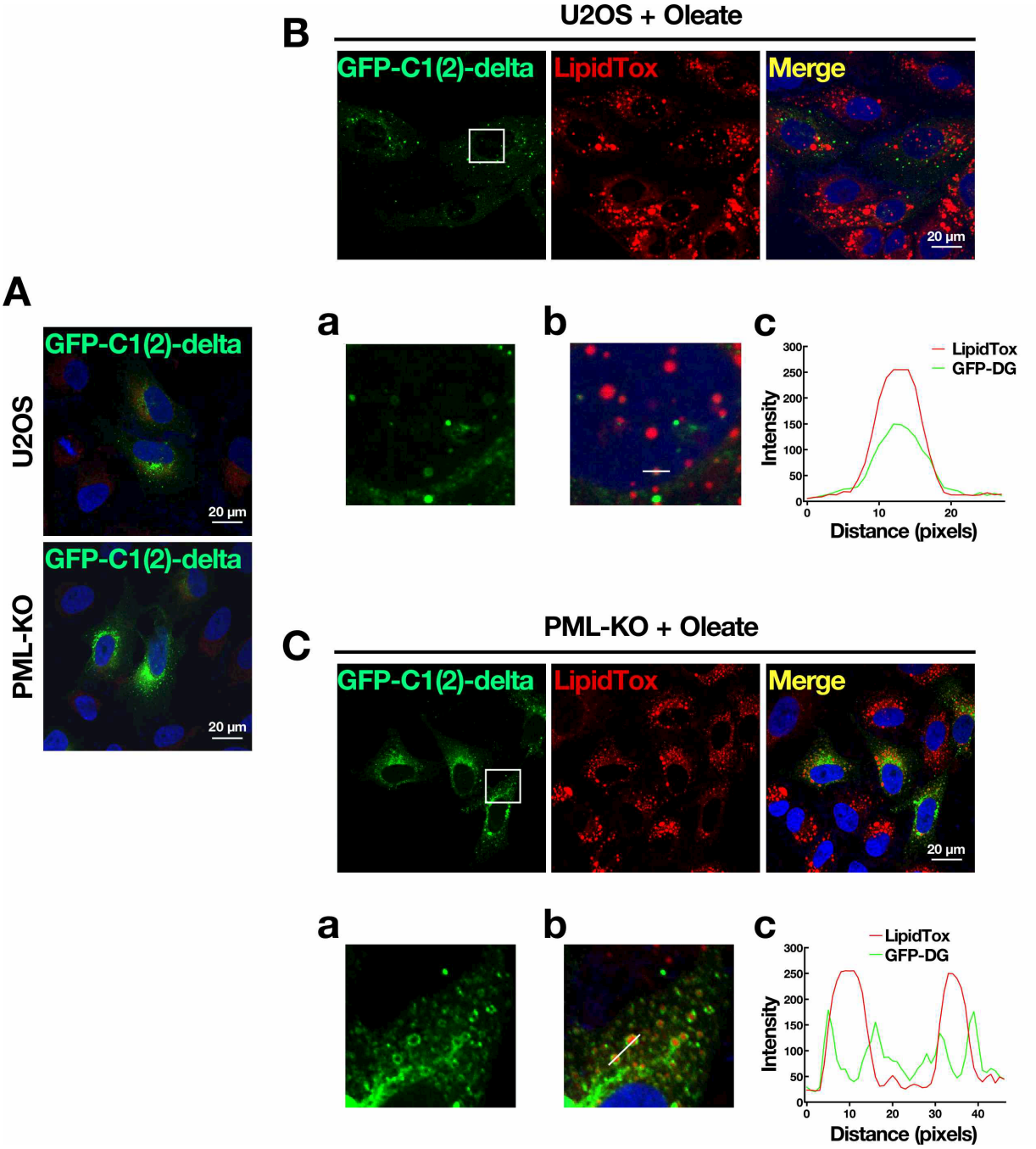

Figure 4.7. **PML affects the partitioning of DG on nLDs and cLDs.** Localization of the DG sensor GFP-C1(2) delta in U2OS and PKL-KO cells **(A)**. U2OS cells expressing GFP-C1(2) delta were treated with oleate/BSA (400 µM) for 24 h. LDs and nuclei were visualized with LipidTox Red and Hoechst 33258, respectively. Highlighted areas from GFP and merged images are shown in panels **a** and **b**. A RGB line plot **(c)** shows the association of the DG sensor with a nLD **(B)**. PML-KO cells were treated as described above. Highlighted areas from GFP and merge images are shown in panels **a** and **b**. RGB line plot (**c**) shows the association of the DG sensor with cLDs.

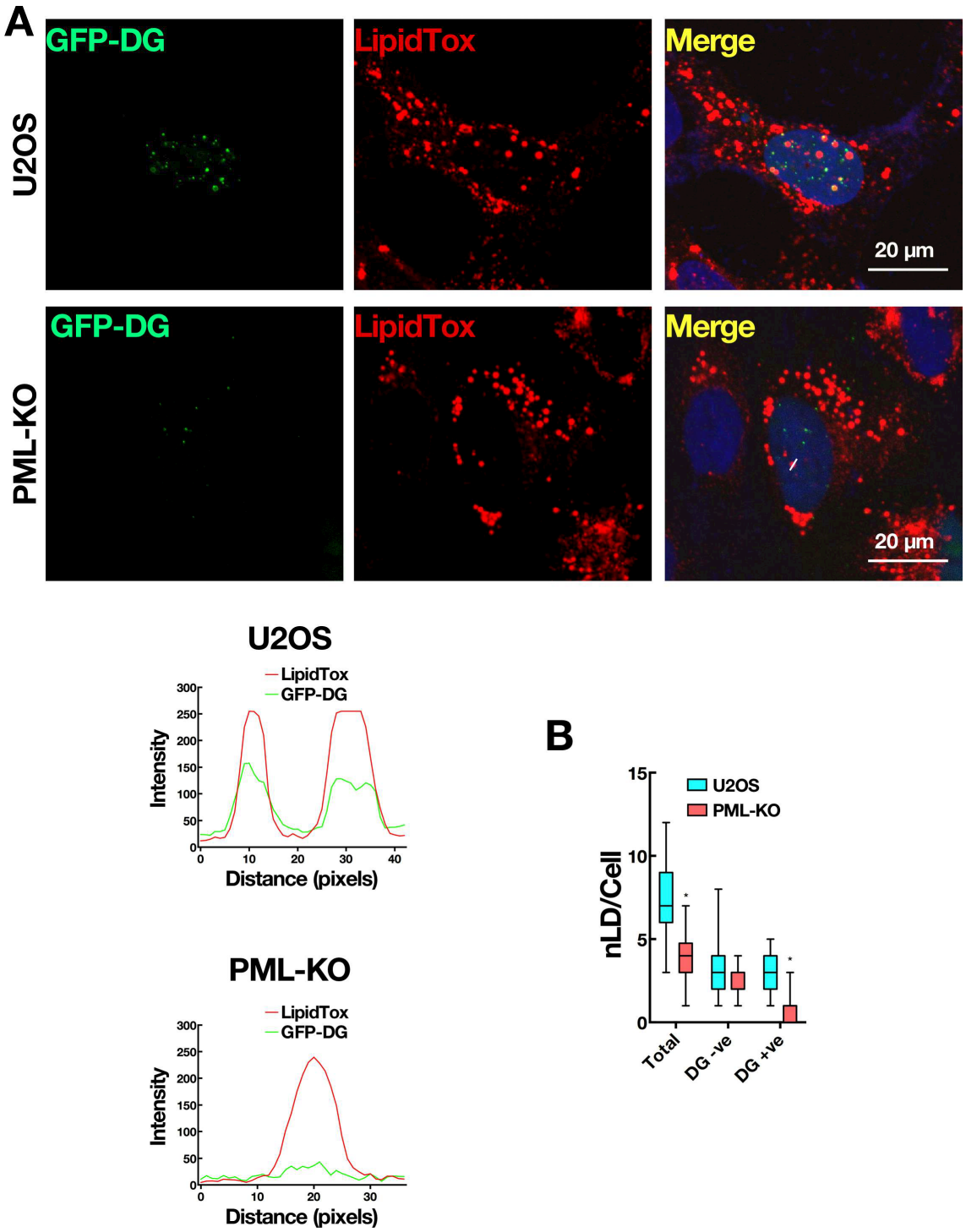

Figure 4.8. **PML expression is required for DG content on nLDs.** U2OS and PML-KO cells expressing the nuclear DG sensor GFP-C1(2) delta-2xNLS (GFP-DG) were treated with oleate/BSA (400 µM) for 24 h. LDs and nuclei were visualized with LipidTox Red and Hoechst 33258. RGB line plots shows the association of the DG sensor with nLDs **(A)**. Quantification of nLDs with (+) or without (-) DG **(B)**. 64 cells from three separate experiments.

populations based on the presence or absence of DG and/or PML; nLDs associated with neither DG or PML (DG/PML-), DG only (DG+), PML only (PML+) and both DG and PML (DG/PML+) (**Fig. 4.9B**). This revealed that 60% of total nLDs were DG/PML- in U2OS cells. The remaining nLDs were primarily DG/PML+ (79%) with a small percentage of DG+ or PML+. The cross-sectional area of DG/PML- nLDs was significantly reduced compared to that of total nLDs (**Fig. 4.9C**). In contrast, PML+ and DG/PML+ nLDs were significantly larger than total nLDs. The DG on LDs could be produced by LIPIN-mediated dephosphorylation of PA. To test this, localization of the PA biosensor GFP-nes-2xPABP (314) was also monitored. The PA biosensor was detected on the plasma membrane and not on nLDs or cLDs in control and PML-KO cells (**Fig. 4.9D**). Collectively, these data indicate that PML expression increases DG levels on the surface of nLDs, and its deficiency caused a notable increase in DG on cLDs.

Since PML expression was positively correlated with CCTα-positive (**Fig. 4.5D**) and DG-positive nLDs (**Fig. 4.9**), and DG is a known activator of CCTα and substrate for PC synthesis, immunofluorescence microscopy was used to determine the distribution of DG and CCTα on nLDs. In U2OS cells, the nuclear DG sensor and CCTα were detected on nLDs (**Fig. 4.10A**). However, in PML-KO cells, CCTα associated with nLDs that lacked DG. As expected, quantification of DG/CCTα distribution on nLDs revealed that all four nLD populations were reduced in PML-KO cells compared to control cells (**Fig. 4.10B**). However, the percent distribution of DG and CCTα on nLDs was similar in control and PML-KO cells, suggesting that CCTα association with nLDs was independent of their

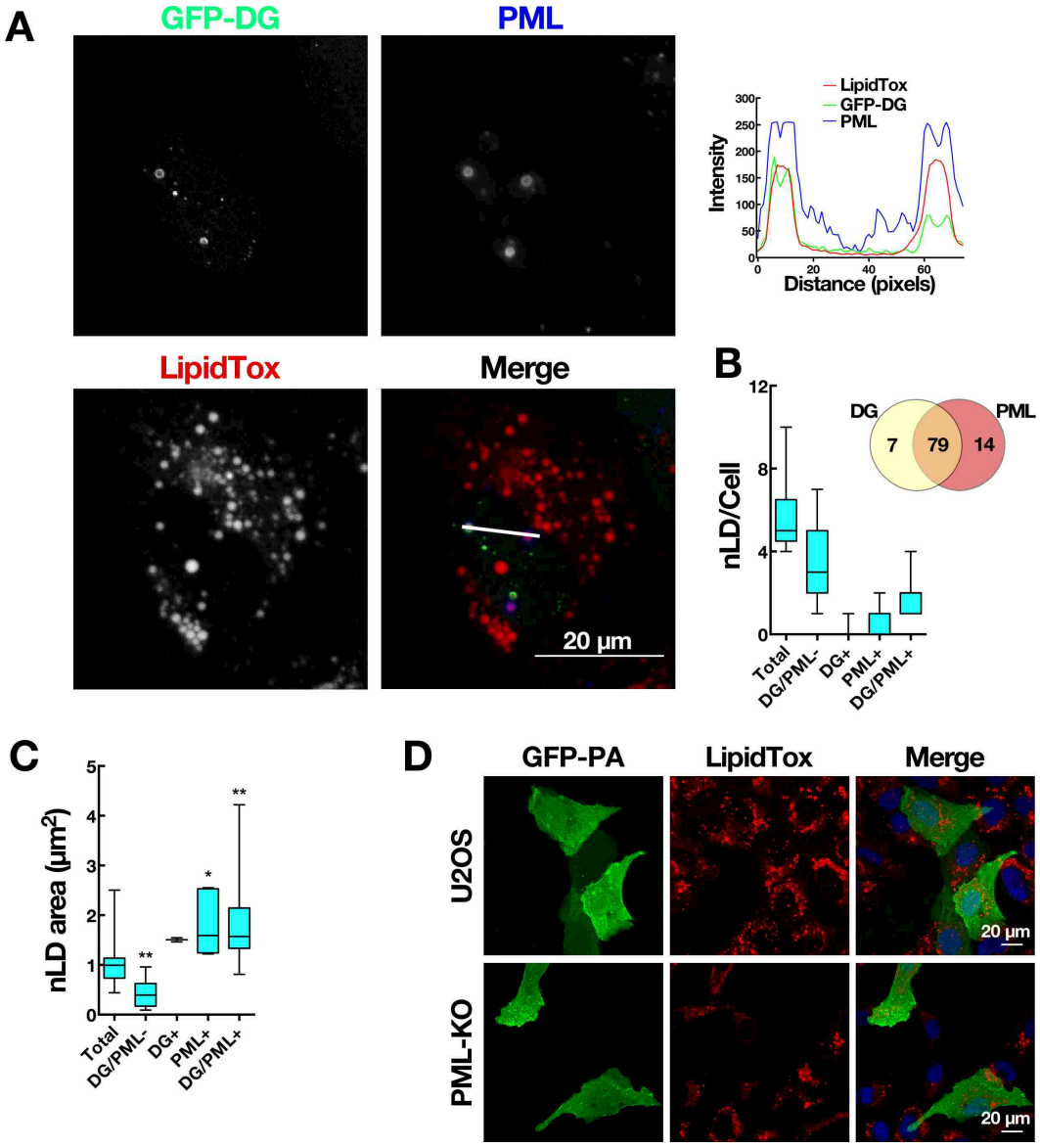

Figure 4.9. PML-positive nLDs are enriched in DG. U2OS cells transiently expressing the nuclear DG sensor GFP-C1(2) delta-2xNLS (GFP-DG) were treated with oleate/BSA (400 µM for 24 h) and immunostained with a PML polyclonal antibody and followed by AlexaFluor-647 secondary antibody. LDs were visualized with LipidTox Red. The RGB line plot shows the localization of GFP-DG with PML and nLDs **(A)**. Quantitation of nLDs containing neither the GFP-DG or PML (DG/PML-), GFP-DG (DG+), PML (PML+) or both (DG/PML+). A Venn diagram shows the percent distribution of GFP-DG and PML positive nLDs **(B)**. The cross-sectional area of nLDs in U2OS cells containing GFP-DG and/or PML as described above **(C)**. 25 cells from three separate experiments. ANOVA $^{**}P<0.01$, $^{*}P<0.05$ compared to total nLD area. U2OS and PML-KO cells transiently expressing the PA biosensor GFP-nes-2xPABP were cultured in media described above. LDs and nuclei were visualized with LipidTox Red and Hoechst 33258, respectively **(D)**.

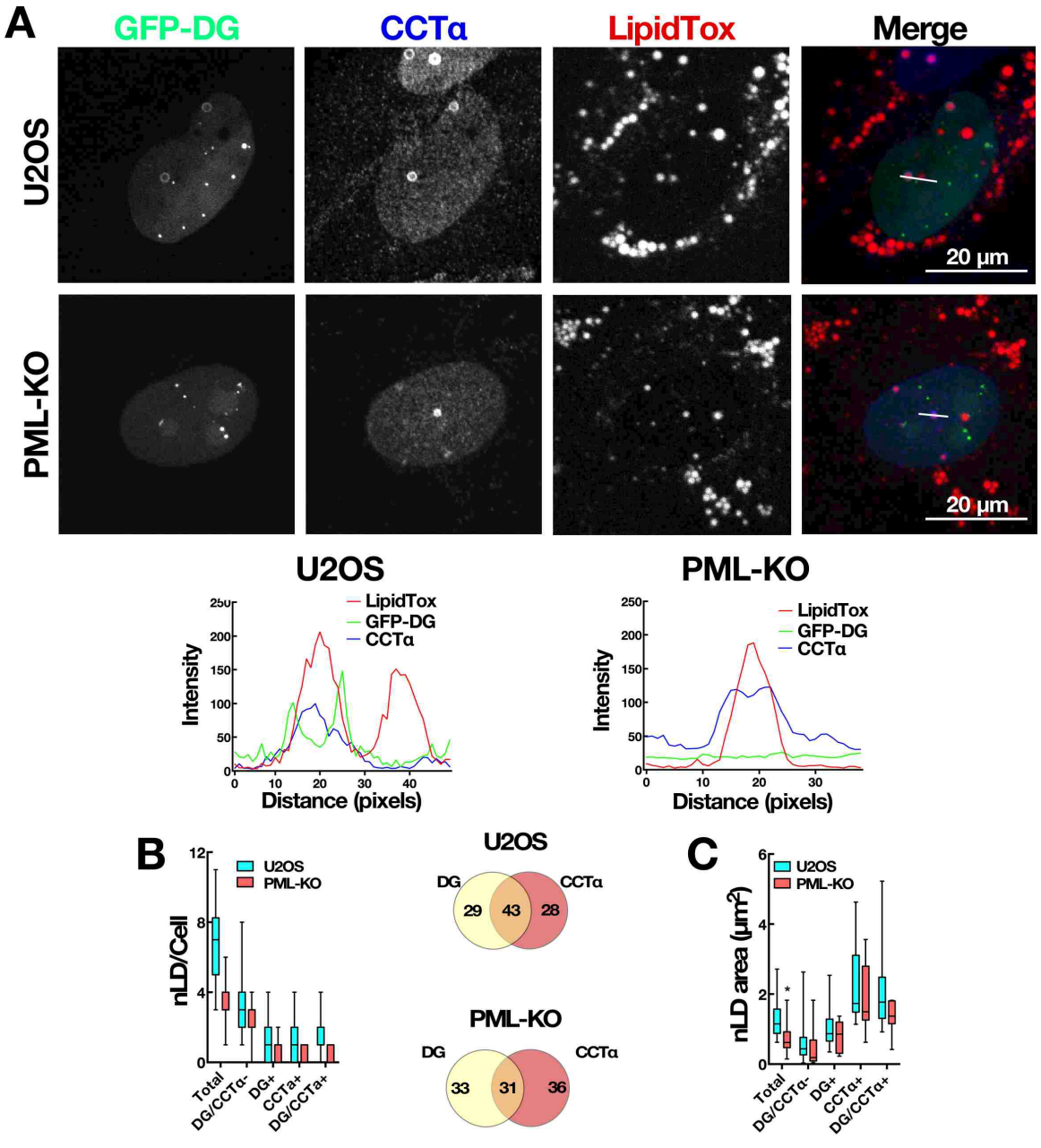

Figure. 4.10. CCTα association with nLDs is not dependent on DG. U2OS and PML-KO cells transiently expressing the nuclear DG sensor GFP-C1(2) delta-2xNLS (GFP-DG) were treated with oleate/BSA (400 μM) for 24 h and immunostained with a CCTα polyclonal antibody and followed by AlexaFluor-647 secondary antibody. LDs were visualized with LipidTox Red. RGB plots through nLDs show association with CCTα and GFP-DG **(A)**. Quantification of nLDs containing neither the GFP-DG or CCTα (DG/CCTα-), GFP-DG (DG+), CCTα (CCTα+) or both (DG/CCTα+). A Venn diagram shows the percent distribution of GFP-DG and CCTα-positive nLDs **(B)**. The cross-sectional area of nLDs population containing GFP-DG and/or CCTα was measured **(C)**. 30 cells from three separate experiments. **P*<0.05.

content of DG. As well, there was no significant difference in the area of DG/CCTα containing nLDs in controls and PML-KO cells (**Fig. 4.10C**).

4.1.3 Association of LIPIN-1 with nLDs is PML-dependent

LIPIN-1 is a PA phosphatase that produces DG for PC, PE and TG synthesis. LIPIN-1α and β isoforms were localized to cLDs in macrophages (66), possibly recruited by seipin for DG production and LD biogenesis. To determine if PML knockout affected LIPIN-1 recruitment to cLDs or nLDs, V5-tagged LIPIN-1α or β were transiently expressed and localized in U2OS and PML-KO cells (**Fig. 4.11** and **Fig. 4.12**). Immunofluorescence revealed that LIPIN-1α was expressed in the nucleus and cytoplasm of untreated U2OS and PML-KO cells (**Fig. 4.11A**). In oleate-treated U2OS cells, LIPIN-1α was extensively associated with nLDs (**Fig. 4.11B, a,b** and **c**). However, LIPIN-1α did not localize to cLDs. In contrast, LIPIN-1α in oleate-treated PML-KO cells was diffusely localized in the nucleus and cytoplasm (**Fig. 4.11C**), and quantification revealed that PML-KO cells had significantly reduced LIPIN-1α association with nLDs (**Fig. 4.11D**). Similar to LIPIN-1α, the LIPIN-1β isoform also associated with the surface of nLDs, but not cLDs, in oleate-treated U2OS cells (**Fig. 4.12B, a,b** and **C**). However, LIPIN-1β was not found on nLDs or cLDs in PML-KO cells (**Fig. 4.12C**). To determine the extent of LIPIN-1α and DG co-localization (**Fig. 4.13A**), the distribution and cross sectional area of LIPIN-1α and DG containing nLDs was quantified in U2OS cells. Of the DG/LIPIN-1α-positive nLDs, 53% contained both (**Fig. 4.13B**), and LIPIN-1α-positive nLDs were significantly larger within the total population (**Fig. 4.13C**). To demonstrate that LIPIN-1α and DG localization on nLDs was not a unique phenomenon in non-TG secreting cells, we

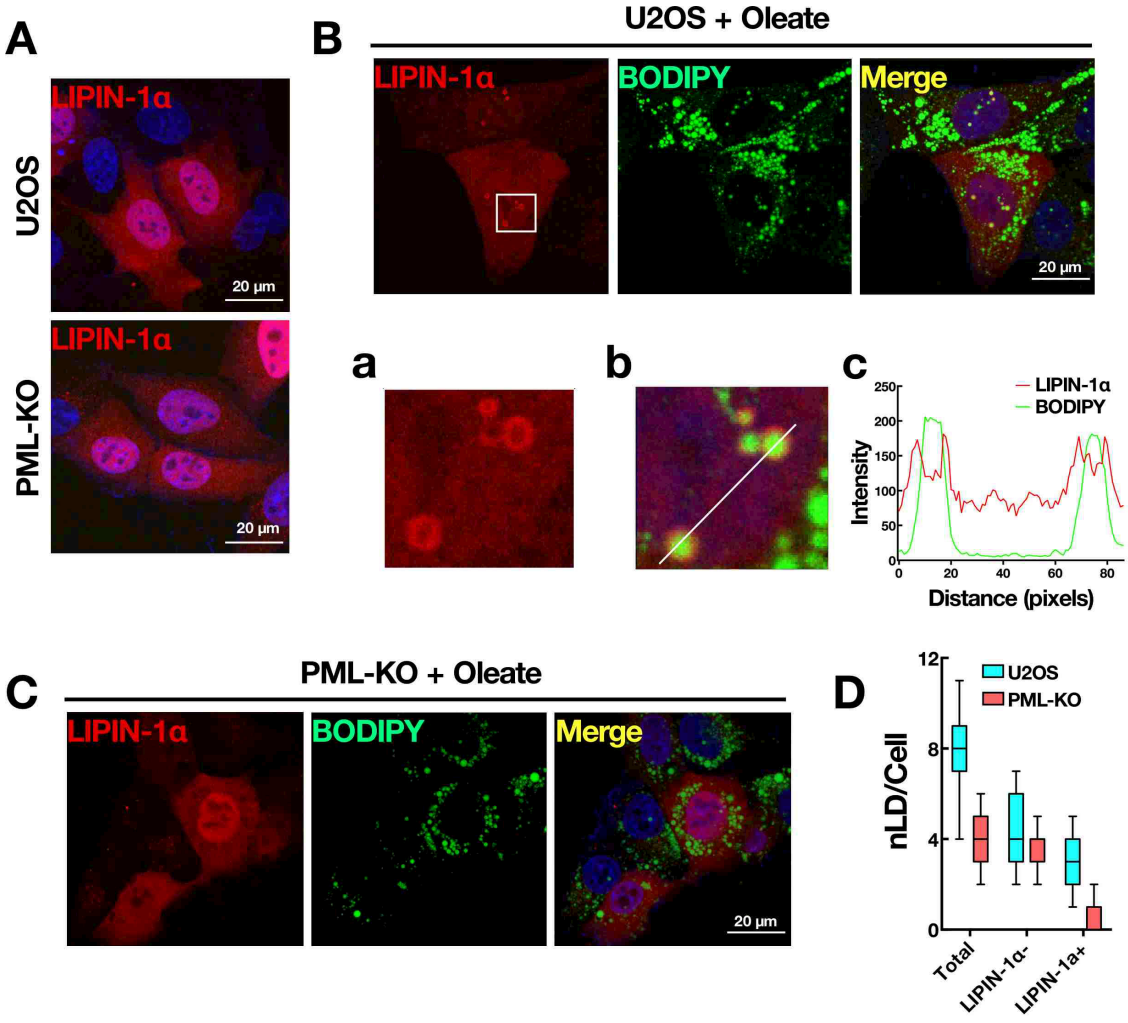

Figure. 4.11. PML is required for LIPIN-1α association with nLDs. Localization of LIPIN-1α-V5 in U2OS and PKL-KO cells **(A)**. U2OS cells expressing LIPIN-1α-V5 were treated with oleate/BSA (400 μM) for 24 h and immunostained with V5 monoclonal antibody followed by AlexaFluor-594 secondary antibody. LDs and nuclei were visualized with BODIPY and Hoechst 33258, respectively. Highlighted areas from LIPIN-1α and merged images are shown in panels **a** and **b**. A RGB line plot **(c)** shows the association of LIPIN-1α with nLDs **(B)**. PML-KO cells were treated as described above **(C)**. Quantification of nLDs with (+) or without (-) LIPIN-1α **(D)**. 50 cells from two separate experiments (50 cells).

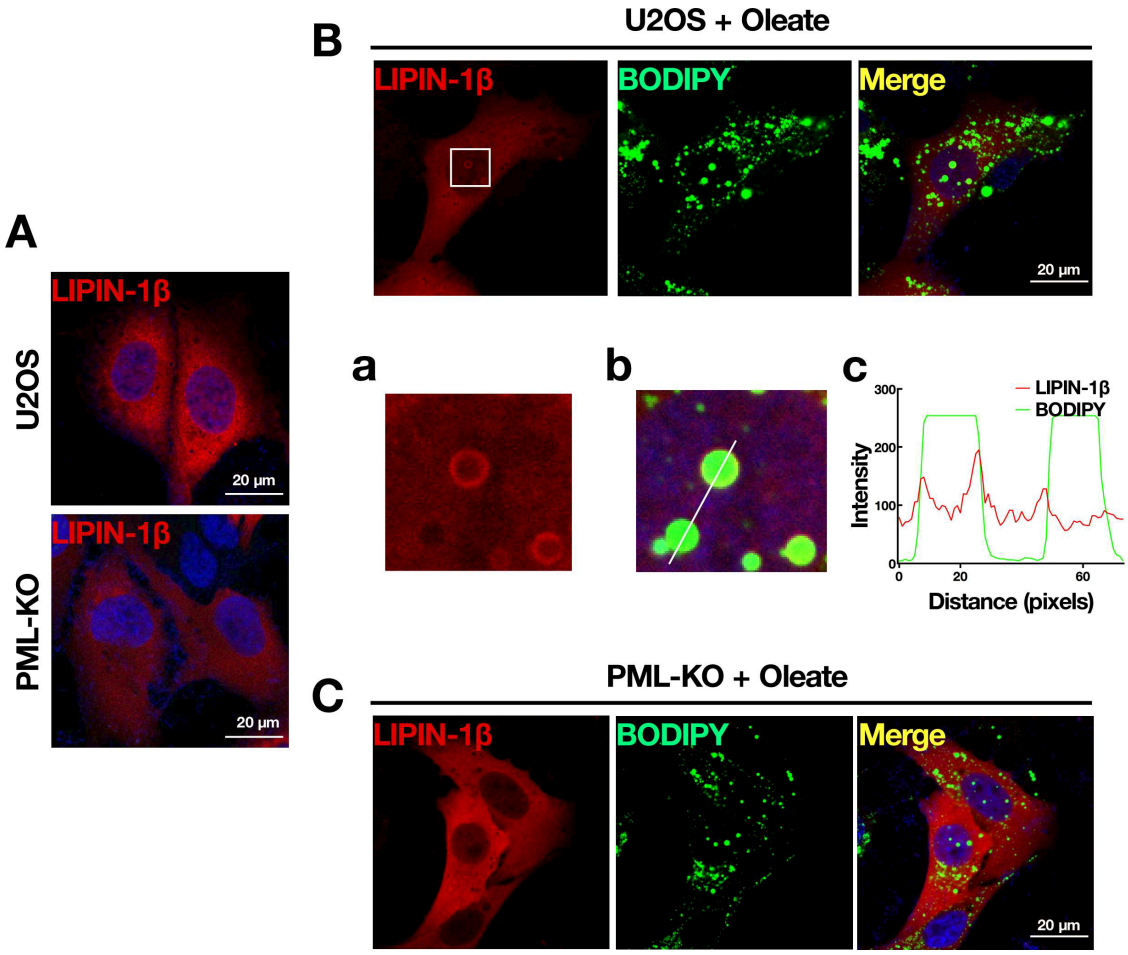

Figure. 4.12. PML is required for LIPIN-1β association with nLDs. Localization of LIPIN-1β-V5 in U2OS and PKL-KO cells **(A)**. U2OS cells expressing LIPIN-1β-V5 were treated with oleate/BSA (400 μM) for 24 h and immunostained with V5 monoclonal antibody followed by AlexaFluor-594 secondary antibody. LDs and nuclei were visualized with BODIPY-493/504 and Hoechst 33258, respectively. Highlighted areas from LIPIN-1β and merged images are shown in panels **a** and **b**. A RGB line plot **(c)** shows the association of LIPIN-1β with nLDs **(B)**. PML-KO cells were treated as described above **(C)**.

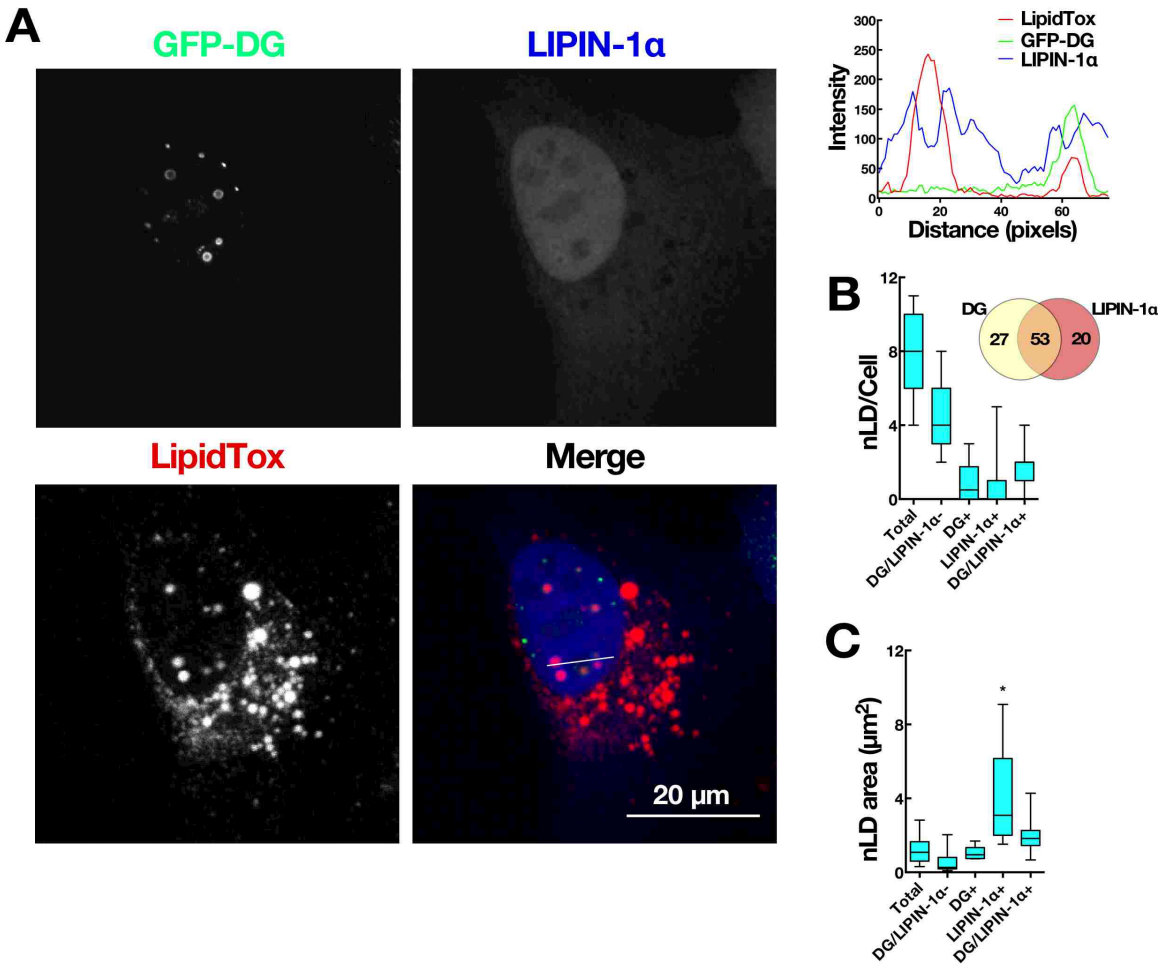

Figure 4.13. LIPIN-1α associates with DG-positive nLDs and requires PML. U2OS cells transiently expressing the nuclear DG sensor GFP-C1(2) delta-2xNLS (GFP-DG) and LIPIN-1α-V5 were treated with oleate/BSA (400 μM) for 24 h and immunostained with V5 monoclonal antibody followed by AlexaFluor-647 secondary antibody. LDs were visualized with LipidTox Red. RGB line plot shows GFP-DG and LIPIN-1α on the surface of nLDs **(A)**. Quantification of nLDs containing neither the GFP-DG or LIPIN-1α (PML/LIPIN-1 -), GFP-DG (DG+), LIPIN-1α (LIPIN-1α+) or both (DG/LIPIN-1α+). A Venn diagram shows the percent distribution of GFP-DG and LIPIN-1α-positive nLDs **(B)**. The cross-sectional area of nLDs containing differing compositions of GFP-DG and LIPIN-1α was quantified **(C)**. 26 cells from three separate experiments. ANOVA *P<0.001 compared with total nLD area.

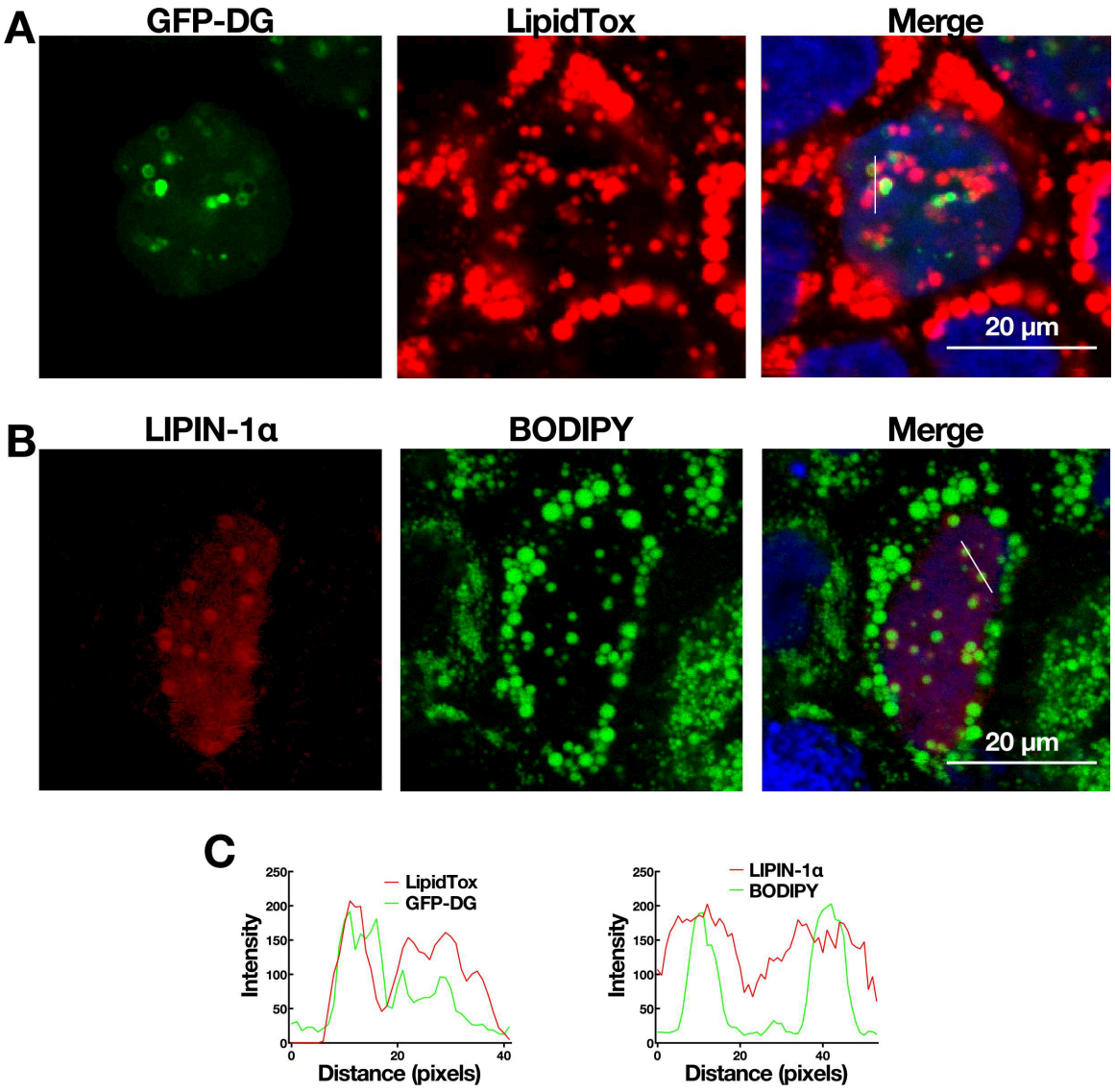

Figure 4.14. Localization of DG and LIPIN-1α in Caco2 cells. Caco2 cells transiently expressing the nuclear DG sensor GFP-C1(2) delta-2xNLS (GFP-DG) were treated with oleate/BSA (400 µM) for 24 h. LDs were visualized with LipidTox Red **(A)**. Caco2 cells expressing LIPIN-1α-V5 were treated as described above and immunostained with V5 monoclonal antibody followed by AlexaFluor-594 secondary antibody. LDs were visualized with BODIPY-493/504 **(B)**. Nuclei were stained with Hoechst 33258 (**A** and **B**) RGB line plots show GFP-DG or LIPIN-1α on the surface of nLDs **(C).**

compared to Caco2 cells that have abundant nLDs associated with PML and CCTα. The nuclear DG biosensor and LIPIN-1α and were also localized to large nLDs in Caco2 (**Fig. 4.14A** and **B**). Collectively, PML regulates LIPIN-1 association with nLDs, which produces DG for TG and PC synthesis required for LD formation. CCTα translocation to nLDs, which required PML-II but not DG, would accommodate monolayer expansion.

4.1.4 PML-KO Cells have Reduced PC and TG Synthesis

To determine whether reduced CCTα translocation to nLDs in PML-KO cells affected PC biosynthesis, cells treated with or without oleate for 24 h were pulse-labelled for up to 4 h in medium containing [^{3}H]choline, and isotope incorporation into PC was measured (**Fig. 4.15**). [^{3}H]Choline incorporation into PC was significantly reduced by approximately 50% in PML-KO cells treated with oleate. Interestingly, [^{3}H]choline incorporation under basal condition was not affected by PML knockout suggesting that nLDs are important sites for CCTα activation.

We next determined whether PML knockout affected synthesis of fatty acids and sterols by measuring [^{3}H]acetate incorporation in cells cultured in FCS or LPDS, the conditions that inhibit or activate SREPBs, respectively (**Fig. 4.16**). However, synthesis of sterols and fatty acids was only activated slightly by culturing U2OS cells in LPDS, and PML knockout had a minor inhibitory effect on *de novo* synthesis of sterols and fatty acids. Significantly reduced synthesis of cholesterol and fatty acids was only observed in cells cultured in FCS and LPDS, respectively.

The effect of PML knockout on *de novo* TG synthesis was determined by incubating cells in medium containing 2 μCi/ml [^{3}H]glycerol with or without 100 μM

oleate for up to 6 h. [^{3}H]Glycerol incorporation into TG was similar in untreated control and PML-KO cells. Interestingly, the incorporation of [^{3}H]glycerol into TG was higher in oleate-treated PML-KO cells compared to controls (**Fig. 4.17A**). The rate of [^{3}H]glycerol incorporation was lower in U2OS cells at early time points (1-4 h) but normalized by 6 h. TG synthesis in control and PML-KO cells was also measured by analysis of 100 μM [^{3}H]oleate incorporation into TG and CE. Using similar labeling and oleate treatment conditions as described for [^{3}H]glycerol, incorporation of [^{3}H]oleate into TG and CE was significantly decreased by approximately 2-fold whether cells were cultured in FCS or LPDS (**Fig. 4.17B** and **C**).

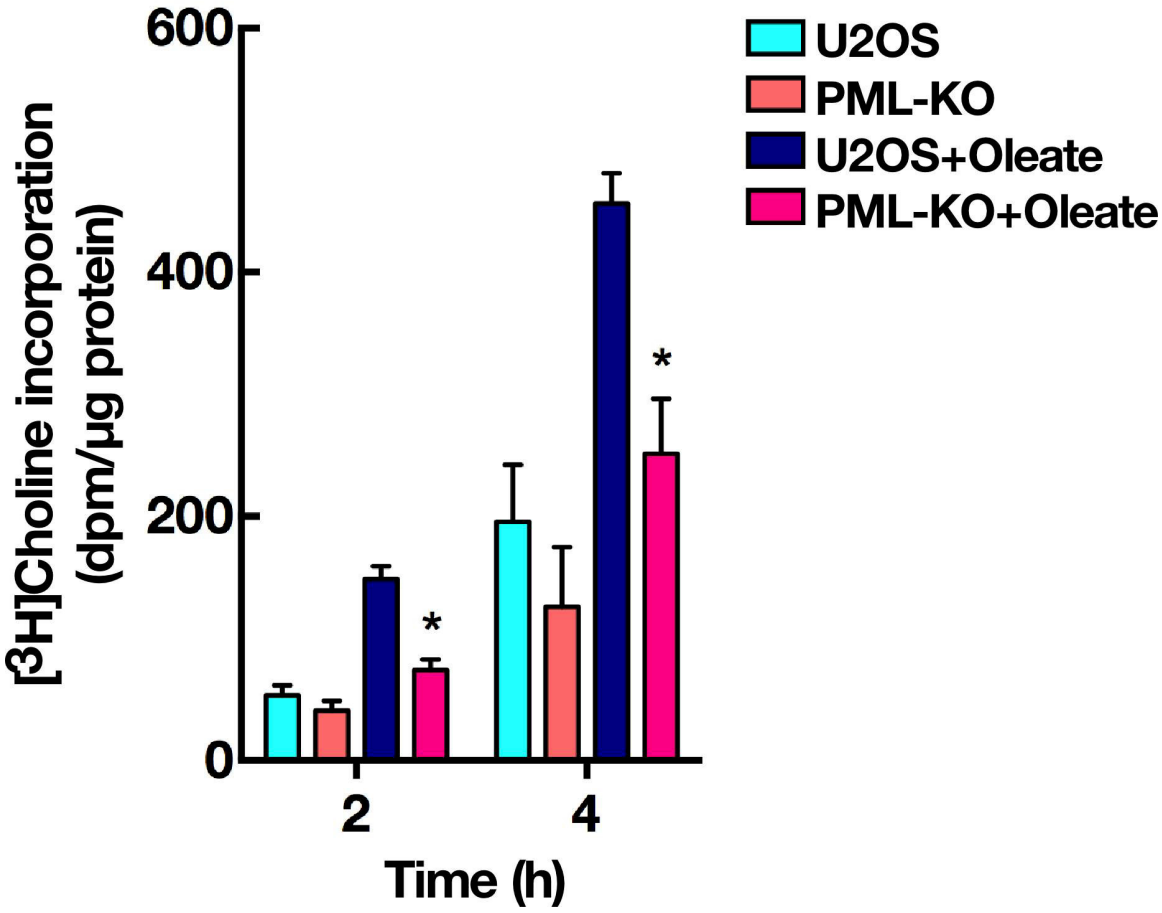

Figure 4.15. Reduced PC synthesis in PML-KO cells. U2OS and PML-KO cells were cultured with or without oleate/BSA (400 µM) for 24 h. Cells were then incubated with choline-free medium containing [^{3}H]choline (2 µCi/ml) and incorporation into PC was measured up to 4 h. Results are the mean and SEM of three experiments. **P*<0.05 compared with matched U2OS controls.

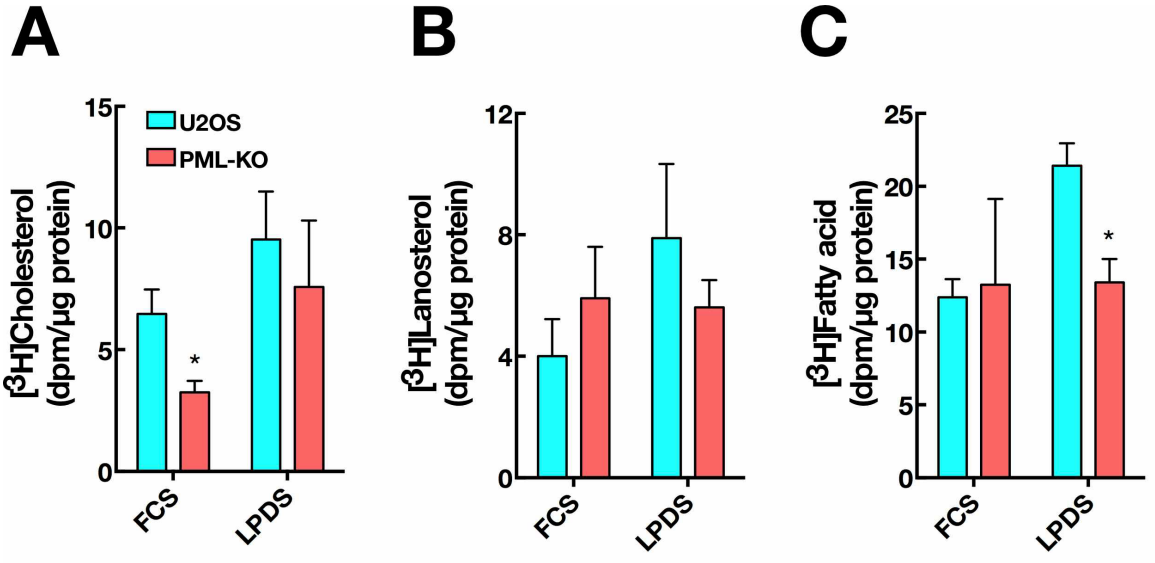

Figure 4.16. PML-KO cells have reduced cholesterol and fatty acid synthesis. U2OS and PML-KO cells were cultured in FCS or lipoprotein-deficient serum (LPDS) for 18 h prior to pulse-labeling with [^{3}H]acetate (2.5 µCi/ml) for 4 h. [^{3}H]Acetate incorporation into cholesterol **(A)**, lanosterol **(B)** and fatty acids **(C)** was determined. Results are the mean and SEM of three experiments. **P*<0.05 compared with matched U2OS controls.

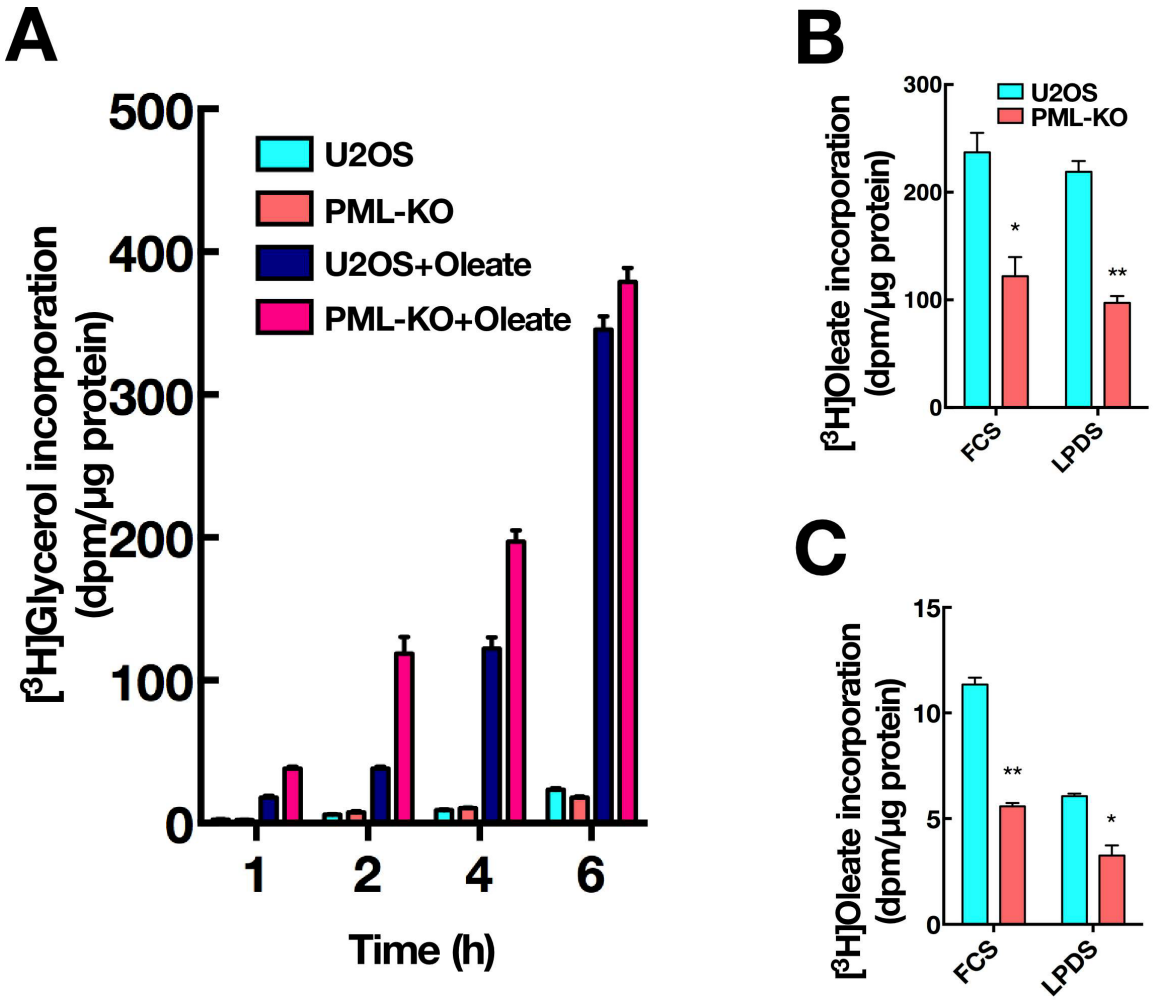

Figure 4.17. PML-KO cells have reduced TG synthesis by exogenous fatty acids. U2OS and PML-KO cells were pulse-labelled with [^{3}H]glycerol (2 µCi/ml) in the presence or absence of oleate/BSA (100 µM) for up to 6 h. [^{3}H]Glycerol incorporation in to TG was determined. Results are the mean and SD of triplicates of one experiment **(A)**. U2OS and PML-KO cells were cultured in FCS or lipoprotein-deficient serum (LPDS) for 18 h prior to pulse-labeling with [^{3}H]oleate/BSA 100 µM for 4 h. [^{3}H]Oleate incorporation into TG **(B)** and CE **(C)** was determined. Results are the mean and SEM of three experiments. $^{**}P<0.001$, $^{*}P<0.01$ compared with matched U2OS controls.

4.2 Discussion

The role of lipids in nuclear function has received little attention beyond their obvious structure role in the NE and as a source of ligands for some transcription factors. The presence of functional lipid biosynthetic pathways and potential interaction with other nuclear activities are suggested by the presence of nuclear CCTα, the rate-limiting enzyme in PC synthesis, and other TG and lipid biosynthetic enzymes such as LIPINs. The recent observation that nLDs form and expand in the nucleus, much like their cytosolic counterparts, is further evidence of dynamic nuclear lipid synthesis and storage.

CCTα is acutely and rapidly activated by translocating from nucleoplasm to the NE and NR in response to acute treatment of lipid activators (i.e. fatty acids) or PC deficiency to increase PC synthesis (2,12). Interestingly, CCTα was recently shown to associate with nLDs that formed in oleate-treated Huh7 human hepatoma cells (14). In hepatoma cells, PML-NBs were co-localized with CCTα on nLDs, and RNAi knockdown of PML-II isoform caused a decrease in the number and size of nLDs. Here we report for the first time that intestinal-derived Caco2 cells have abundant nLDs that are affected by CCTα deficiency. We also used U2OS cells with a knockout of all PML isoforms to understand how PML-NBs regulate TG and PC biosynthesis for nLD biogenesis and cellular lipid homeostasis.

Consistent with previous reports in Huh7 cells (14), BODIPY-stained nLDs associated with PML-NBs and CCTα in 24 h oleate-treated U2OS, Caco2 and HepG2 cells (**Fig. 4.1**). Since CCTα did not associate with nLDs in Caco2 cells treated for 12 h with oleate (**Fig. 3.4**), the association between nLDs and CCTα may reflect increased PC synthesis required for formation of both cLDs and nLDs after prolonged exposure to oleate

(24 h) (**Fig. 4.2** and **4.3**). Interestingly, CCTα knockout in Caco2 cells showed a similar effect on cLD and nLD morphology size and abundance. CCTα-KO cells had fewer larger LDs in both cytoplasm and nucleus (**Fig. 4.2** and **4.3A** and **B**) as a result of the shift toward large LDs (**Fig. 4.3B**). These indicate that LD biogenesis in the nucleus and cytoplasm is regulated by a similar mechanism, which could involve fusion of small-PC poor nLDs into large nLDs.

The positive correlation between the size of nLDs and PML association, which was apparent in both Caco2 and CCTα-KO cells (**Fig. 4.3C**), suggests that PML recruitment was enhanced by lipid-dependent stress. One potential explanation could be that PML proteins polymerize on the surface of nLDs to increase fatty acid flux into storage pathway and to activate CCTα to increase PC synthesis required for expanding nLDs. Support for this comes from previous observations that overexpression of PML-II increased nLDs (14) and inhibition of nLD formation reduced PC synthesis (288) in Huh7 cells. These data indicate that nLDs in Caco2 cells, which secrete TG-containing chylomicrons, may form and interact with PML and CCTα in a similar manner as those in hepatocytes (**Fig. 1.7**). However, the presence of nLD-association with PML-NBs/CCTα in U2OS cells (**Fig. 4.1A**), in which nLDs are formed by a mechanism that does not involve release of apoB-free luminal LDs from type I NR (**Fig. 1.7**), suggests that this association could be involved in TG and PC synthesis in non-lipoprotein secreting cells as well. As expected, loss of PML proteins in U2OS cells caused a significant reduction in the number and size of nLDs in response to oleate (**Fig. 4.5B** and **E**). In addition, we found that PML-KO cells had a reduced number of cLDs (**Fig. 4.5C**) but did not affect the size distribution (**Fig. 4.5F**), an initial indication of PML exerts regulatory control outside the nucleus. However, why

cLDs were less severely affected by PML knockout compared to nLDs is unclear. It is feasible that nuclear TG is in equilibrium with the cytoplasmic pool through diffusion within the INM and ER. In this respect, inability to form nLDs in PML-KO cells could divert TG into the cytoplasm but TG availability could still be insufficient since nLDs account for less than 10% of total LDs in the cell. Alternately, PML may differentially regulate nLD and cLD formation, as indicated by increased and decreased localization of the DG biosensors on cLDs and nLDs, respectively (**Fig. 4.7** and **Fig. 4.8**).

Transiently expressed GFP-PML-II associated with nLDs in PML-KO cells and restored both nLD and cLD size and number (**Fig. 4.6A, B** and **C**), confirming that this isoform is critical for both nLD and cLD biogenesis. Unlike PML-II, other GFP-tagged PML isoforms did not exhibit localization on nLDs (**Fig. 4.6A**). This could be related to unique C-terminal domain of PML-II (14,315), which contains the nuclear periphery-binding motif that mediates distribution of PML-II along the nucleoplasmic surface of the INM and promotes formation of type I NR, which were correlated with the ability of PML-II to increase nLDs (14). However, nLDs showed minimal association with NE protein emerin (**Fig. 4.4B** and **C**) and endogenous PML-NBs in U2OS cells (**Fig. 4.1A**) and GFP-PML-II (**Fig. 4.6A)** in PML-KO cells did not localize to the NE or NR, indicating that nLDs in U2OS cells are formed by different mechanism from those in hepatocytes.

Since CCTα recognizes and binds to membranes with packing defects due to elevated DG content (9,10), diminished CCTα translocation to nLDs in PML-KO cells (**Fig. 4.5D**) was thought to be due to reduced DG levels (**Fig. 4.8**). Furthermore, co-localization of the nuclear DG sensor and PML showed that DG+ nLDs, of which 79% were associated with PML in U2OS cells, were larger than DG/PML- nLDs (**Fig. 4.9A, B** and **C**), indicating

a positive correlation between PML expression and the number and size of DG-positive nLDs. These data suggested that PML maintains DG synthesis for nLD formation and promotes CCTα recruitment to the surface of nLDs enriched in DG. However, these two PML functions are not inter-dependent since CCTα associated with nLDs that lacked DG in PML-KO cells (**Fig. 4.10A**) and CCTα associated with nLDs by a mechanism that is independent of DG levels in wild-type U2OS cells (**Fig. 4.10B** and **C**).

nLDs are important sites of CCTα regulation as indicated by the reduced nLD association of CCTα (**Fig. 4.5D**) and incorporation of [^{3}H]choline into PC in oleate-treated PML-KO cells (**Fig. 4.15**). PC deficiency due to reduced CCTα activity leads to LD coalescence (2,4,32), resulting in fewer and larger particles. Paradoxically, PML-KO cells had fewer and smaller nLDs and fewer cLDs with no evidence for change in size (**Fig. 4.5**), suggesting that sufficient PC was available. A potential explanation is that the decrease in LD size and number in PML-KO cells was accompanied by reduced PC synthesis with a corresponding decrease in TG synthesis. Thus, loss of PML downregulated CCTα-nLD association and PC synthesis due to reduced total LD surface area. It was also unclear why CCTα translocates to nLDs but not cLDs. This could be due to its nuclear localization, with substrates and product freely diffusing in and out of the nucleus. However, insect and mammalian CCTs in *Drosophila* S2 cells were exported from the nucleus and localized to cLDs during oleate loading (12), and in some mammalian cells, CCTα is frequently observed in the cytoplasm with no evidence for cLD localization (2). Similar to cLDs from S2 cells, the surface of mammalian nLDs may have higher PE/PC ratio compared to cLDs making them a more optimal binding site for CCTα.

DG is the substrate shared by the final enzymes of PC and TG biosynthesis. Because PML expression was positively correlated with DG levels on nLDs and CCTα-nLD association, PML could be a positive regulator of DG production by LIPINs. Consistent with a previous study using neuronal cells (316), LIPIN-1α and β were predominantly expressed in the nucleus and cytoplasm, respectively (**Fig. 4.11** and **Fig. 4.12**). Interestingly, knockout of PML reduced LIPIN-1α and β recruitment to nLDs when treated with oleate, suggesting that PML is an effector of LIPIN-1. Similar to PML and CCTα, LIPIN-1α co-localized with the nuclear DG sensor on nLDs (**Fig. 4.13A** and **B**), and DG and/or LIPIN-1α containing nLDs were larger than those that lack DG and LIPIN-1α (**Fig. 4.13C**). Taken together, these data indicate that LIPIN-1α association with nLDs is PML-dependent and maintains DG production that is used to produce TG and PC for nLD formation. However, a PA biosensor was not detected on nLDs in control cells (**Fig. 4.9D**). This was surprising because LIPIN-1 is recruited to membranes enriched in PA which it then dephosphorylates to DG. One possible explanation could be that PA is rapidly converted into DG and does not reach levels detectable by the probe. Since nLDs containing DG/PML (**Fig. 4.9C**), DG/CCTα (**Fig. 4.10C**) or DG/LIPIN-1α (**Fig. 4.13C**) are similar in size, it is possible that a multi-protein complex composed of G3P pathway enzymes could form on nLDs by a mechanism dependent on PML. Whether GPAT4 localizes to nLDs is not determined yet, however, overexpressed DGAT2 was shown to co-localize with PML on nLDs in oleate-treated Huh7 cells (14). In addition, the nuclear DG biosensor and LIPIN-1α were localized to large nLDs, which are possibly PML/CCTα-positive, in Caco2 cells (**Fig. 4.14**).

Accompanying reduced LIPIN-1 translocation and LD formation, PML-KO cells also had significantly reduced tracer [^{3}H]oleate incorporation into TG (**Figure. 4.17B**). Since PML regulates gene transcription by modulating the function of transcription factors (317), reduced TG synthesis in PML-KO cells could be due to inhibition of expression of genes involved in TG biosynthesis. However, this is unlikely because free fatty acids resulting from reduced TG synthesis must be oxidized but PML is responsible for PGC-1α deacetylation and activation (303), which is predicted to increase β-oxidation (318). Furthermore, PML knockout did not inhibit *de novo* TG synthesis (**Fig. 4.17A**). Considering that PML is a potent activator of PGC-1α/PPAR and fatty acid oxidation and its deficiency had a minimal effect on *de novo* fatty acid synthesis (**Fig. 4.16C**), one potential explanation for the reduction in [^{3}H]oleate-labeled TG could be reduced fatty acid uptake at the plasma membrane. In support of this, the fatty acid translocase *FAT*, a well-known PPAR target gene, was reduced in *Pml*$^{-/-}$ mouse WAT (319). It is possible that loss of nLD interaction with PML-NBs induces a transcriptional response that is dependent on PGC-1α/PPAR/FAT signaling pathway to avoid fatty acid overload. Thus, reduced fatty acid availability for TG and PC synthesis consequently diminished both nLD and cLD formation. However, the reason for increased level of [^{3}H]glycerol-labeled TG in oleate-treated PML-KO cells is not clear (**Fig. 4.17A**). It is feasible that reduced fatty acid uptake also resulted in reduced hydrolysis of TG from LDs by lipases. Collectively, this study demonstrates that assembly of PML-NBs on nLDs elicit a defensive response to fatty acid loading by recruiting TG and PC biosynthetic enzymes to generate LDs. PML deficiency diminishes LIPIN-1 and CCTα translocation to nLDs, which results in TG and PC synthesis required for LD biogenesis.

CHAPTER 5: Conclusion

LDs are dynamic organelles that store or release fatty acids and cholesterol depending on cellular metabolic states. Since an imbalance between storage and mobilization can lead to pathological conditions, it is important to understand mechanisms involved in regulating LD biogenesis and TG metabolism.

PC is the primary phospholipid component of the surface monolayer of LDs that stabilizes and regulates their capacity to store and mobilize lipids. Chapter 3 of this thesis explored the precise role of intestinal *de novo* PC synthesis by the CDP-choline pathway in TG metabolism. This was based on the evidence that 1) knockdown of CCTα impairs LD morphology and TG storage in mammalian cells and 2) PC deficiency in mouse liver causes TG accumulation due to impaired VLDL secretion. Consistent with other cell types, knockout of CCTα in Caco2 cells caused TG accumulation in abnormal LDs, which reduced transfer of cytosolic TG to the ER for secretion in chylomicrons (**Fig. 5.1**).

Interestingly, it has recently shown that intestine-specific knockout of CCTα in mouse reduced the uptake of fatty acid from the intestinal lumen into enterocytes (275). However, metabolic labeling in our study demonstrated that there was 50% residual PC synthesis and fatty acid uptake and TG synthesis was normal in CCTα-KO cells. A potential reason for this dissimilarity could relate to the expression of CCTβ2 in Caco2 cells but not in normal intestinal epithelial cells. As a result, PC synthesis by CCTβ2 could partially compensate for the loss of CCTα but still be limiting for LD biogenesis and chylomicron secretion. It would be interesting to determine whether knockout of CCTβ2 in Caco2 cells exerts a similar effect as CCTα knockout. Alternately, since CCTβ2

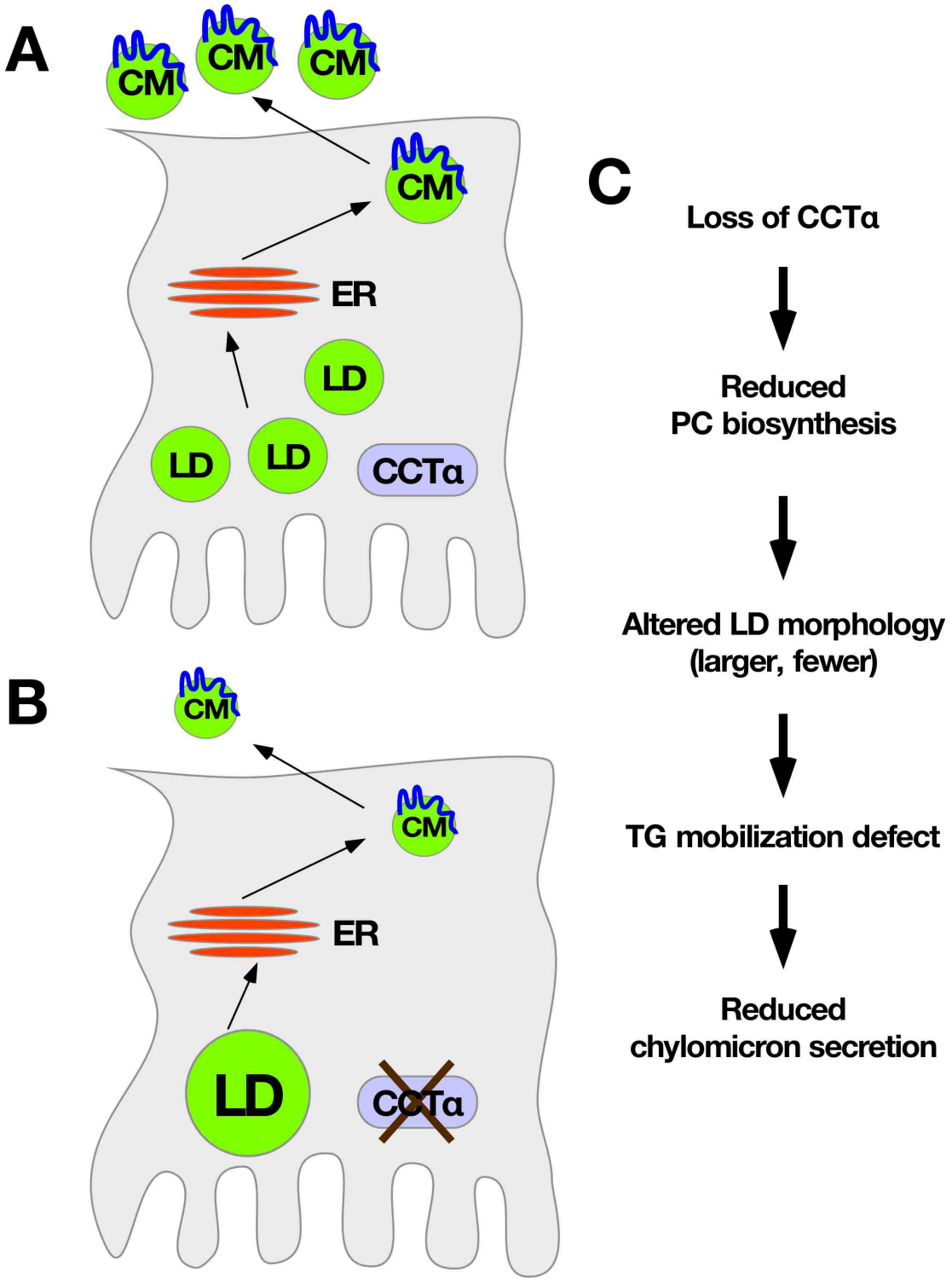

Figure 5.1. Consequences of loss of CCTα in Caco2 cells. In normal Caco2 cells, TG stored in LDs is hydrolyzed and assembled into chylomicrons for secretion at the basolateral membrane **(A)**. In CCTα-KO cells, reduced *de novo* PC synthesis leads to formation of fewer, larger LDs, resulting in partial defective TG mobilization. This reduces TG availability for chylomicron assembly in the ER and secretion **(B** and **C)**.

expression and apoB-100 secretion disappear during development (4) and CCTα knockout had no effect on apoB-100 secretion, CCTβ2 expression could be specifically linked to apoB-100 secretion. If CCTβ2 knockout reduces apoB-100 secretion, but not apoB-48 secretion, this would provide the first evidence that nuclear and cytoplasmic arm of the CDP-choline pathway differentially regulate TG secretion.

One of the consequence of blocking PC synthesis is the redistribution of DG toward TG synthesis and LD formation. Surprisingly, there was no evidence for such substrate diversion in CCTα-KO cells despite the accumulation of TG. Instead, the increase in TG deposition was a result of defective turnover, which was potentially linked to decreased LD-associated lipase activity. Because decreased TG mobilization from the storage pool can result in reduced oxidation, it is feasible that an inability to utilize fatty acid for PC synthesis may increase flux into oxidation pathways as a defensive mechanism against fatty-acid induced toxicity. Taken together, this study shows a specific requirement for PC synthesis by the nuclear arm of the CDP-choline pathway for TG storage and secretion, and disruption in LD biogenesis lead to impaired lipid metabolism.

Data presented in Chapter 4 identified nLDs as novel sites for cellular lipid metabolism. The initial hypothesis was that loss of PML would decrease nLD biogenesis. This hypothesis was based on evidence that 1) nLDs are dynamic like their cLD counterparts, 2) nLDs association with PML-NBs and CCTα and 3) loss of PML decreased nLD size and number during oleate load. The findings in this study demonstrate that the interaction of nLDs with PML-NBs is not only involved in nLDs biogenesis but also affects cLDs and cellular TG homeostasis. Loss of PML leads to reduced TG and PC synthesis

and LD formation as a result of decreased LIPIN-1 and CCTα translocation to nLDs (**Fig. 5.2**).

An important question is how nLDs are formed in cells that do not secrete lipoproteins. Although data indicate that loss of PML caused more profound effects on nLDs compared to cLDs, it is feasible that TG stored in cLDs is in equilibrium with the cytoplasmic pool through diffusion within the ER and INM in U2OS cells. In this regard, the presence of TG and PC biosynthetic enzymes in the INM suggest that nLDs in non-lipoprotein secreting cells may be generated in the INM and bud into the nucleoplasm by seipin-dependent mechanism as shown in yeast (292). Interestingly, Ohsaki et al. showed a discrete nuclear periphery localization of PML-II in Huh7 cells but not in cells that do not produce nLDs (14). Since TG biosynthetic enzymes form a complex involving seipin in response to fatty acids, we speculate that PML is recruited to the nLD nucleation sites in the INM to regulate fatty acid partitioning.

Our results show that nLDs associate with PML-NBs and CCTα in Caco2 and HepG2 cells, and that knockout of CCTα exerts similar effects on nLD and cLD morphology. Since the source of nLDs in these cells are proposed to be ER-luminal apoB-free LDs (288), it would be interesting to determine whether PML plays a critical role in TG secretion in lipoproteins. Suppressed nLD formation in PML-deficient cells could partition lipids into secretory pathway, cytoplasmic storage pool or β-oxidation. Alternately, loss of nLD interaction with PML-NBs could exert a transcriptional response to compromise fatty acid uptake. Lipidomic and transcriptomic analysis in the presence or absence of oleate could provide a broader view of PML-regulated TG secretion.

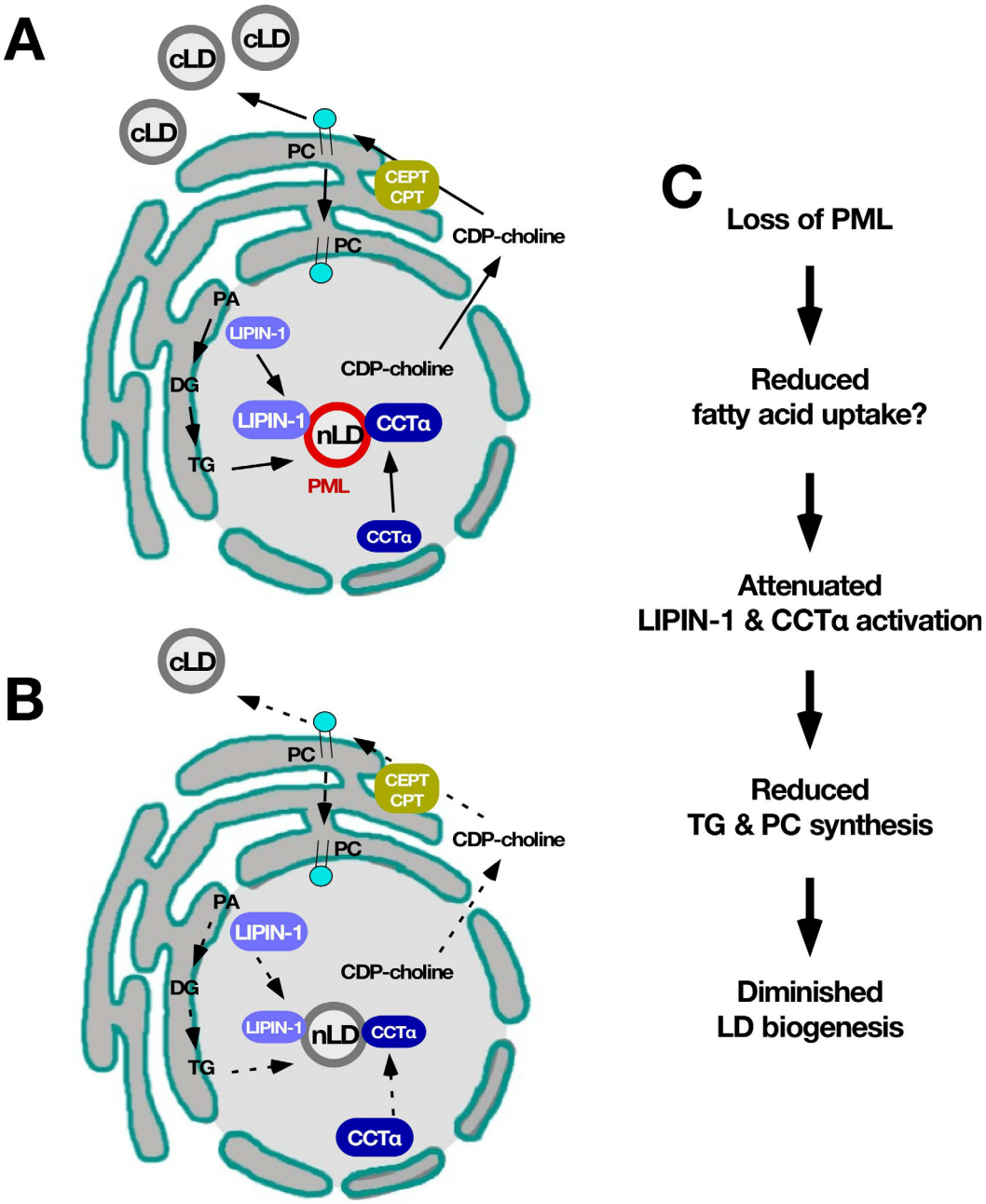

Figure 5.2. Consequences of loss of PML in U2OS cells. As local synthesis of TG increases in the INM, nLDs are formed and interact with PML. This interaction recruits and activates LIPIN-1 and CCTα for TG and PC synthesis. CDP-choline produced by CCTα can be sued by CEPT/CPT at the INM for PC synthesis required for nLDs or can be transported into the cytoplasm for PC required for cLDs **(A)**. Loss of PML-nLD interaction induces a transcriptional response to reduce fatty acid uptake to prevent cells from lipotoxicity. Consequently, LIPIN-1 and CCTα translocation/activation on the surface of nLDs is attenuated. This reduces TG and PC synthesis, resulting in diminished LD biogenesis **(B** and **C)**. Dashed arrows indicate reduced substrate flux or translocation of enzymes.

Nevertheless, this study provides the first evidence that nLDs are key regulators of lipid homeostasis.

In conclusion, data presented in this thesis demonstrate how PC and TG biosynthesis regulates formation and function of LDs and provide evidence that nLDs more broadly control cellular fatty acid metabolism. Our research extends current understanding of the biology of LDs and would provide a basis for future studies related to LD-associated metabolic disorders.

References

1. Bell, R. M., and Coleman, R. A. (1980) Enzymes of glycerolipid synthesis in eukaryotes. *Annu Rev Biochem* **49**, 459-487

2. Aitchison, A. J., Arsenault, D. J., and Ridgway, N. D. (2015) Nuclear-localized CTP:phosphocholine cytidylyltransferase alpha regulates phosphatidylcholine synthesis required for lipid droplet biogenesis. *Mol Biol Cell* **26**, 2927-2938

3. Lee, J., and Ridgway, N. D. (2019) Substrate channeling in the glycerol-3-phosphate pathway regulates the synthesis, storage and secretion of glycerolipids. *Biochim Biophys Acta Mol Cell Biol Lipids*

4. Lee, J., and Ridgway, N. D. (2018) Phosphatidylcholine synthesis regulates triglyceride storage and chylomicron secretion by Caco2 cells. *J Lipid Res* **59**, 1940-1950

5. Langin, D., Dicker, A., Tavernier, G., Hoffstedt, J., Mairal, A., Ryden, M., Arner, E., Sicard, A., Jenkins, C. M., Viguerie, N., van Harmelen, V., Gross, R. W., Holm, C., and Arner, P. (2005) Adipocyte lipases and defect of lipolysis in human obesity. *Diabetes* **54**, 3190-3197

6. Nagle, C. A., Klett, E. L., and Coleman, R. A. (2009) Hepatic triacylglycerol accumulation and insulin resistance. *J Lipid Res* **50 Suppl**, S74-79

7. Boutet, E., El Mourabit, H., Prot, M., Nemani, M., Khallouf, E., Colard, O., Maurice, M., Durand-Schneider, A. M., Chretien, Y., Gres, S., Wolf, C., Saulnier-Blache, J. S., Capeau, J., and Magre, J. (2009) Seipin deficiency alters fatty acid Delta9 desaturation and lipid droplet formation in Berardinelli-Seip congenital lipodystrophy. *Biochimie* **91**, 796-803

8. Fagone, P., and Jackowski, S. (2013) Phosphatidylcholine and the CDP-choline cycle. *Biochim Biophys Acta* **1831**, 523-532

9. Cornell, R. B. (2016) Membrane lipid compositional sensing by the inducible amphipathic helix of CCT. *Biochim Biophys Acta* **1861**, 847-861

10. Cornell, R. B., and Ridgway, N. D. (2015) CTP:phosphocholine cytidylyltransferase: Function, regulation, and structure of an amphitropic enzyme required for membrane biogenesis. *Prog Lipid Res* **59**, 147-171

11. Jacobs, R. L., Devlin, C., Tabas, I., and Vance, D. E. (2004) Targeted deletion of hepatic CTP:phosphocholine cytidylyltransferase alpha in mice decreases plasma high density and very low density lipoproteins. *J Biol Chem* **279**, 47402-47410

12. Krahmer, N., Guo, Y., Wilfling, F., Hilger, M., Lingrell, S., Heger, K., Newman, H. W., Schmidt-Supprian, M., Vance, D. E., Mann, M., Farese, R. V., Jr., and Walther, T. C. (2011) Phosphatidylcholine synthesis for lipid droplet expansion is mediated by localized activation of CTP:phosphocholine cytidylyltransferase. *Cell Metab* **14**, 504-515

13. Lagrutta, L. C., Montero-Villegas, S., Layerenza, J. P., Sisti, M. S., Garcia de Bravo, M. M., and Ves-Losada, A. (2017) Reversible Nuclear-Lipid-Droplet Morphology Induced by Oleic Acid: A Link to Cellular-Lipid Metabolism. *PLoS One* **12**, e0170608

14. Ohsaki, Y., Kawai, T., Yoshikawa, Y., Cheng, J., Jokitalo, E., and Fujimoto, T. (2016) PML isoform II plays a critical role in nuclear lipid droplet formation. *J Cell Biol* **212**, 29-38

15. Yen, C. L., Stone, S. J., Koliwad, S., Harris, C., and Farese, R. V., Jr. (2008) Thematic review series: glycerolipids. DGAT enzymes and triacylglycerol biosynthesis. *J Lipid Res* **49**, 2283-2301

16. Lagace, T. A., and Ridgway, N. D. (2013) The role of phospholipids in the biological activity and structure of the endoplasmic reticulum. *Biochim Biophys Acta* **1833**, 2499-2510

17. Listenberger, L. L., Han, X., Lewis, S. E., Cases, S., Farese, R. V., Jr., Ory, D. S., and Schaffer, J. E. (2003) Triglyceride accumulation protects against fatty acid-induced lipotoxicity. *Proc Natl Acad Sci U S A* **100**, 3077-3082

18. Dowhan, W. (1997) Molecular basis for membrane phospholipid diversity: why are there so many lipids? *Annu Rev Biochem* **66**, 199-232

19. Cullis, P. R., and de Kruijff, B. (1979) Lipid polymorphism and the functional roles of lipids in biological membranes. *Biochim Biophys Acta* **559**, 399-420

20. Essen, L. O., Perisic, O., Katan, M., Wu, Y., Roberts, M. F., and Williams, R. L. (1997) Structural mapping of the catalytic mechanism for a mammalian phosphoinositide-specific phospholipase C. *Biochemistry* **36**, 1704-1718

21. Fadok, V. A., Bratton, D. L., Frasch, S. C., Warner, M. L., and Henson, P. M. (1998) The role of phosphatidylserine in recognition of apoptotic cells by phagocytes. *Cell Death Differ* **5**, 551-562

22. Daleke, D. L. (2003) Regulation of transbilayer plasma membrane phospholipid asymmetry. *J Lipid Res* **44**, 233-242

23. Brugger, B., Erben, G., Sandhoff, R., Wieland, F. T., and Lehmann, W. D. (1997) Quantitative analysis of biological membrane lipids at the low picomole level by nano-electrospray ionization tandem mass spectrometry. *Proc Natl Acad Sci U S A* **94**, 2339-2344

24. Nakamura, T., Lin, L. L., Kharbanda, S., Knopf, J., and Kufe, D. (1992) Macrophage colony stimulating factor activates phosphatidylcholine hydrolysis by cytoplasmic phospholipase A2. *EMBO J* **11**, 4917-4922

25. Liscovitch, M., Ben-Av, P., Danin, M., Faiman, G., Eldar, H., and Livneh, E. (1993) Phospholipase D-mediated hydrolysis of phosphatidylcholine: role in cell signalling. *J Lipid Mediat* **8**, 177-182

26. Billah, M. M., Eckel, S., Mullmann, T. J., Egan, R. W., and Siegel, M. I. (1989) Phosphatidylcholine hydrolysis by phospholipase D determines phosphatidate and diglyceride levels in chemotactic peptide-stimulated human neutrophils. Involvement of phosphatidate phosphohydrolase in signal transduction. *J Biol Chem* **264**, 17069-17077

27. Sakai, T., Sugiyama, T., Banno, Y., Kato, Y., and Nozawa, Y. (2004) Involvement of phosphatidylcholine hydrolysis by phospholipase C in prostaglandin F2alpha-induced 1,2-diacylglycerol formation in osteoblast-like MC3T3-E1 cells. *J Bone Miner Metab* **22**, 198-206

28. Greenberg, A. S., Coleman, R. A., Kraemer, F. B., McManaman, J. L., Obin, M. S., Puri, V., Yan, Q. W., Miyoshi, H., and Mashek, D. G. (2011) The role of lipid droplets in metabolic disease in rodents and humans. *J Clin Invest* **121**, 2102-2110

29. Fujimoto, T., and Parton, R. G. (2011) Not just fat: the structure and function of the lipid droplet. *Cold Spring Harb Perspect Biol* **3**

30. Guo, Y., Walther, T. C., Rao, M., Stuurman, N., Goshima, G., Terayama, K., Wong, J. S., Vale, R. D., Walter, P., and Farese, R. V. (2008) Functional genomic screen reveals genes involved in lipid-droplet formation and utilization. *Nature* **453**, 657-661

31. Thiam, A. R., Farese, R. V., Jr., and Walther, T. C. (2013) The biophysics and cell biology of lipid droplets. *Nat Rev Mol Cell Biol* **14**, 775-786

32. Krahmer, N., Farese, R. V., Jr., and Walther, T. C. (2013) Balancing the fat: lipid droplets and human disease. *EMBO Mol Med* **5**, 973-983

33. Caceres, M., Teran, C. G., Rodriguez, S., and Medina, M. (2008) Prevalence of insulin resistance and its association with metabolic syndrome criteria among Bolivian children and adolescents with obesity. *BMC Pediatr* **8**, 31

34. Sayiner, M., Koenig, A., Henry, L., and Younossi, Z. M. (2016) Epidemiology of Nonalcoholic Fatty Liver Disease and Nonalcoholic Steatohepatitis in the United States and the Rest of the World. *Clin Liver Dis* **20**, 205-214

35. Coleman, R. A., Lewin, T. M., Van Horn, C. G., and Gonzalez-Baro, M. R. (2002) Do long-chain acyl-CoA synthetases regulate fatty acid entry into synthetic versus degradative pathways? *J Nutr* **132**, 2123-2126

36. Kayden, H. J., Senior, J. R., and Mattson, F. H. (1967) The monoglyceride pathway of fat absorption in man. *J Clin Invest* **46**, 1695-1703

37. Nelson, D. W., Gao, Y., Yen, M. I., and Yen, C. L. (2014) Intestine-specific deletion of acyl-CoA:monoacylglycerol acyltransferase (MGAT) 2 protects mice from diet-induced obesity and glucose intolerance. *J Biol Chem* **289**, 17338-17349

38. Takeuchi, K., and Reue, K. (2009) Biochemistry, physiology, and genetics of GPAT, AGPAT, and lipin enzymes in triglyceride synthesis. *Am J Physiol Endocrinol Metab* **296**, E1195-1209

39. Coleman, R. A., and Lee, D. P. (2004) Enzymes of triacylglycerol synthesis and their regulation. *Prog Lipid Res* **43**, 134-176

40. Wilfling, F., Wang, H., Haas, J. T., Krahmer, N., Gould, T. J., Uchida, A., Cheng, J. X., Graham, M., Christiano, R., Frohlich, F., Liu, X., Buhman, K. K., Coleman, R. A., Bewersdorf, J., Farese, R. V., Jr., and Walther, T. C. (2013) Triacylglycerol synthesis enzymes mediate lipid droplet growth by relocalizing from the ER to lipid droplets. *Dev Cell* **24**, 384-399

41. McFie, P. J., Banman, S. L., Kary, S., and Stone, S. J. (2011) Murine diacylglycerol acyltransferase-2 (DGAT2) can catalyze triacylglycerol synthesis and promote lipid droplet formation independent of its localization to the endoplasmic reticulum. *J Biol Chem* **286**, 28235-28246

42. Wendel, A. A., Lewin, T. M., and Coleman, R. A. (2009) Glycerol-3-phosphate acyltransferases: rate limiting enzymes of triacylglycerol biosynthesis. *Biochim Biophys Acta* **1791**, 501-506

43. Yamashita, A., Hayashi, Y., Matsumoto, N., Nemoto-Sasaki, Y., Oka, S., Tanikawa, T., and Sugiura, T. (2014) Glycerophosphate/Acylglycerophosphate acyltransferases. *Biology (Basel)* **3**, 801-830

44. Gonzalez-Baro, M. R., and Coleman, R. A. (2017) Mitochondrial acyltransferases and glycerophospholipid metabolism. *Biochim Biophys Acta Mol Cell Biol Lipids* **1862**, 49-55

45. Dircks, L. K., Ke, J., and Sul, H. S. (1999) A conserved seven amino acid stretch important for murine mitochondrial glycerol-3-phosphate acyltransferase activity. Significance of arginine 318 in catalysis. *J Biol Chem* **274**, 34728-34734

46. Heath, R. J., and Rock, C. O. (1998) A conserved histidine is essential for glycerolipid acyltransferase catalysis. *J Bacteriol* **180**, 1425-1430

47. Lewin, T. M., Wang, P., and Coleman, R. A. (1999) Analysis of amino acid motifs diagnostic for the sn-glycerol-3-phosphate acyltransferase reaction. *Biochemistry* **38**, 5764-5771

48. Vancura, A., and Haldar, D. (1994) Purification and characterization of glycerophosphate acyltransferase from rat liver mitochondria. *J Biol Chem* **269**, 27209-27215

49. Wang, S., Lee, D. P., Gong, N., Schwerbrock, N. M., Mashek, D. G., Gonzalez-Baro, M. R., Stapleton, C., Li, L. O., Lewin, T. M., and Coleman, R. A. (2007) Cloning and functional characterization of a novel mitochondrial N-ethylmaleimide-sensitive glycerol-3-phosphate acyltransferase (GPAT2). *Arch Biochem Biophys* **465**, 347-358

50. Lewin, T. M., Schwerbrock, N. M., Lee, D. P., and Coleman, R. A. (2004) Identification of a new glycerol-3-phosphate acyltransferase isoenzyme, mtGPAT2, in mitochondria. *J Biol Chem* **279**, 13488-13495

51. Cao, J., Li, J. L., Li, D., Tobin, J. F., and Gimeno, R. E. (2006) Molecular identification of microsomal acyl-CoA:glycerol-3-phosphate acyltransferase, a key enzyme in de novo triacylglycerol synthesis. *Proc Natl Acad Sci U S A* **103**, 19695-19700

52. Nagle, C. A., Vergnes, L., Dejong, H., Wang, S., Lewin, T. M., Reue, K., and Coleman, R. A. (2008) Identification of a novel sn-glycerol-3-phosphate acyltransferase isoform, GPAT4, as the enzyme deficient in Agpat6-/- mice. *J Lipid Res* **49**, 823-831

53. Beigneux, A. P., Vergnes, L., Qiao, X., Quatela, S., Davis, R., Watkins, S. M., Coleman, R. A., Walzem, R. L., Philips, M., Reue, K., and Young, S. G. (2006) Agpat6--a novel lipid biosynthetic gene required for triacylglycerol production in mammary epithelium. *J Lipid Res* **47**, 734-744

54. Aguado, B., and Campbell, R. D. (1998) Characterization of a human lysophosphatidic acid acyltransferase that is encoded by a gene located in the class III region of the human major histocompatibility complex. *J Biol Chem* **273**, 4096-4105

55. Hollenback, D., Bonham, L., Law, L., Rossnagle, E., Romero, L., Carew, H., Tompkins, C. K., Leung, D. W., Singer, J. W., and White, T. (2006) Substrate specificity of lysophosphatidic acid acyltransferase beta -- evidence from membrane and whole cell assays. *J Lipid Res* **47**, 593-604

56. Agarwal, A. K., and Garg, A. (2003) Congenital generalized lipodystrophy: significance of triglyceride biosynthetic pathways. *Trends Endocrinol Metab* **14**, 214-221

57. Eberhardt, C., Gray, P. W., and Tjoelker, L. W. (1997) Human lysophosphatidic acid acyltransferase. cDNA cloning, expression, and localization to chromosome 9q34.3. *J Biol Chem* **272**, 20299-20305

58. West, J., Tompkins, C. K., Balantac, N., Nudelman, E., Meengs, B., White, T., Bursten, S., Coleman, J., Kumar, A., Singer, J. W., and Leung, D. W. (1997) Cloning and expression of two human lysophosphatidic acid acyltransferase cDNAs that enhance cytokine-induced signaling responses in cells. *DNA Cell Biol* **16**, 691-701

59. Gale, S. E., Frolov, A., Han, X., Bickel, P. E., Cao, L., Bowcock, A., Schaffer, J. E., and Ory, D. S. (2006) A regulatory role for 1-acylglycerol-3-phosphate-O-acyltransferase 2 in adipocyte differentiation. *J Biol Chem* **281**, 11082-11089

60. Agarwal, A. K., Arioglu, E., De Almeida, S., Akkoc, N., Taylor, S. I., Bowcock, A. M., Barnes, R. I., and Garg, A. (2002) AGPAT2 is mutated in congenital generalized lipodystrophy linked to chromosome 9q34. *Nat Genet* **31**, 21-23

61. Prasad, S. S., Garg, A., and Agarwal, A. K. (2011) Enzymatic activities of the human AGPAT isoform 3 and isoform 5: localization of AGPAT5 to mitochondria. *J Lipid Res* **52**, 451-462

62. Yuki, K., Shindou, H., Hishikawa, D., and Shimizu, T. (2009) Characterization of mouse lysophosphatidic acid acyltransferase 3: an enzyme with dual functions in the testis. *J Lipid Res* **50**, 860-869

63. Eto, M., Shindou, H., and Shimizu, T. (2014) A novel lysophosphatidic acid acyltransferase enzyme (LPAAT4) with a possible role for incorporating docosahexaenoic acid into brain glycerophospholipids. *Biochem Biophys Res Commun* **443**, 718-724

64. Lu, B., Jiang, Y. J., Zhou, Y., Xu, F. Y., Hatch, G. M., and Choy, P. C. (2005) Cloning and characterization of murine 1-acyl-sn-glycerol 3-phosphate acyltransferases and their regulation by PPARalpha in murine heart. *Biochem J* **385**, 469-477

65. Eaton, J. M., Takkellapati, S., Lawrence, R. T., McQueeney, K. E., Boroda, S., Mullins, G. R., Sherwood, S. G., Finck, B. N., Villen, J., and Harris, T. E. (2014) Lipin 2 binds phosphatidic acid by the electrostatic hydrogen bond switch mechanism independent of phosphorylation. *J Biol Chem* **289**, 18055-18066

66. Valdearcos, M., Esquinas, E., Meana, C., Gil-de-Gomez, L., Guijas, C., Balsinde, J., and Balboa, M. A. (2011) Subcellular localization and role of lipin-1 in human macrophages. *J Immunol* **186**, 6004-6013

67. Wang, H., Zhang, J., Qiu, W., Han, G. S., Carman, G. M., and Adeli, K. (2011) Lipin-1gamma isoform is a novel lipid droplet-associated protein highly expressed in the brain. *FEBS Lett* **585**, 1979-1984

68. Donkor, J., Sariahmetoglu, M., Dewald, J., Brindley, D. N., and Reue, K. (2007) Three mammalian lipins act as phosphatidate phosphatases with distinct tissue expression patterns. *J Biol Chem* **282**, 3450-3457

69. Grimsey, N., Han, G. S., O'Hara, L., Rochford, J. J., Carman, G. M., and Siniossoglou, S. (2008) Temporal and spatial regulation of the phosphatidate phosphatases lipin 1 and 2. *J Biol Chem* **283**, 29166-29174

70. Csaki, L. S., Dwyer, J. R., Li, X., Nguyen, M. H., Dewald, J., Brindley, D. N., Lusis, A. J., Yoshinaga, Y., de Jong, P., Fong, L., Young, S. G., and Reue, K. (2014) Lipin-1 and lipin-3 together determine adiposity in vivo. *Mol Metab* **3**, 145-154

71. Cases, S., Stone, S. J., Zhou, P., Yen, E., Tow, B., Lardizabal, K. D., Voelker, T., and Farese, R. V., Jr. (2001) Cloning of DGAT2, a second mammalian diacylglycerol acyltransferase, and related family members. *J Biol Chem* **276**, 38870-38876

72. McFie, P. J., Stone, S. L., Banman, S. L., and Stone, S. J. (2010) Topological orientation of acyl-CoA:diacylglycerol acyltransferase-1 (DGAT1) and identification of a putative active site histidine and the role of the n terminus in dimer/tetramer formation. *J Biol Chem* **285**, 37377-37387

73. Cases, S., Smith, S. J., Zheng, Y. W., Myers, H. M., Lear, S. R., Sande, E., Novak, S., Collins, C., Welch, C. B., Lusis, A. J., Erickson, S. K., and Farese, R. V., Jr. (1998) Identification of a gene encoding an acyl CoA:diacylglycerol acyltransferase, a key enzyme in triacylglycerol synthesis. *Proc Natl Acad Sci U S A* **95**, 13018-13023

74. McFie, P. J., Banman, S. L., and Stone, S. J. (2018) Diacylglycerol acyltransferase-2 contains a c-terminal sequence that interacts with lipid droplets. *Biochim Biophys Acta Mol Cell Biol Lipids* **1863**, 1068-1081

75. Coleman, R. A., Lewin, T. M., and Muoio, D. M. (2000) Physiological and nutritional regulation of enzymes of triacylglycerol synthesis. *Annu Rev Nutr* **20**, 77-103

76. Linden, D., William-Olsson, L., Ahnmark, A., Ekroos, K., Hallberg, C., Sjogren, H. P., Becker, B., Svensson, L., Clapham, J. C., Oscarsson, J., and Schreyer, S. (2006) Liver-directed overexpression of mitochondrial glycerol-3-phosphate acyltransferase results in hepatic steatosis, increased triacylglycerol secretion and reduced fatty acid oxidation. *FASEB J* **20**, 434-443

77. Linden, D., William-Olsson, L., Rhedin, M., Asztely, A. K., Clapham, J. C., and Schreyer, S. (2004) Overexpression of mitochondrial GPAT in rat hepatocytes leads to decreased fatty acid oxidation and increased glycerolipid biosynthesis. *J Lipid Res* **45**, 1279-1288

78. Nagle, C. A., An, J., Shiota, M., Torres, T. P., Cline, G. W., Liu, Z. X., Wang, S., Catlin, R. L., Shulman, G. I., Newgard, C. B., and Coleman, R. A. (2007) Hepatic overexpression of glycerol-sn-3-phosphate acyltransferase 1 in rats causes insulin resistance. *J Biol Chem* **282**, 14807-14815

79. Hammond, L. E., Neschen, S., Romanelli, A. J., Cline, G. W., Ilkayeva, O. R., Shulman, G. I., Muoio, D. M., and Coleman, R. A. (2005) Mitochondrial glycerol-3-phosphate acyltransferase-1 is essential in liver for the metabolism of excess acyl-CoAs. *J Biol Chem* **280**, 25629-25636

80. Neschen, S., Morino, K., Hammond, L. E., Zhang, D., Liu, Z. X., Romanelli, A. J., Cline, G. W., Pongratz, R. L., Zhang, X. M., Choi, C. S., Coleman, R. A., and Shulman, G. I. (2005) Prevention of hepatic steatosis and hepatic insulin resistance in mitochondrial acyl-CoA:glycerol-sn-3-phosphate acyltransferase 1 knockout mice. *Cell Metab* **2**, 55-65

81. Cao, J., Perez, S., Goodwin, B., Lin, Q., Peng, H., Qadri, A., Zhou, Y., Clark, R. W., Perreault, M., Tobin, J. F., and Gimeno, R. E. (2014) Mice deleted for GPAT3 have reduced GPAT activity in white adipose tissue and altered energy and cholesterol homeostasis in diet-induced obesity. *Am J Physiol Endocrinol Metab* **306**, E1176-1187

82. Khatun, I., Clark, R. W., Vera, N. B., Kou, K., Erion, D. M., Coskran, T., Bobrowski, W. F., Okerberg, C., and Goodwin, B. (2016) Characterization of a Novel Intestinal Glycerol-3-phosphate Acyltransferase Pathway and Its Role in Lipid Homeostasis. *J Biol Chem* **291**, 2602-2615

83. Wendel, A. A., Cooper, D. E., Ilkayeva, O. R., Muoio, D. M., and Coleman, R. A. (2013) Glycerol-3-phosphate acyltransferase (GPAT)-1, but not GPAT4, incorporates newly synthesized fatty acids into triacylglycerol and diminishes fatty acid oxidation. *J Biol Chem* **288**, 27299-27306

84. Chen, Y. Q., Kuo, M. S., Li, S., Bui, H. H., Peake, D. A., Sanders, P. E., Thibodeaux, S. J., Chu, S., Qian, Y. W., Zhao, Y., Bredt, D. S., Moller, D. E., Konrad, R. J., Beigneux, A. P., Young, S. G., and Cao, G. (2008) AGPAT6 is a novel microsomal glycerol-3-phosphate acyltransferase. *J Biol Chem* **283**, 10048-10057

85. Cao, J., Shan, D., Revett, T., Li, D., Wu, L., Liu, W., Tobin, J. F., and Gimeno, R. E. (2008) Molecular identification of a novel mammalian brain isoform of acyl-CoA:lysophospholipid acyltransferase with prominent ethanolamine lysophospholipid acylating activity, LPEAT2. *J Biol Chem* **283**, 19049-19057

86. Hishikawa, D., Hashidate, T., Shimizu, T., and Shindou, H. (2014) Diversity and function of membrane glycerophospholipids generated by the remodeling pathway in mammalian cells. *J Lipid Res* **55**, 799-807

87. Kume, K., and Shimizu, T. (1997) cDNA cloning and expression of murine 1-acyl-sn-glycerol-3-phosphate acyltransferase. *Biochem Biophys Res Commun* **237**, 663-666

88. Ruan, H., and Pownall, H. J. (2001) Overexpression of 1-acyl-glycerol-3-phosphate acyltransferase-alpha enhances lipid storage in cellular models of adipose tissue and skeletal muscle. *Diabetes* **50**, 233-240

89. Cortes, V. A., Curtis, D. E., Sukumaran, S., Shao, X., Parameswara, V., Rashid, S., Smith, A. R., Ren, J., Esser, V., Hammer, R. E., Agarwal, A. K., Horton, J. D., and Garg, A. (2009) Molecular mechanisms of hepatic steatosis and insulin resistance in the AGPAT2-deficient mouse model of congenital generalized lipodystrophy. *Cell Metab* **9**, 165-176

90. Agarwal, A. K., Tunison, K., Dalal, J. S., Yen, C. L., Farese, R. V., Jr., Horton, J. D., and Garg, A. (2016) Mogat1 deletion does not ameliorate hepatic steatosis in lipodystrophic (Agpat2-/-) or obese (ob/ob) mice. *J Lipid Res* **57**, 616-630

91. Koeberle, A., Shindou, H., Harayama, T., Yuki, K., and Shimizu, T. (2012) Polyunsaturated fatty acids are incorporated into maturating male mouse germ cells by lysophosphatidic acid acyltransferase 3. *FASEB J* **26**, 169-180

92. Soupene, E., Fyrst, H., and Kuypers, F. A. (2008) Mammalian acyl-CoA:lysophosphatidylcholine acyltransferase enzymes. *Proc Natl Acad Sci U S A* **105**, 88-93

93. Nakanishi, H., Shindou, H., Hishikawa, D., Harayama, T., Ogasawara, R., Suwabe, A., Taguchi, R., and Shimizu, T. (2006) Cloning and characterization of mouse lung-type acyl-CoA:lysophosphatidylcholine acyltransferase 1 (LPCAT1). Expression in alveolar type II cells and possible involvement in surfactant production. *J Biol Chem* **281**, 20140-20147

94. Harayama, T., Eto, M., Shindou, H., Kita, Y., Otsubo, E., Hishikawa, D., Ishii, S., Sakimura, K., Mishina, M., and Shimizu, T. (2014) Lysophospholipid acyltransferases mediate phosphatidylcholine diversification to achieve the physical properties required in vivo. *Cell Metab* **20**, 295-305

95. Bridges, J. P., Ikegami, M., Brilli, L. L., Chen, X., Mason, R. J., and Shannon, J. M. (2010) LPCAT1 regulates surfactant phospholipid synthesis and is required for transitioning to air breathing in mice. *J Clin Invest* **120**, 1736-1748

96. Shindou, H., Hishikawa, D., Nakanishi, H., Harayama, T., Ishii, S., Taguchi, R., and Shimizu, T. (2007) A single enzyme catalyzes both platelet-activating factor production and membrane biogenesis of inflammatory cells. Cloning and characterization of acetyl-CoA:LYSO-PAF acetyltransferase. *J Biol Chem* **282**, 6532-6539

97. Shindou, H., Ishii, S., Yamamoto, M., Takeda, K., Akira, S., and Shimizu, T. (2005) Priming effect of lipopolysaccharide on acetyl-coenzyme A:lyso-platelet-activating factor acetyltransferase is MyD88 and TRIF independent. *J Immunol* **175**, 1177-1183

98. Shindou, H., Hishikawa, D., Harayama, T., Yuki, K., and Shimizu, T. (2009) Recent progress on acyl CoA: lysophospholipid acyltransferase research. *J Lipid Res* **50 Suppl**, S46-51

99. Hashidate-Yoshida, T., Harayama, T., Hishikawa, D., Morimoto, R., Hamano, F., Tokuoka, S. M., Eto, M., Tamura-Nakano, M., Yanobu-Takanashi, R., Mukumoto, Y., Kiyonari, H., Okamura, T., Kita, Y., Shindou, H., and Shimizu, T. (2015) Fatty acid remodeling by LPCAT3 enriches arachidonate in phospholipid membranes and regulates triglyceride transport. *Elife* **4**

100. Rong, X., Wang, B., Dunham, M. M., Hedde, P. N., Wong, J. S., Gratton, E., Young, S. G., Ford, D. A., and Tontonoz, P. (2015) Lpcat3-dependent production of arachidonoyl phospholipids is a key determinant of triglyceride secretion. *Elife* **4**

101. Hishikawa, D., Shindou, H., Kobayashi, S., Nakanishi, H., Taguchi, R., and Shimizu, T. (2008) Discovery of a lysophospholipid acyltransferase family essential for membrane asymmetry and diversity. *Proc Natl Acad Sci U S A* **105**, 2830-2835

102. Kurabe, N., Hayasaka, T., Ogawa, M., Masaki, N., Ide, Y., Waki, M., Nakamura, T., Kurachi, K., Kahyo, T., Shinmura, K., Midorikawa, Y., Sugiyama, Y., Setou, M., and Sugimura, H. (2013) Accumulated phosphatidylcholine (16:0/16:1) in human colorectal cancer; possible involvement of LPCAT4. *Cancer Sci* **104**, 1295-1302

103. Han, G. S., Wu, W. I., and Carman, G. M. (2006) The Saccharomyces cerevisiae Lipin homolog is a Mg2+-dependent phosphatidate phosphatase enzyme. *J Biol Chem* **281**, 9210-9218

104. Peterfy, M., Phan, J., Xu, P., and Reue, K. (2001) Lipodystrophy in the fld mouse results from mutation of a new gene encoding a nuclear protein, lipin. *Nat Genet* **27**, 121-124

105. Peterfy, M., Phan, J., and Reue, K. (2005) Alternatively spliced lipin isoforms exhibit distinct expression pattern, subcellular localization, and role in adipogenesis. *J Biol Chem* **280**, 32883-32889

106. Harris, T. E., Huffman, T. A., Chi, A., Shabanowitz, J., Hunt, D. F., Kumar, A., and Lawrence, J. C., Jr. (2007) Insulin controls subcellular localization and multisite phosphorylation of the phosphatidic acid phosphatase, lipin 1. *J Biol Chem* **282**, 277-286

107. Phan, J., Peterfy, M., and Reue, K. (2004) Lipin expression preceding peroxisome proliferator-activated receptor-gamma is critical for adipogenesis in vivo and in vitro. *J Biol Chem* **279**, 29558-29564

108. Zeharia, A., Shaag, A., Houtkooper, R. H., Hindi, T., de Lonlay, P., Erez, G., Hubert, L., Saada, A., de Keyzer, Y., Eshel, G., Vaz, F. M., Pines, O., and Elpeleg, O. (2008) Mutations in LPIN1 cause recurrent acute myoglobinuria in childhood. *Am J Hum Genet* **83**, 489-494

109. Dwyer, J. R., Donkor, J., Zhang, P., Csaki, L. S., Vergnes, L., Lee, J. M., Dewald, J., Brindley, D. N., Atti, E., Tetradis, S., Yoshinaga, Y., De Jong, P. J., Fong, L. G., Young, S. G., and Reue, K. (2012) Mouse lipin-1 and lipin-2 cooperate to maintain glycerolipid homeostasis in liver and aging cerebellum. *Proc Natl Acad Sci U S A* **109**, E2486-2495

110. Finck, B. N., Gropler, M. C., Chen, Z., Leone, T. C., Croce, M. A., Harris, T. E., Lawrence, J. C., Jr., and Kelly, D. P. (2006) Lipin 1 is an inducible amplifier of the hepatic PGC-1alpha/PPARalpha regulatory pathway. *Cell Metab* **4**, 199-210

111. Harris, T. E., and Finck, B. N. (2011) Dual function lipin proteins and glycerolipid metabolism. *Trends Endocrinol Metab* **22**, 226-233

112. Weiss, S. B., Kennedy, E. P., and Kiyasu, J. Y. (1960) The enzymatic synthesis of triglycerides. *J Biol Chem* **235**, 40-44

113. Walther, T. C., and Farese, R. V., Jr. (2009) The life of lipid droplets. *Biochim Biophys Acta* **1791**, 459-466

114. Lin, S., Cheng, D., Liu, M. S., Chen, J., and Chang, T. Y. (1999) Human acyl-CoA:cholesterol acyltransferase-1 in the endoplasmic reticulum contains seven transmembrane domains. *J Biol Chem* **274**, 23276-23285

115. Waterman, I. J., Price, N. T., and Zammit, V. A. (2002) Distinct ontogenic patterns of overt and latent DGAT activities of rat liver microsomes. *J Lipid Res* **43**, 1555-1562

116. Villanueva, C. J., Monetti, M., Shih, M., Zhou, P., Watkins, S. M., Bhanot, S., and Farese, R. V., Jr. (2009) Specific role for acyl CoA:Diacylglycerol acyltransferase 1 (Dgat1) in hepatic steatosis due to exogenous fatty acids. *Hepatology* **50**, 434-442

117. Li, C., Li, L., Lian, J., Watts, R., Nelson, R., Goodwin, B., and Lehner, R. (2015) Roles of Acyl-CoA:Diacylglycerol Acyltransferases 1 and 2 in Triacylglycerol Synthesis and Secretion in Primary Hepatocytes. *Arterioscler Thromb Vasc Biol* **35**, 1080-1091

118. Lehner, R., Lian, J., and Quiroga, A. D. (2012) Lumenal lipid metabolism: implications for lipoprotein assembly. *Arterioscler Thromb Vasc Biol* **32**, 1087-1093

119. Stone, S. J., Levin, M. C., and Farese, R. V., Jr. (2006) Membrane topology and identification of key functional amino acid residues of murine acyl-CoA:diacylglycerol acyltransferase-2. *J Biol Chem* **281**, 40273-40282

120. Thiele, C., and Spandl, J. (2008) Cell biology of lipid droplets. *Curr Opin Cell Biol* **20**, 378-385

121. van Meer, G. (2001) Caveolin, cholesterol, and lipid droplets? *J Cell Biol* **152**, F29-34

122. Han, G. S., Siniossoglou, S., and Carman, G. M. (2007) The cellular functions of the yeast lipin homolog PAH1p are dependent on its phosphatidate phosphatase activity. *J Biol Chem* **282**, 37026-37035

123. Cascales, C., Mangiapane, E. H., and Brindley, D. N. (1984) Oleic acid promotes the activation and translocation of phosphatidate phosphohydrolase from the cytosol to particulate fractions of isolated rat hepatocytes. *Biochem J* **219**, 911-916

124. Sim, M. F., Dennis, R. J., Aubry, E. M., Ramanathan, N., Sembongi, H., Saudek, V., Ito, D., O'Rahilly, S., Siniossoglou, S., and Rochford, J. J. (2012) The human lipodystrophy protein seipin is an ER membrane adaptor for the adipogenic PA phosphatase lipin 1. *Mol Metab* **2**, 38-46

125. Sui, X., Arlt, H., Brock, K. P., Lai, Z. W., DiMaio, F., Marks, D. S., Liao, M., Farese, R. V., Jr., and Walther, T. C. (2018) Cryo-electron microscopy structure of the lipid droplet-formation protein seipin. *J Cell Biol* **217**, 4080-4091

126. Szymanski, K. M., Binns, D., Bartz, R., Grishin, N. V., Li, W. P., Agarwal, A. K., Garg, A., Anderson, R. G., and Goodman, J. M. (2007) The lipodystrophy protein seipin is found at endoplasmic reticulum lipid droplet junctions and is important for droplet morphology. *Proc Natl Acad Sci U S A* **104**, 20890-20895

127. Yan, R., Qian, H., Lukmantara, I., Gao, M., Du, X., Yan, N., and Yang, H. (2018) Human SEIPIN Binds Anionic Phospholipids. *Dev Cell* **47**, 248-256 e244

128. Talukder, M. M., Sim, M. F., O'Rahilly, S., Edwardson, J. M., and Rochford, J. J. (2015) Seipin oligomers can interact directly with AGPAT2 and lipin 1, physically scaffolding critical regulators of adipogenesis. *Mol Metab* **4**, 199-209

129. Pagac, M., Cooper, D. E., Qi, Y., Lukmantara, I. E., Mak, H. Y., Wu, Z., Tian, Y., Liu, Z., Lei, M., Du, X., Ferguson, C., Kotevski, D., Sadowski, P., Chen, W., Boroda, S., Harris, T. E., Liu, G., Parton, R. G., Huang, X., Coleman, R. A., and Yang, H. (2016) SEIPIN Regulates Lipid Droplet Expansion and Adipocyte Development by Modulating the Activity of Glycerol-3-phosphate Acyltransferase. *Cell Rep* **17**, 1546-1559

130. Lehner, R., and Kuksis, A. (1995) Triacylglycerol synthesis by purified triacylglycerol synthetase of rat intestinal mucosa. Role of acyl-CoA acyltransferase. *J Biol Chem* **270**, 13630-13636

131. Man, W. C., Miyazaki, M., Chu, K., and Ntambi, J. (2006) Colocalization of SCD1 and DGAT2: implying preference for endogenous monounsaturated fatty acids in triglyceride synthesis. *J Lipid Res* **47**, 1928-1939

132. Vance, J. E. (2014) MAM (mitochondria-associated membranes) in mammalian cells: lipids and beyond. *Biochim Biophys Acta* **1841**, 595-609

133. Jin, Y., McFie, P. J., Banman, S. L., Brandt, C., and Stone, S. J. (2014) Diacylglycerol acyltransferase-2 (DGAT2) and monoacylglycerol acyltransferase-2 (MGAT2) interact to promote triacylglycerol synthesis. *J Biol Chem* **289**, 28237-28248

134. Xu, N., Zhang, S. O., Cole, R. A., McKinney, S. A., Guo, F., Haas, J. T., Bobba, S., Farese, R. V., Jr., and Mak, H. Y. (2012) The FATP1-DGAT2 complex facilitates lipid droplet expansion at the ER-lipid droplet interface. *J Cell Biol* **198**, 895-911

135. Vance, J. E., and Vance, D. E. (2004) Phospholipid biosynthesis in mammalian cells. *Biochem Cell Biol* **82**, 113-128

136. Ridgway, N. D., and Vance, D. E. (1987) Purification of phosphatidylethanolamine N-methyltransferase from rat liver. *J Biol Chem* **262**, 17231-17239

137. Cole, L. K., and Vance, D. E. (2010) A role for Sp1 in transcriptional regulation of phosphatidylethanolamine N-methyltransferase in liver and 3T3-L1 adipocytes. *J Biol Chem* **285**, 11880-11891

138. Kennedy, E. P., and Weiss, S. B. (1956) The function of cytidine coenzymes in the biosynthesis of phospholipides. *J Biol Chem* **222**, 193-214

139. Li, Z., and Vance, D. E. (2008) Phosphatidylcholine and choline homeostasis. *J Lipid Res* **49**, 1187-1194

140. Michel, V., Yuan, Z., Ramsubir, S., and Bakovic, M. (2006) Choline transport for phospholipid synthesis. *Exp Biol Med (Maywood)* **231**, 490-504

141. Lever, M., and Slow, S. (2010) The clinical significance of betaine, an osmolyte with a key role in methyl group metabolism. *Clin Biochem* **43**, 732-744

142. Roth, M., Obaidat, A., and Hagenbuch, B. (2012) OATPs, OATs and OCTs: the organic anion and cation transporters of the SLCO and SLC22A gene superfamilies. *Br J Pharmacol* **165**, 1260-1287

143. Nies, A. T., Koepsell, H., Winter, S., Burk, O., Klein, K., Kerb, R., Zanger, U. M., Keppler, D., Schwab, M., and Schaeffeler, E. (2009) Expression of organic cation transporters OCT1 (SLC22A1) and OCT3 (SLC22A3) is affected by genetic factors and cholestasis in human liver. *Hepatology* **50**, 1227-1240

144. Wu, X., Kekuda, R., Huang, W., Fei, Y. J., Leibach, F. H., Chen, J., Conway, S. J., and Ganapathy, V. (1998) Identity of the organic cation transporter OCT3 as the extraneuronal monoamine transporter (uptake2) and evidence for the expression of the transporter in the brain. *J Biol Chem* **273**, 32776-32786

145. Okuda, M., Saito, H., Urakami, Y., Takano, M., and Inui, K. (1996) cDNA cloning and functional expression of a novel rat kidney organic cation transporter, OCT2. *Biochem Biophys Res Commun* **224**, 500-507

146. Apparsundaram, S., Ferguson, S. M., George, A. L., Jr., and Blakely, R. D. (2000) Molecular cloning of a human, hemicholinium-3-sensitive choline transporter. *Biochem Biophys Res Commun* **276**, 862-867

147. Traiffort, E., Ruat, M., O'Regan, S., and Meunier, F. M. (2005) Molecular characterization of the family of choline transporter-like proteins and their splice variants. *J Neurochem* **92**, 1116-1125

148. Machova, E., O'Regan, S., Newcombe, J., Meunier, F. M., Prentice, J., Dove, R., Lisa, V., and Dolezal, V. (2009) Detection of choline transporter-like 1 protein CTL1 in neuroblastoma x glioma cells and in the CNS, and its role in choline uptake. *J Neurochem* **110**, 1297-1309

149. Michel, V., and Bakovic, M. (2012) The ubiquitous choline transporter SLC44A1. *Cent Nerv Syst Agents Med Chem* **12**, 70-81

150. Nakamura, T., Fujiwara, R., Ishiguro, N., Oyabu, M., Nakanishi, T., Shirasaka, Y., Maeda, T., and Tamai, I. (2010) Involvement of choline transporter-like proteins, CTL1 and CTL2, in glucocorticoid-induced acceleration of phosphatidylcholine synthesis via increased choline uptake. *Biol Pharm Bull* **33**, 691-696

151. Ishiguro, N., Oyabu, M., Sato, T., Maeda, T., Minami, H., and Tamai, I. (2008) Decreased biosynthesis of lung surfactant constituent phosphatidylcholine due to inhibition of choline transporter by gefitinib in lung alveolar cells. *Pharm Res* **25**, 417-427

152. Aoyama, C., Liao, H., and Ishidate, K. (2004) Structure and function of choline kinase isoforms in mammalian cells. *Prog Lipid Res* **43**, 266-281

153. Aoyama, C., Yamazaki, N., Terada, H., and Ishidate, K. (2000) Structure and characterization of the genes for murine choline/ethanolamine kinase isozymes alpha and beta. *J Lipid Res* **41**, 452-464

154. Aoyama, C., Ohtani, A., and Ishidate, K. (2002) Expression and characterization of the active molecular forms of choline/ethanolamine kinase-alpha and -beta in mouse tissues, including carbon tetrachloride-induced liver. *Biochem J* **363**, 777-784

155. Wu, G., Aoyama, C., Young, S. G., and Vance, D. E. (2008) Early embryonic lethality caused by disruption of the gene for choline kinase alpha, the first enzyme in phosphatidylcholine biosynthesis. *J Biol Chem* **283**, 1456-1462

156. Wu, G., Sher, R. B., Cox, G. A., and Vance, D. E. (2009) Understanding the muscular dystrophy caused by deletion of choline kinase beta in mice. *Biochim Biophys Acta* **1791**, 347-356

157. McMaster, C. R., and Bell, R. M. (1997) CDP-choline:1,2-diacylglycerol cholinephosphotransferase. *Biochim Biophys Acta* **1348**, 100-110

158. Henneberry, A. L., Wistow, G., and McMaster, C. R. (2000) Cloning, genomic organization, and characterization of a human cholinephosphotransferase. *J Biol Chem* **275**, 29808-29815

159. Henneberry, A. L., and McMaster, C. R. (1999) Cloning and expression of a human choline/ethanolaminephosphotransferase: synthesis of phosphatidylcholine and phosphatidylethanolamine. *Biochem J* **339 (Pt 2)**, 291-298

160. Horibata, Y., and Hirabayashi, Y. (2007) Identification and characterization of human ethanolaminephosphotransferase1. *J Lipid Res* **48**, 503-508

161. Henneberry, A. L., Wright, M. M., and McMaster, C. R. (2002) The major sites of cellular phospholipid synthesis and molecular determinants of Fatty Acid and lipid head group specificity. *Mol Biol Cell* **13**, 3148-3161

162. Wright, M. M., Henneberry, A. L., Lagace, T. A., Ridgway, N. D., and McMaster, C. R. (2001) Uncoupling farnesol-induced apoptosis from its inhibition of phosphatidylcholine synthesis. *J Biol Chem* **276**, 25254-25261

163. Sriburi, R., Jackowski, S., Mori, K., and Brewer, J. W. (2004) XBP1: a link between the unfolded protein response, lipid biosynthesis, and biogenesis of the endoplasmic reticulum. *J Cell Biol* **167**, 35-41

164. Lykidis, A., Murti, K. G., and Jackowski, S. (1998) Cloning and characterization of a second human CTP:phosphocholine cytidylyltransferase. *J Biol Chem* **273**, 14022-14029

165. Veitch, D. P., Gilham, D., and Cornell, R. B. (1998) The role of histidine residues in the HXGH site of CTP:phosphocholine cytidylyltransferase in CTP binding and catalysis. *Eur J Biochem* **255**, 227-234

166. Dennis, M. K., Taneva, S. G., and Cornell, R. B. (2011) The intrinsically disordered nuclear localization signal and phosphorylation segments distinguish the membrane affinity of two cytidylyltransferase isoforms. *J Biol Chem* **286**, 12349-12360

167. Tang, W., Keesler, G. A., and Tabas, I. (1997) The structure of the gene for murine CTP:phosphocholine cytidylyltransferase, Ctpct. Relationship of exon structure to functional domains and identification of transcriptional start sites and potential upstream regulatory elements. *J Biol Chem* **272**, 13146-13151

168. Wang, Y., MacDonald, J. I., and Kent, C. (1995) Identification of the nuclear localization signal of rat liver CTP:phosphocholine cytidylyltransferase. *J Biol Chem* **270**, 354-360

169. Hood, J. K., and Silver, P. A. (1999) In or out? Regulating nuclear transport. *Curr Opin Cell Biol* **11**, 241-247

170. Lykidis, A., Baburina, I., and Jackowski, S. (1999) Distribution of CTP:phosphocholine cytidylyltransferase (CCT) isoforms. Identification of a new CCTbeta splice variant. *J Biol Chem* **274**, 26992-27001

171. Karim, M., Jackson, P., and Jackowski, S. (2003) Gene structure, expression and identification of a new CTP:phosphocholine cytidylyltransferase beta isoform. *Biochim Biophys Acta* **1633**, 1-12

172. Carter, J. M., Waite, K. A., Campenot, R. B., Vance, J. E., and Vance, D. E. (2003) Enhanced expression and activation of CTP:phosphocholine cytidylyltransferase beta2 during neurite outgrowth. *J Biol Chem* **278**, 44988-44994

173. Jackowski, S., Rehg, J. E., Zhang, Y. M., Wang, J., Miller, K., Jackson, P., and Karim, M. A. (2004) Disruption of CCTbeta2 expression leads to gonadal dysfunction. *Mol Cell Biol* **24**, 4720-4733

174. Strakova, J., Demizieux, L., Campenot, R. B., Vance, D. E., and Vance, J. E. (2011) Involvement of CTP:phosphocholine cytidylyltransferase-beta2 in axonal phosphatidylcholine synthesis and branching of neurons. *Biochim Biophys Acta* **1811**, 617-625

175. Gunter, C., Frank, M., Tian, Y., Murti, K. G., Rehg, J. E., and Jackowski, S. (2007) Probucol therapy overcomes the reproductive defect in CTP: phosphocholine cytidylyltransferase beta2 knockout mice. *Biochim Biophys Acta* **1771**, 845-852

176. Wang, L., Magdaleno, S., Tabas, I., and Jackowski, S. (2005) Early embryonic lethality in mice with targeted deletion of the CTP:phosphocholine cytidylyltransferase alpha gene (Pcyt1a). *Mol Cell Biol* **25**, 3357-3363

177. Zhang, D., Tang, W., Yao, P. M., Yang, C., Xie, B., Jackowski, S., and Tabas, I. (2000) Macrophages deficient in CTP:Phosphocholine cytidylyltransferase-alpha are viable under normal culture conditions but are highly susceptible to free cholesterol-induced death. Molecular genetic evidence that the induction of phosphatidylcholine biosynthesis in free cholesterol-loaded macrophages is an adaptive response. *J Biol Chem* **275**, 35368-35376

178. Ridsdale, R., Tseu, I., Wang, J., and Post, M. (2001) CTP:phosphocholine cytidylyltransferase alpha is a cytosolic protein in pulmonary epithelial cells and tissues. *J Biol Chem* **276**, 49148-49155

179. Henderson, F. C., Miakotina, O. L., and Mallampalli, R. K. (2006) Proapoptotic effects of P. aeruginosa involve inhibition of surfactant phosphatidylcholine synthesis. *J Lipid Res* **47**, 2314-2324

180. MacKinnon, M. A., Curwin, A. J., Gaspard, G. J., Suraci, A. B., Fernandez-Murray, J. P., and McMaster, C. R. (2009) The Kap60-Kap95 karyopherin complex directly regulates phosphatidylcholine synthesis. *J Biol Chem* **284**, 7376-7384

181. Fagone, P., Gunter, C., Sage, C. R., Gunn, K. E., Brewer, J. W., and Jackowski, S. (2009) CTP:phosphocholine cytidylyltransferase alpha is required for B-cell proliferation and class switch recombination. *J Biol Chem* **284**, 6847-6854

182. Chen, B. B., and Mallampalli, R. K. (2009) Masking of a nuclear signal motif by monoubiquitination leads to mislocalization and degradation of the regulatory enzyme cytidylyltransferase. *Mol Cell Biol* **29**, 3062-3075

183. Gehrig, K., Morton, C. C., and Ridgway, N. D. (2009) Nuclear export of the rate-limiting enzyme in phosphatidylcholine synthesis is mediated by its membrane binding domain. *J Lipid Res* **50**, 966-976

184. Veitch, D. P., and Cornell, R. B. (1996) Substitution of serine for glycine-91 in the HXGH motif of CTP:phosphocholine cytidylyltransferase implicates this motif in CTP binding. *Biochemistry* **35**, 10743-10750

185. Kalmar, G. B., Kay, R. J., LaChance, A. C., and Cornell, R. B. (1994) Primary structure and expression of a human CTP:phosphocholine cytidylyltransferase. *Biochim Biophys Acta* **1219**, 328-334

186. Xie, M., Smith, J. L., Ding, Z., Zhang, D., and Cornell, R. B. (2004) Membrane binding modulates the quaternary structure of CTP:phosphocholine cytidylyltransferase. *J Biol Chem* **279**, 28817-28825

187. Lee, J., Johnson, J., Ding, Z., Paetzel, M., and Cornell, R. B. (2009) Crystal structure of a mammalian CTP: phosphocholine cytidylyltransferase catalytic domain reveals novel active site residues within a highly conserved nucleotidyltransferase fold. *J Biol Chem* **284**, 33535-33548

188. Clement, J. M., and Kent, C. (1999) CTP:phosphocholine cytidylyltransferase: insights into regulatory mechanisms and novel functions. *Biochem Biophys Res Commun* **257**, 643-650

189. Helmink, B. A., Braker, J. D., Kent, C., and Friesen, J. A. (2003) Identification of lysine 122 and arginine 196 as important functional residues of rat CTP:phosphocholine cytidylyltransferase alpha. *Biochemistry* **42**, 5043-5051

190. Sweitzer, T. D., and Kent, C. (1994) Expression of wild-type and mutant rat liver CTP: phosphocholine cytidylyltransferase in a cytidylyltransferase-deficient Chinese hamster ovary cell line. *Arch Biochem Biophys* **311**, 107-116

191. Johnson, J. E., Rao, N. M., Hui, S. W., and Cornell, R. B. (1998) Conformation and lipid binding properties of four peptides derived from the membrane-binding domain of CTP:phosphocholine cytidylyltransferase. *Biochemistry* **37**, 9509-9519

192. Dunne, S. J., Cornell, R. B., Johnson, J. E., Glover, N. R., and Tracey, A. S. (1996) Structure of the membrane binding domain of CTP:phosphocholine cytidylyltransferase. *Biochemistry* **35**, 11975-11984

193. Attard, G. S., Templer, R. H., Smith, W. S., Hunt, A. N., and Jackowski, S. (2000) Modulation of CTP:phosphocholine cytidylyltransferase by membrane curvature elastic stress. *Proc Natl Acad Sci U S A* **97**, 9032-9036

194. Sleight, R. G., and Dao, H. N. (1990) Synergistic activation of CTP:phosphocholine cytidylyltransferase by phosphatidylethanolamine and oleic acid. *Lipids* **25**, 100-107

195. Seddon, J. M., Templer, R. H., Warrender, N. A., Huang, Z., Cevc, G., and Marsh, D. (1997) Phosphatidylcholine-fatty acid membranes: effects of headgroup hydration on the phase behaviour and structural parameters of the gel and inverse hexagonal (H(II)) phases. *Biochim Biophys Acta* **1327**, 131-147

196. van der Veen, J. N., Lingrell, S., and Vance, D. E. (2012) The membrane lipid phosphatidylcholine is an unexpected source of triacylglycerol in the liver. *J Biol Chem* **287**, 23418-23426

197. Jamil, H., Hatch, G. M., and Vance, D. E. (1993) Evidence that binding of CTP:phosphocholine cytidylyltransferase to membranes in rat hepatocytes is modulated by the ratio of bilayer- to non-bilayer-forming lipids. *Biochem J* **291 (Pt 2)**, 419-427

198. Wang, Y., and Kent, C. (1995) Effects of altered phosphorylation sites on the properties of CTP:phosphocholine cytidylyltransferase. *J Biol Chem* **270**, 17843-17849

199. MacDonald, J. I., and Kent, C. (1994) Identification of phosphorylation sites in rat liver CTP: phosphocholine cytidylyltransferase. *J Biol Chem* **269**, 10529-10537

200. Wieprecht, M., Wieder, T., Paul, C., Geilen, C. C., and Orfanos, C. E. (1996) Evidence for phosphorylation of CTP:phosphocholine cytidylyltransferase by multiple proline-directed protein kinases. *J Biol Chem* **271**, 9955-9961

201. Wieprecht, M., Wieder, T., Geilen, C. C., and Orfanos, C. E. (1994) Growth factors stimulate phosphorylation of CTP:phosphocholine cytidylyltransferase in HeLa cells. *FEBS Lett* **353**, 221-224

202. Houweling, M., Jamil, H., Hatch, G. M., and Vance, D. E. (1994) Dephosphorylation of CTP-phosphocholine cytidylyltransferase is not required for binding to membranes. *J Biol Chem* **269**, 7544-7551

203. Bakovic, M., Waite, K. A., and Vance, D. E. (2000) Functional significance of Sp1, Sp2, and Sp3 transcription factors in regulation of the murine CTP:phosphocholine cytidylyltransferase alpha promoter. *J Lipid Res* **41**, 583-594

204. Banchio, C., Schang, L. M., and Vance, D. E. (2004) Phosphorylation of Sp1 by cyclin-dependent kinase 2 modulates the role of Sp1 in CTP:phosphocholine cytidylyltransferase alpha regulation during the S phase of the cell cycle. *J Biol Chem* **279**, 40220-40226

205. Banchio, C., Schang, L. M., and Vance, D. E. (2003) Activation of CTP:phosphocholine cytidylyltransferase alpha expression during the S phase of the cell cycle is mediated by the transcription factor Sp1. *J Biol Chem* **278**, 32457-32464

206. Banchio, C., Lingrell, S., and Vance, D. E. (2007) Sp-1 binds promoter elements that are regulated by retinoblastoma and regulate CTP:phosphocholine cytidylyltransferase-alpha transcription. *J Biol Chem* **282**, 14827-14835

207. Bakovic, M., Waite, K., and Vance, D. E. (2003) Oncogenic Ha-Ras transformation modulates the transcription of the CTP:phosphocholine cytidylyltransferase alpha gene via p42/44MAPK and transcription factor Sp3. *J Biol Chem* **278**, 14753-14761

208. Foretz, M., Guichard, C., Ferre, P., and Foufelle, F. (1999) Sterol regulatory element binding protein-1c is a major mediator of insulin action on the hepatic expression of glucokinase and lipogenesis-related genes. *Proc Natl Acad Sci U S A* **96**, 12737-12742

209. Jerkins, A. A., Liu, W. R., Lee, S., and Sul, H. S. (1995) Characterization of the murine mitochondrial glycerol-3-phosphate acyltransferase promoter. *J Biol Chem* **270**, 1416-1421

210. Brown, M. S., and Goldstein, J. L. (1997) The SREBP pathway: regulation of cholesterol metabolism by proteolysis of a membrane-bound transcription factor. *Cell* **89**, 331-340

211. Kast, H. R., Nguyen, C. M., Anisfeld, A. M., Ericsson, J., and Edwards, P. A. (2001) CTP:phosphocholine cytidylyltransferase, a new sterol- and SREBP-responsive gene. *J Lipid Res* **42**, 1266-1272

212. Lagace, T. A., Storey, M. K., and Ridgway, N. D. (2000) Regulation of phosphatidylcholine metabolism in Chinese hamster ovary cells by the sterol regulatory element-binding protein (SREBP)/SREBP cleavage-activating protein pathway. *J Biol Chem* **275**, 14367-14374

213. Wilfling, F., Haas, J. T., Walther, T. C., and Farese, R. V., Jr. (2014) Lipid droplet biogenesis. *Curr Opin Cell Biol* **29**, 39-45

214. Khandelia, H., Duelund, L., Pakkanen, K. I., and Ipsen, J. H. (2010) Triglyceride blisters in lipid bilayers: implications for lipid droplet biogenesis and the mobile lipid signal in cancer cell membranes. *PLoS One* **5**, e12811

215. Kassan, A., Herms, A., Fernandez-Vidal, A., Bosch, M., Schieber, N. L., Reddy, B. J., Fajardo, A., Gelabert-Baldrich, M., Tebar, F., Enrich, C., Gross, S. P., Parton, R. G., and Pol, A. (2013) Acyl-CoA synthetase 3 promotes lipid droplet biogenesis in ER microdomains. *J Cell Biol* **203**, 985-1001

216. Jacquier, N., Choudhary, V., Mari, M., Toulmay, A., Reggiori, F., and Schneiter, R. (2011) Lipid droplets are functionally connected to the endoplasmic reticulum in Saccharomyces cerevisiae. *J Cell Sci* **124**, 2424-2437

217. Wilfling, F., Thiam, A. R., Olarte, M. J., Wang, J., Beck, R., Gould, T. J., Allgeyer, E. S., Pincet, F., Bewersdorf, J., Farese, R. V., Jr., and Walther, T. C. (2014) Arf1/COPI machinery acts directly on lipid droplets and enables their connection to the ER for protein targeting. *Elife* **3**, e01607

218. Olzmann, J. A., and Carvalho, P. (2019) Dynamics and functions of lipid droplets. *Nat Rev Mol Cell Biol* **20**, 137-155

219. Beller, M., Sztalryd, C., Southall, N., Bell, M., Jackle, H., Auld, D. S., and Oliver, B. (2008) COPI complex is a regulator of lipid homeostasis. *PLoS Biol* **6**, e292

220. Soni, K. G., Mardones, G. A., Sougrat, R., Smirnova, E., Jackson, C. L., and Bonifacino, J. S. (2009) Coatomer-dependent protein delivery to lipid droplets. *J Cell Sci* **122**, 1834-1841

221. Gao, G., Chen, F. J., Zhou, L., Su, L., Xu, D., Xu, L., and Li, P. (2017) Control of lipid droplet fusion and growth by CIDE family proteins. *Biochim Biophys Acta Mol Cell Biol Lipids* **1862**, 1197-1204

222. Gong, J., Sun, Z., Wu, L., Xu, W., Schieber, N., Xu, D., Shui, G., Yang, H., Parton, R. G., and Li, P. (2011) Fsp27 promotes lipid droplet growth by lipid exchange and transfer at lipid droplet contact sites. *J Cell Biol* **195**, 953-963

223. Jambunathan, S., Yin, J., Khan, W., Tamori, Y., and Puri, V. (2011) FSP27 promotes lipid droplet clustering and then fusion to regulate triglyceride accumulation. *PLoS One* **6**, e28614

224. Sun, Z., Gong, J., Wu, H., Xu, W., Wu, L., Xu, D., Gao, J., Wu, J. W., Yang, H., Yang, M., and Li, P. (2013) Perilipin1 promotes unilocular lipid droplet formation through the activation of Fsp27 in adipocytes. *Nat Commun* **4**, 1594

225. Grahn, T. H., Zhang, Y., Lee, M. J., Sommer, A. G., Mostoslavsky, G., Fried, S. K., Greenberg, A. S., and Puri, V. (2013) FSP27 and PLIN1 interaction promotes the formation of large lipid droplets in human adipocytes. *Biochem Biophys Res Commun* **432**, 296-301

226. Ye, J., Li, J. Z., Liu, Y., Li, X., Yang, T., Ma, X., Li, Q., Yao, Z., and Li, P. (2009) Cideb, an ER- and lipid droplet-associated protein, mediates VLDL lipidation and maturation by interacting with apolipoprotein B. *Cell Metab* **9**, 177-190

227. Ducharme, N. A., and Bickel, P. E. (2008) Lipid droplets in lipogenesis and lipolysis. *Endocrinology* **149**, 942-949

228. Haemmerle, G., Lass, A., Zimmermann, R., Gorkiewicz, G., Meyer, C., Rozman, J., Heldmaier, G., Maier, R., Theussl, C., Eder, S., Kratky, D., Wagner, E. F., Klingenspor, M., Hoefler, G., and Zechner, R. (2006) Defective lipolysis and altered energy metabolism in mice lacking adipose triglyceride lipase. *Science* **312**, 734-737

229. Ong, K. T., Mashek, M. T., Davidson, N. O., and Mashek, D. G. (2014) Hepatic ATGL mediates PPAR-alpha signaling and fatty acid channeling through an L-FABP independent mechanism. *J Lipid Res* **55**, 808-815

230. Wu, J. W., Wang, S. P., Casavant, S., Moreau, A., Yang, G. S., and Mitchell, G. A. (2012) Fasting energy homeostasis in mice with adipose deficiency of desnutrin/adipose triglyceride lipase. *Endocrinology* **153**, 2198-2207

231. Reid, B. N., Ables, G. P., Otlivanchik, O. A., Schoiswohl, G., Zechner, R., Blaner, W. S., Goldberg, I. J., Schwabe, R. F., Chua, S. C., Jr., and Huang, L. S. (2008) Hepatic overexpression of hormone-sensitive lipase and adipose triglyceride lipase promotes fatty acid oxidation, stimulates direct release of free fatty acids, and ameliorates steatosis. *J Biol Chem* **283**, 13087-13099

232. Sathyanarayan, A., Mashek, M. T., and Mashek, D. G. (2017) ATGL Promotes Autophagy/Lipophagy via SIRT1 to Control Hepatic Lipid Droplet Catabolism. *Cell Rep* **19**, 1-9

233. Lu, X., Yang, X., and Liu, J. (2010) Differential control of ATGL-mediated lipid droplet degradation by CGI-58 and G0S2. *Cell Cycle* **9**, 2719-2725

234. Lefevre, C., Jobard, F., Caux, F., Bouadjar, B., Karaduman, A., Heilig, R., Lakhdar, H., Wollenberg, A., Verret, J. L., Weissenbach, J., Ozguc, M., Lathrop, M., Prud'homme, J. F., and Fischer, J. (2001) Mutations in CGI-58, the gene encoding a new protein of the esterase/lipase/thioesterase subfamily, in Chanarin-Dorfman syndrome. *Am J Hum Genet* **69**, 1002-1012

235. Yamaguchi, T., Omatsu, N., Matsushita, S., and Osumi, T. (2004) CGI-58 interacts with perilipin and is localized to lipid droplets. Possible involvement of CGI-58 mislocalization in Chanarin-Dorfman syndrome. *J Biol Chem* **279**, 30490-30497

236. Lass, A., Zimmermann, R., Haemmerle, G., Riederer, M., Schoiswohl, G., Schweiger, M., Kienesberger, P., Strauss, J. G., Gorkiewicz, G., and Zechner, R. (2006) Adipose triglyceride lipase-mediated lipolysis of cellular fat stores is activated by CGI-58 and defective in Chanarin-Dorfman Syndrome. *Cell Metab* **3**, 309-319

237. Haemmerle, G., Zimmermann, R., Hayn, M., Theussl, C., Waeg, G., Wagner, E., Sattler, W., Magin, T. M., Wagner, E. F., and Zechner, R. (2002) Hormone-sensitive lipase deficiency in mice causes diglyceride accumulation in adipose tissue, muscle, and testis. *J Biol Chem* **277**, 4806-4815

238. Albert, J. S., Yerges-Armstrong, L. M., Horenstein, R. B., Pollin, T. I., Sreenivasan, U. T., Chai, S., Blaner, W. S., Snitker, S., O'Connell, J. R., Gong, D. W., Breyer, R. J., 3rd, Ryan, A. S., McLenithan, J. C., Shuldiner, A. R., Sztalryd, C., and Damcott, C. M. (2014) Null mutation in hormone-sensitive lipase gene and risk of type 2 diabetes. *N Engl J Med* **370**, 2307-2315

239. Douglass, J. D., Zhou, Y. X., Wu, A., Zadroga, J. A., Gajda, A. M., Lackey, A. I., Lang, W., Chevalier, K. M., Sutton, S. W., Zhang, S. P., Flores, C. M., Connelly, M. A., and Storch, J. (2015) Global deletion of MGL in mice delays lipid absorption and alters energy homeostasis and diet-induced obesity. *J Lipid Res* **56**, 1153-1171

240. Taschler, U., Radner, F. P., Heier, C., Schreiber, R., Schweiger, M., Schoiswohl, G., Preiss-Landl, K., Jaeger, D., Reiter, B., Koefeler, H. C., Wojciechowski, J., Theussl, C., Penninger, J. M., Lass, A., Haemmerle, G., Zechner, R., and Zimmermann, R. (2011) Monoglyceride lipase deficiency in mice impairs lipolysis and attenuates diet-induced insulin resistance. *J Biol Chem* **286**, 17467-17477

241. Singh, R., Kaushik, S., Wang, Y., Xiang, Y., Novak, I., Komatsu, M., Tanaka, K., Cuervo, A. M., and Czaja, M. J. (2009) Autophagy regulates lipid metabolism. *Nature* **458**, 1131-1135

242. Martinez-Vicente, M., Talloczy, Z., Wong, E., Tang, G., Koga, H., Kaushik, S., de Vries, R., Arias, E., Harris, S., Sulzer, D., and Cuervo, A. M. (2010) Cargo recognition failure is responsible for inefficient autophagy in Huntington's disease. *Nat Neurosci* **13**, 567-576

243. Martinez-Lopez, N., Garcia-Macia, M., Sahu, S., Athonvarangkul, D., Liebling, E., Merlo, P., Cecconi, F., Schwartz, G. J., and Singh, R. (2016) Autophagy in the CNS and Periphery Coordinate Lipophagy and Lipolysis in the Brown Adipose Tissue and Liver. *Cell Metab* **23**, 113-127

244. Ouimet, M., Franklin, V., Mak, E., Liao, X., Tabas, I., and Marcel, Y. L. (2011) Autophagy regulates cholesterol efflux from macrophage foam cells via lysosomal acid lipase. *Cell Metab* **13**, 655-667

245. Khaldoun, S. A., Emond-Boisjoly, M. A., Chateau, D., Carriere, V., Lacasa, M., Rousset, M., Demignot, S., and Morel, E. (2014) Autophagosomes contribute to intracellular lipid distribution in enterocytes. *Mol Biol Cell* **25**, 118-132

246. Khan, S. A., Sathyanarayan, A., Mashek, M. T., Ong, K. T., Wollaston-Hayden, E. E., and Mashek, D. G. (2015) ATGL-catalyzed lipolysis regulates SIRT1 to control PGC-1alpha/PPAR-alpha signaling. *Diabetes* **64**, 418-426

247. Schott, M. B., Weller, S. G., Schulze, R. J., Krueger, E. W., Drizyte-Miller, K., Casey, C. A., and McNiven, M. A. (2019) Lipid droplet size directs lipolysis and lipophagy catabolism in hepatocytes. *J Cell Biol* **218**, 3320-3335

248. Feingold, K. R., and Grunfeld, C. (2000) Introduction to Lipids and Lipoproteins. in *Endotext* (Feingold, K. R., Anawalt, B., Boyce, A., Chrousos, G., Dungan, K., Grossman, A., Hershman, J. M., Kaltsas, G., Koch, C., Kopp, P., Korbonits, M., McLachlan, R., Morley, J. E., New, M., Perreault, L., Purnell, J., Rebar, R., Singer, F., Trence, D. L., Vinik, A., and Wilson, D. P. eds.), South Dartmouth (MA). pp

249. Veniant, M. M., Zlot, C. H., Walzem, R. L., Pierotti, V., Driscoll, R., Dichek, D., Herz, J., and Young, S. G. (1998) Lipoprotein clearance mechanisms in LDL receptor-deficient "Apo-B48-only" and "Apo-B100-only" mice. *J Clin Invest* **102**, 1559-1568

250. Mahley, R. W., Innerarity, T. L., Rall, S. C., Jr., and Weisgraber, K. H. (1984) Plasma lipoproteins: apolipoprotein structure and function. *J Lipid Res* **25**, 1277-1294

251. Demignot, S., Beilstein, F., and Morel, E. (2014) Triglyceride-rich lipoproteins and cytosolic lipid droplets in enterocytes: key players in intestinal physiology and metabolic disorders. *Biochimie* **96**, 48-55

252. Dash, S., Xiao, C., Morgantini, C., and Lewis, G. F. (2015) New Insights into the Regulation of Chylomicron Production. *Annu Rev Nutr* **35**, 265-294

253. Aalto-Setala, K., Bisgaier, C. L., Ho, A., Kieft, K. A., Traber, M. G., Kayden, H. J., Ramakrishnan, R., Walsh, A., Essenburg, A. D., and Breslow, J. L. (1994) Intestinal expression of human apolipoprotein A-IV in transgenic mice fails to influence dietary lipid absorption or feeding behavior. *J Clin Invest* **93**, 1776-1786

254. Weinstock, P. H., Bisgaier, C. L., Hayek, T., Aalto-Setala, K., Sehayek, E., Wu, L., Sheiffele, P., Merkel, M., Essenburg, A. D., and Breslow, J. L. (1997) Decreased HDL cholesterol levels but normal lipid absorption, growth, and feeding behavior in apolipoprotein A-IV knockout mice. *J Lipid Res* **38**, 1782-1794

255. Rensen, P. C., and van Berkel, T. J. (1996) Apolipoprotein E effectively inhibits lipoprotein lipase-mediated lipolysis of chylomicron-like triglyceride-rich lipid emulsions in vitro and in vivo. *J Biol Chem* **271**, 14791-14799

256. Tall, A. R., Green, P. H., Glickman, R. M., and Riley, J. W. (1979) Metabolic fate of chylomicron phospholipids and apoproteins in the rat. *J Clin Invest* **64**, 977-989

257. Gibbons, G. F., Islam, K., and Pease, R. J. (2000) Mobilisation of triacylglycerol stores. *Biochim Biophys Acta* **1483**, 37-57

258. Olofsson, S. O., Bostrom, P., Andersson, L., Rutberg, M., Perman, J., and Boren, J. (2009) Lipid droplets as dynamic organelles connecting storage and efflux of lipids. *Biochim Biophys Acta* **1791**, 448-458

259. Uchida, A., Whitsitt, M. C., Eustaquio, T., Slipchenko, M. N., Leary, J. F., Cheng, J. X., and Buhman, K. K. (2012) Reduced triglyceride secretion in response to an acute dietary fat challenge in obese compared to lean mice. *Front Physiol* **3**, 26

260. Obrowsky, S., Chandak, P. G., Patankar, J. V., Povoden, S., Schlager, S., Kershaw, E. E., Bogner-Strauss, J. G., Hoefler, G., Levak-Frank, S., and Kratky, D. (2013) Adipose triglyceride lipase is a TG hydrolase of the small intestine and regulates intestinal PPARalpha signaling. *J Lipid Res* **54**, 425-435

261. Obrowsky, S., Chandak, P. G., Patankar, J. V., Pfeifer, T., Povoden, S., Schreiber, R., Haemmerle, G., Levak-Frank, S., and Kratky, D. (2012) Cholesteryl ester accumulation and accelerated cholesterol absorption in intestine-specific hormone sensitive lipase-null mice. *Biochim Biophys Acta* **1821**, 1406-1414

262. Coates, P. M., Brown, S. A., Jumawan, J., and Koldovsky, O. (1977) Characteristics and postnatal development of the acid lipase activity of the rat small intestine. *Biochem J* **166**, 331-338

263. Mansbach, C. M., 2nd, Arnold, A., and Garrett, M. (1987) Effect of chloroquine on intestinal lipid metabolism. *Am J Physiol* **253**, G673-678

264. Xie, P., Guo, F., Ma, Y., Zhu, H., Wang, F., Xue, B., Shi, H., Yang, J., and Yu, L. (2014) Intestinal Cgi-58 deficiency reduces postprandial lipid absorption. *PLoS One* **9**, e91652

265. Sturley, S. L., and Hussain, M. M. (2012) Lipid droplet formation on opposing sides of the endoplasmic reticulum. *J Lipid Res* **53**, 1800-1810

266. Jamil, H., Dickson, J. K., Jr., Chu, C. H., Lago, M. W., Rinehart, J. K., Biller, S. A., Gregg, R. E., and Wetterau, J. R. (1995) Microsomal triglyceride transfer protein. Specificity of lipid binding and transport. *J Biol Chem* **270**, 6549-6554

267. Xiao, C., Stahel, P., and Lewis, G. F. (2019) Regulation of Chylomicron Secretion: Focus on Post-Assembly Mechanisms. *Cell Mol Gastroenterol Hepatol* **7**, 487-501

268. Lev, S. (2010) Non-vesicular lipid transport by lipid-transfer proteins and beyond. *Nat Rev Mol Cell Biol* **11**, 739-750

269. Horl, G., Wagner, A., Cole, L. K., Malli, R., Reicher, H., Kotzbeck, P., Kofeler, H., Hofler, G., Frank, S., Bogner-Strauss, J. G., Sattler, W., Vance, D. E., and Steyrer, E. (2011) Sequential synthesis and methylation of phosphatidylethanolamine promote lipid droplet biosynthesis and stability in tissue culture and in vivo. *J Biol Chem* **286**, 17338-17350

270. Moessinger, C., Kuerschner, L., Spandl, J., Shevchenko, A., and Thiele, C. (2011) Human lysophosphatidylcholine acyltransferases 1 and 2 are located in lipid droplets where they catalyze the formation of phosphatidylcholine. *J Biol Chem* **286**, 21330-21339

271. Yao, Z. M., and Vance, D. E. (1990) Reduction in VLDL, but not HDL, in plasma of rats deficient in choline. *Biochem Cell Biol* **68**, 552-558

272. Noga, A. A., Zhao, Y., and Vance, D. E. (2002) An unexpected requirement for phosphatidylethanolamine N-methyltransferase in the secretion of very low density lipoproteins. *J Biol Chem* **277**, 42358-42365

273. Jacobs, R. L., Zhao, Y., Koonen, D. P., Sletten, T., Su, B., Lingrell, S., Cao, G., Peake, D. A., Kuo, M. S., Proctor, S. D., Kennedy, B. P., Dyck, J. R., and Vance, D. E. (2010) Impaired de novo choline synthesis explains why phosphatidylethanolamine N-methyltransferase-deficient mice are protected from diet-induced obesity. *J Biol Chem* **285**, 22403-22413

274. da Silva, R. P., Kelly, K. B., Lewis, E. D., Leonard, K. A., Goruk, S., Curtis, J. M., Vine, D. F., Proctor, S. D., Field, C. J., and Jacobs, R. L. (2015) Choline deficiency impairs intestinal lipid metabolism in the lactating rat. *J Nutr Biochem* **26**, 1077-1083

275. Kennelly, J. P., van der Veen, J. N., Nelson, R. C., Leonard, K. A., Havinga, R., Buteau, J., Kuipers, F., and Jacobs, R. L. (2018) Intestinal de novo phosphatidylcholine synthesis is required for dietary lipid absorption and metabolic homeostasis. *J Lipid Res* **59**, 1695-1708

276. La Cour, L. F., Chayen, J., and Gahan, P. S. (1958) Evidence for lipid material in chromosomes. *Exp Cell Res* **14**, 469-485

277. Gurr, M. I., Finean, J. B., and Hawthorne, J. N. (1963) The Phospholipids of Liver-Cell Fractions. I. The Phospholipid Composition of the Liver-Cell Nucleus. *Biochim Biophys Acta* **70**, 406-416

278. Layerenza, J. P., Gonzalez, P., Garcia de Bravo, M. M., Polo, M. P., Sisti, M. S., and Ves-Losada, A. (2013) Nuclear lipid droplets: a novel nuclear domain. *Biochim Biophys Acta* **1831**, 327-340

279. Khandwala, A. S., and Kasper, C. B. (1971) The fatty acid composition of individual phospholipids from rat liver nuclear membrane and nuclei. *J Biol Chem* **246**, 6242-6246

280. James, J. L., Clawson, G. A., Chan, C. H., and Smuckler, E. A. (1981) Analysis of the phospholipid of the nuclear envelope and endoplasmic reticulum of liver cells by high pressure liquid chromatography. *Lipids* **16**, 541-545

281. Keenan, T. W., Berezney, R., and Crane, F. L. (1972) Lipid composition of further purified bovine liver nuclear membranes. *Lipids* **7**, 212-215

282. Alroy, J., Merk, F. B., Goyal, V., and Ucci, A. (1981) Heterogeneous distribution of filipin-sterol complexes in nuclear membranes. *Biochim Biophys Acta* **649**, 239-243

283. Ledeen, R. W., and Wu, G. (2004) Nuclear lipids: key signaling effectors in the nervous system and other tissues. *J Lipid Res* **45**, 1-8

284. Irvine, R. F. (2003) Nuclear lipid signalling. *Nat Rev Mol Cell Biol* **4**, 349-360

285. Hardingham, G. E., Cruzalegui, F. H., Chawla, S., and Bading, H. (1998) Mechanisms controlling gene expression by nuclear calcium signals. *Cell Calcium* **23**, 131-134

286. Neri, L. M., Borgatti, P., Capitani, S., and Martelli, A. M. (1998) Nuclear diacylglycerol produced by phosphoinositide-specific phospholipase C is responsible for nuclear translocation of protein kinase C-alpha. *J Biol Chem* **273**, 29738-29744

287. Sun, B., Murray, N. R., and Fields, A. P. (1997) A role for nuclear phosphatidylinositol-specific phospholipase C in the G2/M phase transition. *J Biol Chem* **272**, 26313-26317

288. Soltysik, K., Ohsaki, Y., Tatematsu, T., Cheng, J., and Fujimoto, T. (2019) Nuclear lipid droplets derive from a lipoprotein precursor and regulate phosphatidylcholine synthesis. *Nat Commun* **10**, 473

289. Uzbekov, R., and Roingeard, P. (2013) Nuclear lipid droplets identified by electron microscopy of serial sections. *BMC Res Notes* **6**, 386

290. Muller, R., Rieck, M., and Muller-Brusselbach, S. (2008) Regulation of Cell Proliferation and Differentiation by PPARbeta/delta. *PPAR Res* **2008**, 614852

291. Walesky, C., and Apte, U. (2015) Role of hepatocyte nuclear factor 4alpha (HNF4alpha) in cell proliferation and cancer. *Gene Expr* **16**, 101-108

292. Romanauska, A., and Kohler, A. (2018) The Inner Nuclear Membrane Is a Metabolically Active Territory that Generates Nuclear Lipid Droplets. *Cell* **174**, 700-715 e718

293. Haider, A., Wei, Y. C., Lim, K., Barbosa, A. D., Liu, C. H., Weber, U., Mlodzik, M., Oras, K., Collier, S., Hussain, M. M., Dong, L., Patel, S., Alvarez-Guaita, A., Saudek, V., Jenkins, B. J., Koulman, A., Dymond, M. K., Hardie, R. C., Siniossoglou, S., and Savage, D. B. (2018) PCYT1A Regulates Phosphatidylcholine Homeostasis from the Inner Nuclear Membrane in Response to Membrane Stored Curvature Elastic Stress. *Dev Cell* **45**, 481-495 e488

294. Smoyer, C. J., Katta, S. S., Gardner, J. M., Stoltz, L., McCroskey, S., Bradford, W. D., McClain, M., Smith, S. E., Slaughter, B. D., Unruh, J. R., and Jaspersen, S. L. (2016) Analysis of membrane proteins localizing to the inner nuclear envelope in living cells. *J Cell Biol* **215**, 575-590

295. de The, H., Lavau, C., Marchio, A., Chomienne, C., Degos, L., and Dejean, A. (1991) The PML-RAR alpha fusion mRNA generated by the t(15;17) translocation in acute promyelocytic leukemia encodes a functionally altered RAR. *Cell* **66**, 675-684

296. Nisole, S., Maroui, M. A., Mascle, X. H., Aubry, M., and Chelbi-Alix, M. K. (2013) Differential Roles of PML Isoforms. *Front Oncol* **3**, 125

297. Van Damme, E., Laukens, K., Dang, T. H., and Van Ostade, X. (2010) A manually curated network of the PML nuclear body interactome reveals an important role for PML-NBs in SUMOylation dynamics. *Int J Biol Sci* **6**, 51-67

298. Boisvert, F. M., Hendzel, M. J., and Bazett-Jones, D. P. (2000) Promyelocytic leukemia (PML) nuclear bodies are protein structures that do not accumulate RNA. *J Cell Biol* **148**, 283-292

299. Dellaire, G., Ching, R. W., Ahmed, K., Jalali, F., Tse, K. C., Bristow, R. G., and Bazett-Jones, D. P. (2006) Promyelocytic leukemia nuclear bodies behave as DNA damage sensors whose response to DNA double-strand breaks is regulated by NBS1 and the kinases ATM, Chk2, and ATR. *J Cell Biol* **175**, 55-66

300. Bernardi, R., and Pandolfi, P. P. (2007) Structure, dynamics and functions of promyelocytic leukaemia nuclear bodies. *Nat Rev Mol Cell Biol* **8**, 1006-1016

301. Hofmann, T. G., Moller, A., Sirma, H., Zentgraf, H., Taya, Y., Droge, W., Will, H., and Schmitz, M. L. (2002) Regulation of p53 activity by its interaction with homeodomain-interacting protein kinase-2. *Nat Cell Biol* **4**, 1-10

302. Ito, K., Carracedo, A., Weiss, D., Arai, F., Ala, U., Avigan, D. E., Schafer, Z. T., Evans, R. M., Suda, T., Lee, C. H., and Pandolfi, P. P. (2012) A PML-PPAR-delta pathway for fatty acid oxidation regulates hematopoietic stem cell maintenance. *Nat Med* **18**, 1350-1358

303. Carracedo, A., Weiss, D., Leliaert, A. K., Bhasin, M., de Boer, V. C., Laurent, G., Adams, A. C., Sundvall, M., Song, S. J., Ito, K., Finley, L. S., Egia, A., Libermann, T., Gerhart-Hines, Z., Puigserver, P., Haigis, M. C., Maratos-Flier, E., Richardson, A. L., Schafer, Z. T., and Pandolfi, P. P. (2012) A metabolic prosurvival role for PML in breast cancer. *J Clin Invest* **122**, 3088-3100

304. Chung, Y. L., and Wu, M. L. (2018) The Role of Promyelocytic Leukemia Protein in Steatosis-Associated Hepatic Tumors Related to Chronic Hepatitis B virus Infection. *Transl Oncol* **11**, 743-754

305. Salsman, J., Stathakis, A., Parker, E., Chung, D., Anthes, L. E., Koskowich, K. L., Lahsaee, S., Gaston, D., Kukurba, K. R., Smith, K. S., Chute, I. C., Leger, D., Frost, L. D., Montgomery, S. B., Lewis, S. M., Eskiw, C., and Dellaire, G. (2017) PML nuclear bodies contribute to the basal expression of the mTOR inhibitor DDIT4. *Sci Rep* **7**, 45038

306. Goldstein, J. L., Basu, S. K., and Brown, M. S. (1983) Receptor-mediated endocytosis of low-density lipoprotein in cultured cells. *Methods Enzymol* **98**, 241-260

307. Lowry, O. H., Rosebrough, N. J., Farr, A. L., and Randall, R. J. (1951) Protein measurement with the Folin phenol reagent. *J Biol Chem* **193**, 265-275

308. Levy, E., Yotov, W., Seidman, E. G., Garofalo, C., Delvin, E., and Menard, D. (1999) Caco-2 cells and human fetal colon: a comparative analysis of their lipid transport. *Biochim Biophys Acta* **1439**, 353-362

309. Luchoomun, J., and Hussain, M. M. (1999) Assembly and secretion of chylomicrons by differentiated Caco-2 cells. Nascent triglycerides and preformed phospholipids are preferentially used for lipoprotein assembly. *J Biol Chem* **274**, 19565-19572

310. Chateau, D., Pauquai, T., Delers, F., Rousset, M., Chambaz, J., and Demignot, S. (2005) Lipid micelles stimulate the secretion of triglyceride-enriched apolipoprotein B48-containing lipoproteins by Caco-2 cells. *J Cell Physiol* **202**, 767-776

311. Tso, P., Drake, D. S., Black, D. D., and Sabesin, S. M. (1984) Evidence for separate pathways of chylomicron and very low-density lipoprotein assembly and transport by rat small intestine. *Am J Physiol* **247**, G599-610

312. Fatma, S., Yakubov, R., Anwar, K., and Hussain, M. M. (2006) Pluronic L81 enhances triacylglycerol accumulation in the cytosol and inhibits chylomicron secretion. *J Lipid Res* **47**, 2422-2432

313. Codazzi, F., Teruel, M. N., and Meyer, T. (2001) Control of astrocyte Ca(2+) oscillations and waves by oscillating translocation and activation of protein kinase C. *Curr Biol* **11**, 1089-1097

314. Bohdanowicz, M., Schlam, D., Hermansson, M., Rizzuti, D., Fairn, G. D., Ueyama, T., Somerharju, P., Du, G., and Grinstein, S. (2013) Phosphatidic acid is required for the constitutive ruffling and macropinocytosis of phagocytes. *Mol Biol Cell* **24**, 1700-1712, S1701-1707

315. Jul-Larsen, A., Grudic, A., Bjerkvig, R., and Boe, S. O. (2010) Subcellular distribution of nuclear import-defective isoforms of the promyelocytic leukemia protein. *BMC Mol Biol* **11**, 89

316. Liu, G. H., and Gerace, L. (2009) Sumoylation regulates nuclear localization of lipin-1alpha in neuronal cells. *PLoS One* **4**, e7031

317. Cheng, X., and Kao, H. Y. (2012) Post-translational modifications of PML: consequences and implications. *Front Oncol* **2**, 210

318. Vega, R. B., Huss, J. M., and Kelly, D. P. (2000) The coactivator PGC-1 cooperates with peroxisome proliferator-activated receptor alpha in transcriptional control of nuclear genes encoding mitochondrial fatty acid oxidation enzymes. *Mol Cell Biol* **20**, 1868-1876

319. Cheng, X., Guo, S., Liu, Y., Chu, H., Hakimi, P., Berger, N. A., Hanson, R. W., and Kao, H. Y. (2013) Ablation of promyelocytic leukemia protein (PML) re-patterns energy balance and protects mice from obesity induced by a Western diet. *J Biol Chem* **288**, 29746-29759